FIBREGY

This project has received funding from the European Union's Horizon 2020 research and innovation programme under grant agreement No 952966.

Development, engineering, production and life cycle management of improved FIBRE-based material solutions for the structure and functional components of large offshore wind enerGY and tidal power platforms

D2.2 (WP2 Task 2.4): Fatigue performance of composite materials.

Responsible Partner: ULIM

Contributor(s): CIMNE, INEGI, CORSO, IXBLUE, TUCO, TSI, ENEROCEAN, BV

This project has received funding from the European Union's Horizon 2020 research and innovation programme under grant agreement No 952966.

DOCUMENT INFORMATION TABLE

CONTRACT NUMBER:	952966	
PROJECT ACRONYM:	FIBREGY	
PROJECT COORDINATOR:	CIMNE	
DOCUMENT RESPONSIBLE	University of Limerick	ULIM
DELIVERABLE TYPE:	Final Report	
DOCUMENT TITLE:	Fatigue performance of composite materials	
DOCUMENT ID:	D2.2	
DISSEMINATION LEVEL:	CO: Confidential, only for members of the consortium	
FILENAME:	FIBREGY_T2.4_D2.2 Report_VF	
STATUS:	Final version	

Authoring & Review

PREPARED / REVIEWED BY				
Name	Role	Partner	Date	Comments
Anthony Comer, Akshay Hejjaji, Gursahib Bhatia, Jayaram R. Pothnis	Creator/co-authors	ULIM	24/05/2023	
João Cardoso	Review	INEGI	26/05/2023	Comments suggested for Section 3.4

This project has received funding from the European Union's Horizon 2020 research and innovation programme under grant agreement No 952966.

EXECUTIVE SUMMARY

This document contains a description of the work performed in Task 2.4 during months 1-29 of the FibreGY project. An interim report D2.2.1 detailing the work performed in Task 2.4 from months 1 to 24 was shared with all the partners in the month 24 (M24) as agreed in the description of action (DoA). The current document is the is the continuation of D2.2.1 encompassing a very brief review of literature related to the fatigue behaviour of fibre reinforced composites in the context of wind turbine blades. This is followed by the description of an extensive experimental fatigue test campaign and the associated results. Furthermore, description of quasi-static compression tests, which were performed in addition to the fatigue tests and the associated results are also included in this report. These tests were conducted to facilitate the development of numerical models by Fibregy partners.

The main objectives addressed in this document can be summarised as follows:

- To describe the methodology employed for an extensive experimental testing campaign conducted to evaluate the fatigue behaviour of the selected fibre reinforced polymers (FRP) composites.
- To analyse and present the data obtained from the fatigue experiments and failure analysis to understand the fatigue behaviour of the selected thermoplastic and thermoset composites.
- To describe the methodology of compression behaviour characterization and discuss the related results.

In Task 2.1 of this project, composite material systems were down selected thorough a review of the open literature, considering the specific requirements for offshore renewable energy applications and the requirements specified in the DoA [1]. This included an in-situ polymerizable (room temperature infusible) thermoplastic from Arkema and a bio-epoxy from Sicomin with reinforcement consisting of carbon fibre from Mitsubishi and glass fibre from NEG. A test campaign was subsequently conducted, and selected material properties under quasi-static loading conditions were established. This forms a baseline, more specifically the quasi-static tensile behaviour characterization for the fatigue work conducted in Task 2.4. A range of glass fibre reinforced laminates with specific lay-ups as specified in the DoA were manufactured using the vacuum assisted liquid resin infusion process, which is representative of the procedure used for the manufacture of very large-scale components. In addition to the fibre reinforced polymer composites, adhesive bonded joints were also tested under fatigue loading. An overview of the test matrix for the fatigue characterization campaign during months 1 to 29 is shown below in Table 1.

Table 1 Test campaign matrix showing characterization tests performed in Task 2.4.

Test Method	Test Standard	Methodology	Material systems	Lay-up & Bonded joint details
Tension – Tension Fatigue	ISO 13003:2003 [2]	S-N Curve Fractography	Glass/Thermoset (GF/Infugreen)	$[90°]_{9S}$ $[\pm45°]_{2S}$ $[0°, +45°, 90°, -45°]_{2S}$ $[\pm30°]_{8S}$ $[0°]_{3S}$
	N/A	Critical Stress Limit (Thermography)	Glass/Thermoplastic (GF/Elium)	
	ISO 13003:2003 [2]	S-N Curve	Single lap -Bonded Joint Carbon/Thermoset (CF/Infugreen)	Araldite® 2015-1 (Marine Grade) Corso Reversible Adhesive

This project has received funding from the European Union's Horizon 2020 research and innovation programme under grant agreement No 952966.

The results from the fatigue test campaign indicate that both material systems (Glass fibre with thermoset and thermoplastic) exhibit typical behaviour in comparison to what is observed in literature. The S-N curves for unidirectional glass fibre composites (90°, 0°) and quasi-isotropic composites were linear when presented on a semi-log plot. However, composites with obliquely oriented fibres (±45° & ±30°) yielded a non-linear S-N curve on a semi-log plot.

In addition to producing S-N curves for the composite material systems, a temperature stabilization technique (Thermography) was used to rapidly determine the critical stress limit (Stress limit beyond which the damage accumulation during fatigue loading occurs at a higher rate leading to failure) of the composites. The technique yielded promising results and the results obtained were in close agreement with the results obtained from the classical S-N curve approach. In addition, failure analysis was performed by visual inspection followed by Scanning Electron Microscopy (SEM) to understand the failure mechanisms. It is to be noted that, the results pertaining to fatigue testing of glass fiber reinforced composites with fibre orientation of ±30° is a novel outcome of this task with limited results available in existing open literature. Additionally, thermography/temperature stabilization is a novel approach employed in this task to determine the critical stress level of composites. Table 2 below gives an overview of all the tests performed including the number of coupons tested.

Table 2 Total number of tests performed in each case in Task 2.4.

Test configuration	Static Tests	S-N Curve tests	Thermography tests
GF/Thermoplastic (Elium) [90°]	2	11 (1)	2
GF/Thermoset (Infugreen) [90°]	2	9 (2)	2
GF/Thermoplastic (Elium) [±45°]	1	8	3
GF/Thermoset (Infugreen) [±45°]	1	9	3
GF/Thermoplastic (Elium) Quasi-isotropic	2	8	2
GF/Thermoset (Infugreen) Quasi-isotropic	2	8	3
GF/Thermoplastic (Elium) [±30°]	2	10 (1)	3
GF/Thermoset (Infugreen) [±30°]	2	10 (1)	3
GF/Thermoplastic (Elium) [0°] [1]	2	11	2
GF/Thermoset (Infugreen) [0°] [1]	2	10 (4)	2
Bonded joint – Araldite 2015-1 adhesive	3	5	N/A
Bonded joint - Reversible adhesive	3 (1)	5 (2)	N/A
Bonded joint - Reversible adhesive (Aged)	0 (2)	-	N/A

Note: Number in brackets indicate invalid tests/Runouts.

This document also provides the details of the tests conducted under quasi-static compression loading. The deliverable D2.1 for the Task 2.1 was successfully completed and submitted as per the DoA, following the agreed timelines. Compression tests were performed in addition to tests performed in Task 2.1 for the purpose of training numerical models currently being developed by other partners of the FibreGY consortium. A summary of the total tests conducted under quasi-static compression loading is presented below in The results from the compression tests indicate that Elium based laminates possess higher

This project has received funding from the European Union's Horizon 2020 research and innovation programme under grant agreement No 952966.

strength characteristics compared to Infugreen based laminates. The fractography revealed typical plastic behaviour of Elium resin with traces of Elium visibly adhering to the fibre surface in the vicinity of the fracture zone. However, the post fracture fibre surface was found to be cleaner in the case of Infugreen based laminates, suggesting brittle behaviour. These observations were found to be consistent with the observations made in Task 2.1.

Table 3. The details about the manufacturing, testing and results pertaining to compression testing are discussed in Section 5 of this report. The results from the compression tests indicate that Elium based laminates possess higher strength characteristics compared to Infugreen based laminates. The fractography revealed typical plastic behaviour of Elium resin with traces of Elium visibly adhering to the fibre surface in the vicinity of the fracture zone. However, the post fracture fibre surface was found to be cleaner in the case of Infugreen based laminates, suggesting brittle behaviour. These observations were found to be consistent with the observations made in Task 2.1.

Table 3 Test campaign matrix showing properties established in compression testing.

Test Method	**Test Standard**	**Properties**	**Material systems**	**Lay-up configurations**
Quasi-Static Compression	ASTM D6641 [3]	Longitudinal Static Strength (σ_{11}) Transverse Static Strength (σ_{22}) Longitudinal Modulus (E_{11}) Transverse Modulus (E_{22})	Glass/Thermoplastic (GF/Elium)	$[0]_{2S}$
				$[90]_{2S}$
			Glass/Thermoset (GF/Infugreen)	$[0]_{2S}$
				$[90]_{2S}$
			Carbon/Thermoplastic (CF/Elium)	$[0]_{4S}$
				$[90]_{2S}$
			Carbon/Thermoset (CF/Infugreen)	$[0]_{4S}$
				$[90]_{4S}$

Overall, the objectives listed in the DoA for Task 2.4 were successfully achieved. In addition, thermography tests were effectively performed to compliment the results obtained from the classical S-N curve approach. Further, the compressive behaviour of laminates was characterized to supplement the work carried out in Task 2.1 in support of numerical model development.

This project has received funding from the European Union's Horizon 2020 research and innovation programme under grant agreement No 952966.

CONTENTS

This project has received funding from the European Union's Horizon 2020 research and innovation programme under grant agreement No 952966.

This project has received funding from the European Union's Horizon 2020 research and innovation programme under grant agreement No 952966.

LIST OF FIGURES

Chapter 2

Chapter 3

Chapter 4

This project has received funding from the European Union's Horizon 2020 research and innovation programme under grant agreement No 952966.

This project has received funding from the European Union's Horizon 2020 research and innovation programme under grant agreement No 952966.

Chapter 5

This project has received funding from the European Union's Horizon 2020 research and innovation programme under grant agreement No 952966.

LIST OF TABLES

Chapter 2

Chapter 4

Chapter 5

Chapter 6

Chapter 7

This project has received funding from the European Union's Horizon 2020 research and innovation programme under grant agreement No 952966.

LIST OF ABBREVIATIONS

Abbreviation	Expanded Form
ASTM	American Society for Testing and Materials
CAI	Compression after Impact
CF	Carbon Fibre
CFRP	Carbon Fibre Reinforced Polymer
CLC	Combined Loading Compression
CR	Corso Reversible
D	Damage Factor
DoA	Description of Action
E_i	Modulus (Dynamic Stiffness)
E_0	Initial Modulus (Static Stiffness)
FRP	Fibre Reinforced Polymer
GF	Glass Fibre
GFRP	Glass Fibre Reinforced Polymer
GSM	Grams Per Square Meter
IPA	Iso Propyl Alcohol
ISO	International Standard Organisation
MA	Marine Grade Adhesive
MD	Multi-Directional
NEG	Nippon Electric Gas Company Limited
OWTP	Offshore Wind and Tidal Power
QI	Quasi Isotropic
R	Stress Ratio
S-N	Stress - Number of Cycles
SEM	Scanning Electron Microscopy
TP	Thermoplastic
TS	Thermoset
UD	Unidirectional
ULIM	University of Limerick
UTS	Ultimate Tensile Strength
V_f	Fiber volume fraction

This project has received funding from the European Union's Horizon 2020 research and innovation programme under grant agreement No 952966.

1. INTRODUCTION

Climate change goals have persuaded industries in all sectors to initiate environment centric actions to reduce the carbon footprint of their respective activities. The energy sector in particular is taking strides in this regard by promoting the development of renewable technology like offshore wind and tidal energy. Offshore wind and tidal energy has the potential to contribute significant supply of renewable and clean energy in the near future. Offshore wind energy is the most mature technology in terms of development, policies, and present and potential installed capacity [4]. While offshore renewable energy has great growth potential, it is not devoid of challenges. The harsh and corrosive marine environment poses a challenge in terms of efficiency, maintenance, and durability of the steel structures, which consequently increase the installation and maintenance costs. The majority of construction material is steel, and all of this is subjected to degradation by corrosion, which accounts for 60% of maintenance costs. As a result of this, the life of these installations is curtailed despite preventive maintenance thus making offshore renewable energy an unfavourable investment [4].

Composites, especially glass fibre reinforced polymer (GFRP) composites can be a suitable alternative to steel, owing to their low cost compared to other polymer composites, high stiffness-to-weight ratio, high strength to weight ratio and most importantly, corrosion resistance. However, despite such advantages, the industry refrains from the large-scale implementation of composite offshore energy structures due to the lack of understanding about the behaviour of such materials under a variety of loading conditions. With the aim of filling these research gaps the FIBREGY Horizon 2020 EU funded project was initiated to enable the extensive use of FRP materials in the next generation of Offshore Wind and Tidal Power (OWTP) structures. As a part of this project, innovative FRP materials, design procedures, guidelines, inspection, and monitoring methodologies will be audited and qualified for offshore applications with the final objective being to realise scaled ($1/6^{th}$) demonstrators including composite tower for off-shore wind turbine and composite tidal turbine housing.

The rotor blades of a wind turbine will undergo approximately 100 million rotations in its 20-year lifetime. During this service time, the structure is exposed to harsh environmental conditions like extreme temperatures, wind gusts, humidity, rain, hail impact, snow, ice, solar radiation, lightning, and salinity [5]. Given that these structures must endure 20+ years of efficient operation withstanding these harsh conditions, adequate knowledge in terms of the fatigue behaviour of the materials used is required for the purpose of design and certification, which forms the focus of the present research.

During the nascent stages of wind turbine development using glass fibre reinforced composites, the design data was simply borrowed from research conducted in the aerospace sector owing to similarities in several aspects of rotor blades and sailplane/glider wings [5]. However, wind turbine blades are expected to endure at least 10^8 cycles which is beyond the range of average aerospace structures. Also, the aerospace industry predominantly focuses on to carbon fibre-based composites whereas glass-fibre dominated in the wind energy structures due to its low-cost. Hence, much of the research on aerospace structures is rendered inadequate for renewable energy structural applications [6]. According to Sørensen *et. al*, composites used in wind energy applications have a service life of over 20 years, which amounts to approximately 150 million cycles. Hence, use of the traditional S-N curve approach is not attractive for such a high number of cycles.

This project has received funding from the European Union's Horizon 2020 research and innovation programme under grant agreement No 952966.

Conducting cyclic tests to establish lifetimes of such high number of cycles is a long and expensive task. As an alternative, it is more efficient to focus on the behaviour of material at high cycles and investigate whether there exists a critical load (Critical stress) below which the material may sustain high number of cycles [7]. Therefore, in this project a relatively novel approach is adopted to investigate the high cycle behaviour of Glass FRP composites along with classical S-N curve approach.

In this study, the response of glass fibre/bio-based InfuGreen 810 GFRP (GF/Infugreen) composite and glass fibre/in-situ infusible and polymerizable thermoplastic Elium (GF/Elium) to fatigue loading is investigated. GFRP composite test coupons with various lay-ups including [90°], [±45°], [±30°], quasi-isotropic and [0°] are subjected to tension-tension fatigue tests instrumented with extensometer and infrared thermal camera. The damage induced by fatigue loading is quantified in terms of heat dissipation (specimen temperature from IR camera). The fatigue loading induced damage is quantified from the heat (rise in test coupon temperature) and is used to estimate the critical stress limit using a fast and innovative temperature stabilisation method. It is important to mention that; the temperature rise due to heat dissipation has been used by several researchers for quicker estimation of the endurance limit by temperature stabilization method without the use of the time-consuming Whöler or S-N curves approach. Initially, this temperature stabilization method was used for metallic materials [8,9]. However some studies have successfully adopted this method for composite materials and produced effective results [10,11]. The S-N curve for the new GFRP material is obtained by performing classical tests and is used to confirm the critical stress limit values obtained by the new method.

In this Task 2.4, an extensive experimental campaign is conducted to characterize the fatigue performance of two material systems targeted by the project i.e., thermoplastic, and thermoset glass fibre reinforced composites. In addition, the fatigue performance of a connection typology relevant to FIBREGY demonstrators i.e., adhesively bonded joints including a traditional structural adhesive and a novel reversible epoxy formulation was also evaluated. Additionally, the experimental data from the fatigue experiments will be used in Task 3.4 to fine tune the numerical tool used for the prediction of the fatigue performance of composites. This deliverable has five main sections viz. introduction, materials and manufacturing, test methodology, results, and conclusion. As already seen, this section presents a very brief survey of fatigue performance of fibre reinforced polymer composites from available research literature. This is followed by materials and manufacturing section which describes all the materials used and manufacturing /processing techniques used. The third section, test methods describe the fatigue testing methodology including S-N curve approach and thermography/temperature stabilisation approach. This section also describes fractography investigation done using scanning electron microscope. In the fourth section, the fatigue characterization of the down selected materials in various lay-up configurations is presented which is an outcome of an extensive experimental test campaign performed at ULIM. The fifth section describes additional quasi-static compression test performed at ULIM to facilitate training of numerical models being developed by Fibregy partners. In this section the materials tested, compression test methods and results relating to compression testing are presented.

This project has received funding from the European Union's Horizon 2020 research and innovation programme under grant agreement No 952966.

The main objectives addressed in this document can be summarised as follows:

- To describe the methodology employed for an extensive experimental testing campaign conducted to evaluate the fatigue behaviour of the selected FRP composites.
- To analyse and present the data obtained from the fatigue experiments and failure analysis to understand the fatigue behaviour of selected thermoplastic and thermoset composites.
- To describe the methodology of compression behaviour characterization and discuss the related results.

In terms of responsibilities, ULIM has the overall responsibility for the delivery of Task 2.4. The task involves fatigue characterization of 5 configurations of FRP composites and 3 different configurations of bonded joints as presented in Table 1. 1. All the composite laminates required for the testing are manufactured at ULIM and the bonded joint coupons were manufactured and supplied by project partner INEGI.

Table 1. 1 Summary of the fatigue experimental campaign of FIBREGY.

Material system	**Configurations**
Glass Fibre – Thermoset (Infugreen)	0°, ±30°, ±45°, 90°, Quasi-isotropic
Glass fibre – Thermoplastic (Elium)	0°, ±30°, ±45°, 90°, Quasi-isotropic
Bonded joints	Marine grade structural adhesive, Corso's reversible adhesive, Corso's reversible adhesive - Aged

Overall, the critical task of fatigue characterization of the materials down selected in Task 2.1 is performed in Task 2.4 and this document presents the test procedures and results from the tests campaign on mechanical characterization of the down selected materials.

This project has received funding from the European Union's Horizon 2020 research and innovation programme under grant agreement No 952966.

2. MATERIALS AND MANUFACTURING

Regarding the laminates manufactured by vacuum assisted liquid resin infusion, a state-of-the-art thermosetting bio-epoxy and an infusible thermoplastic were studied during the test campaign consistent with the materials down selected in Task 2.1. The resin systems, ratios of curing agent, curing and post-curing conditions for each system are shown in Table 2. 1.

Table 2. 1 Resin systems for manufacturing processes and properties according to manufacturer datasheets [12–14]

	Thermoplastic Acrylic based	**Thermosetting Bioepoxy**
	Arkema	Sicomin
Name	Elium 188XO	SR Infugreen 810
Curing Agent	Perkadox GB-50X	SD8824
Mix Ratio by Wt (Resin : Curing Agent)	100 : 3	100 : 22
Viscosity	100 mPa.s @25°C	120-320 mPa.s @25°C
Curing time at ambient	24 hr	16 hr
Post-cure temperature	60 °C	60 °C
Post-cure time	24 h	16 h
Storage Life	6 months	24 months
Tensile Strength	56 MPa	65 MPa
Tensile Modulus	2.6 GPa	2.8 GPa

The reinforcement fabric studied are unidirectional and quasi-unidirectional non-crimp fabrics, composed predominantly with glass fibres as listed below:

- Saertex UD 1182 g/m^2 E-Glass fibre based on non-crimp Hybon 2026 1200 fibre (Quasi-UD)
- Gerster UD 320 g/m^2 E-Glass fibre based on non-crimp Hybon 2026 1200 fibre (UD)

Specific details of the fabric construction/architecture are provided in Table 2. 2. The Saertex glass-based fabric has over 95% of the glass fibres in the 0° warp direction and 3% of the glass fibre tows in the 90° weft direction.

Table 2. 2 Non-crimp reinforcement fabrics and fibres studied in the test campaign.

	Construction	**Sub layer**	**Fibre**	**Areal Weight (gsm)**	**Total Areal weight (gsm)**
Saertex Glass fibre-based fabric	90°	1	NEG Hybon 2026	36 (3%)	1182
	0°	2	NEG Hybon 2026	1134 (95%)	
			Synthetic stitching	12 (2%)	
Gerster Glass fibre-based fabric	0°	1	NEG Hybon 2026	320 (100%)	≈ 320
			Synthetic stitching	Not Available	

This project has received funding from the European Union's Horizon 2020 research and innovation programme under grant agreement No 952966.

A list of all the layups prepared for vacuum assisted liquid resin infusion specifying the fabric and resin employed is presented in Table 2. 3. All laminates were manufactured by placing the dry reinforcement fabric, peel ply and flow medium on a glass tool. Figure 2. 1 depicts the images of fabric cutting being done by automated fabric cutter and the laying up of cut fabric plies over the glass surface. The lay-up was then enclosed using a vacuum bag secured to a glass tool using sealant tape. The pictures of different laminates being infused are depicted in Figure 2. 2. This approach is commonly referred to as vacuum assisted liquid resin infusion and is typically used for the manufacturing large structures including wind turbine blades. All resin systems were infused without prior degassing at ambient temperature (approximately 20 °C). A vacuum pump was used to obtain a pressure in the range 10–20 mbar (absolute) inside the vacuum bag. Monomer boiling was not observed. The outlet was closed on observing bubble-free resin in the outlet tube. Laminates were allowed to cure at ambient temperature in accordance with the parameters specified in the Table 2. 1. Test samples were then extracted by water jet cutting. Post curing was performed on the test samples post extraction again in accordance with the parameters specified in Table 2. 1. The quality of the laminates was verified by determining the fibre volume fraction (V_f). This was achieved by performing burn-off test, where samples extracted from three different locations are extracted from a laminate. The volume and density of the samples are determined using pycnometer. Then the samples are placed in a crucible and heated to 540 °C in an oven until all the matrix material is burnt off leaving behind clean fibres. Then the clean fibres are weighed, and the fibre volume fraction is determined.

However, the fibre volume fraction (V_f) for the 0° laminates was determined using thickness measurement in accordance with ISO 14127 [2]. The thickness of the laminate is measured at various locations and the areal weight (320 gsm) of the fabric and fibre density is obtained from the manufacturer's datasheet. Finally, Equation 1is used to calculate the fibre volume fraction.

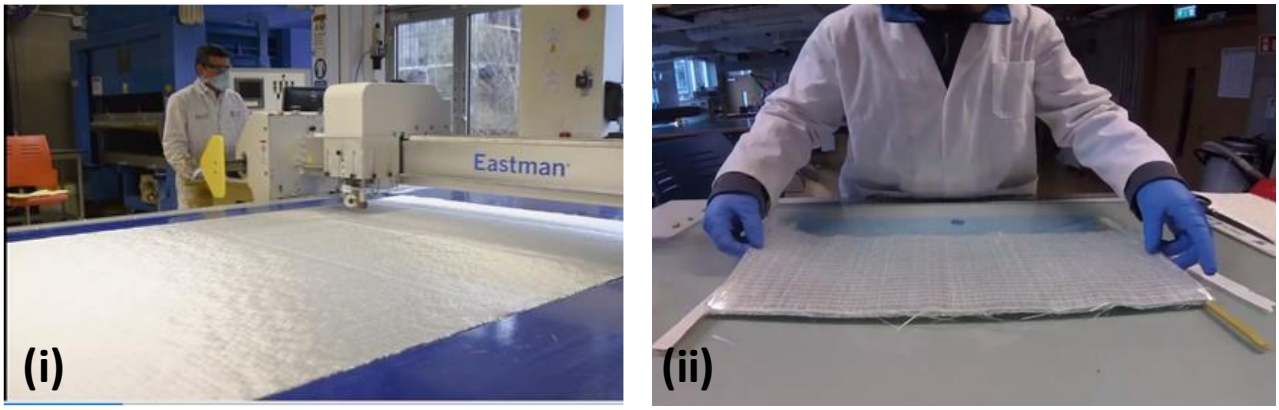

Figure 2. 1 Pictures depicting (i) Fibre Cutting (ii) Lay-up of non-crimp fabric reinforcement.

$$v_f = \frac{Number\ of\ plies\ \times mass\ per\ unit\ area\ of\ fabric\ (\frac{g}{m^2})}{thickness\ (mm) \times fibre\ density\ (\frac{g}{cm^3})}$$

Equation 1

This project has received funding from the European Union's Horizon 2020 research and innovation programme under grant agreement No 952966.

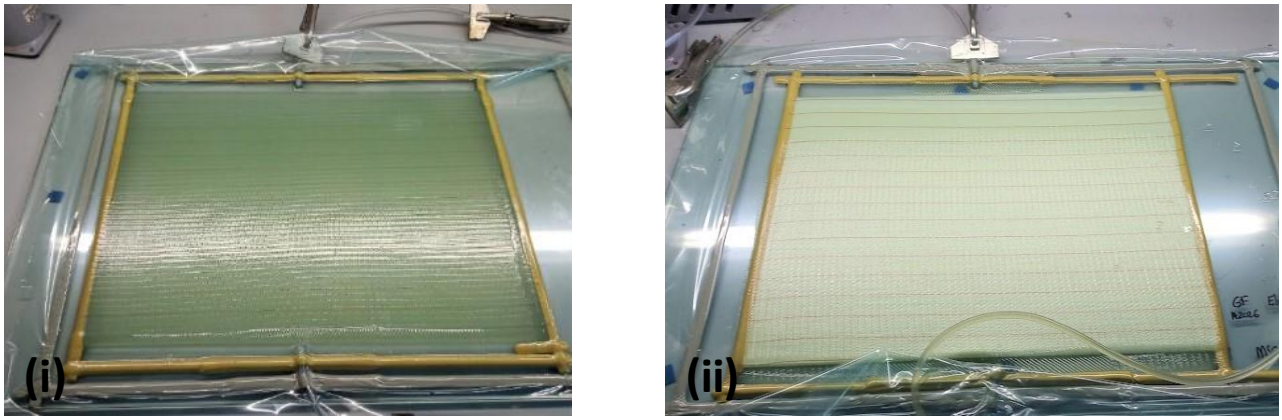

Figure 2. 2 Vacuum assisted liquid resin infusion of laminates 600 x 400 mm (i) GF Hybon 2026/Elium 188 XO (ii) GF Hybon 2026/Infugreen 810.

Table 2. 3 Lay-up, laminate constituents, and fibre volume fraction of composites manufactured using vacuum assisted liquid resin infusion.

	Lay-up	**Reinforcement**	**Resin**	**Initiator**	**Fibre Volume fraction (V_f)**
GF/Elium	$[90]_{9S}$	Glass - Gerster UD	Elium 188 XO	Perkadox GB-50X	55.85 %
	$[\pm45]_{2S}$	Glass - Saertex Quasi-UD	Elium 188 XO		60.91 %
	Quasi-Isotropic $[0°, +45°, 90°, -45°]_S$	Glass - Gerster UD	Elium 188 XO		47.11 %
	$[\pm30°]_{8S}$	Glass - Gerster UD	Elium 188 XO		52.36 %
	$[0]_{6S}$	Glass - Gerster UD	Elium 188 XO		46.06 % *
GF/Infugreen	$[90]_{9S}$	Glass - Gerster UD	SR Infugreen 810	SD 8824	52.47 %
	$[\pm45]_{2S}$	Glass - Saertex Quasi-UD	SR Infugreen 810		57.99 %
	Quasi-Isotropic $[0°, +45°, 90°, -45°]_S$	Glass - Gerster UD	SR Infugreen 810		55.60 %
	$[\pm30°]_{8S}$	Glass - Gerster UD	SR Infugreen 810		49.69 %
	$[0]_{6S}$	Glass - Gerster UD	SR Infugreen 810		44.34 % *

Note: * Denotes Fiber volume fraction was obtained by volume measurement whereas rest of the values were obtained from burn-off test.

This project has received funding from the European Union's Horizon 2020 research and innovation programme under grant agreement No 952966.

3. TEST METHODS

In this section, the test methods associated with each test are described along with the data processing employed to generate the various material properties. The recommendations of ISO 13003:2003 [2] were followed for conducting the fatigue tests and as suggested in the standard the test coupon geometry was based on ISO 527-4:2009 [15]. Figure 3. 1 shows the schematic of the test coupon geometry used for fatigue tests having a width of 25 mm. Two kinds of fatigue testing approach were adopted viz:

- Classic tests: S-N Curve
- Stepwise tests: Thermography

3.1. S-N Curve tests

The loading parameters for the tension-tension fatigue tests ware based on the ultimate static tensile strength of the composite material. Quasi-static tensile tests were carried out to obtain the ultimate tensile strength. The mechanical tests (static tensile and fatigue loading tests) were performed on a Zwick Roell servo-hydraulic load frame instrumented with 100 kN load cell and an extensometer, in which specimens were held in the test frame using hydraulic grips. The loading rate was 1 mm/min. The average tensile strength (F_{uts}= Load at σ_{uts} (UTS = Ultimate tensile strength) values obtained from three tests was considered for the design of the tension-tension fatigue tests. The tension-tension fatigue tests were conducted on the same machine used for the static tests instrumented with 100 kN load cell. In addition, instrumentation including, extensometer and infrared thermal camera were used as shown in Figure 3. 2. The S-N curve was obtained by conducting constant amplitude tension-tension fatigue tests at different maximum cyclic stress levels below σ_{uts} (until failure) where the stress ratio, R was 0.1 and frequency of loading was 8 Hz for 90° coupons and 5 Hz for ±45°, ±30°, 0° and quasi-isotropic specimens.

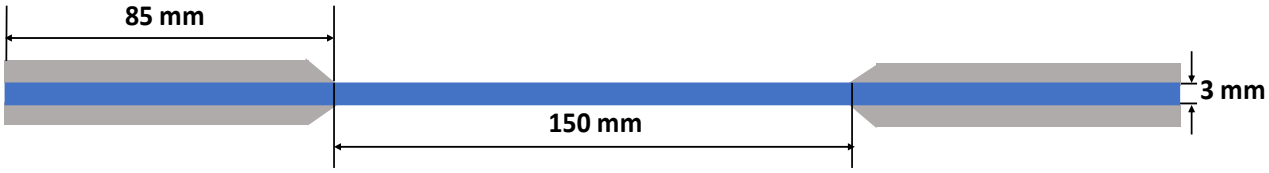

Figure 3. 1 Geometry of the fatigue test coupons according to the ISO:13003:2003 standard with a width of 25 mm.

3.2. Temperature stabilisation test

Some metals and alloys like steel can undergo infinite number of fatigue loading cycles below a certain stress limit. This stress level below which the material can sustain sufficiently high number of loading cycles (>10 million) is called fatigue limit or endurance limit. The fatigue limit of a material is generally obtained by Whöler curves (stress vs. cycles). These fatigue tests are long and tedious, requiring many specimens and time to obtain a fatigue limit. However, the fatigue limit can also be obtained from the temperature stabilization method by interpolation of two intersecting straight lines of different slopes that fits the stabilization temperature when plotted against the corresponding stress level [8–11]. This method is based on the fact that part of the energy required to start the damage propagation is irreversibly transformed into heat and hence, any deformation and damage in the specimen is followed by an increase in temperature.

This project has received funding from the European Union's Horizon 2020 research and innovation programme under grant agreement No 952966.

However, all materials do not exhibit a clear fatigue limit, meaning, the materials will evntually fail at a relatively low number of loading cycles, irespective of the stress level it is loaded at. Fiber reinforced composites belong to this category and do not exhibit fatigue limit. However, the temperature stabilisation method can be used to estimate crtical stress level, below which the damage accumulation during fatigue loading occurs at a lower rate compare to damage accumulation above this stress level.

To obtain the critical stress limit by this method, load controlled tension-tension step-wise fatigues tests were performed using the setup as shown in Figure 3. 2. The test coupons were subjected to 7000/8000 tension-tension sinusoidal load cycles (Stress Ratio, R ratio of 0.1) at a frequency of 5/8 Hz at room temperature (≈ 20° C). The increment between each stress step was approximately 5-7 % of F_{uts} for each block. Each load block was separated with a dwell time of 10 minutes to allow the specimens return to room temperature. The tension-tension fatigue test loading protocol is shown in Figure 3. 3. Up to three such tests were conducted for each configuration and material system combination to evaluate the repeatability. An infrared thermal camera Micro Epsilon TIM VGA thermal IMAGER with 33° lens was used to record the temperature of the specimen surface during loading. The thermal data was analysed to estimate the critical stress limit of the specimens using the temperature stabilization method [8–11].

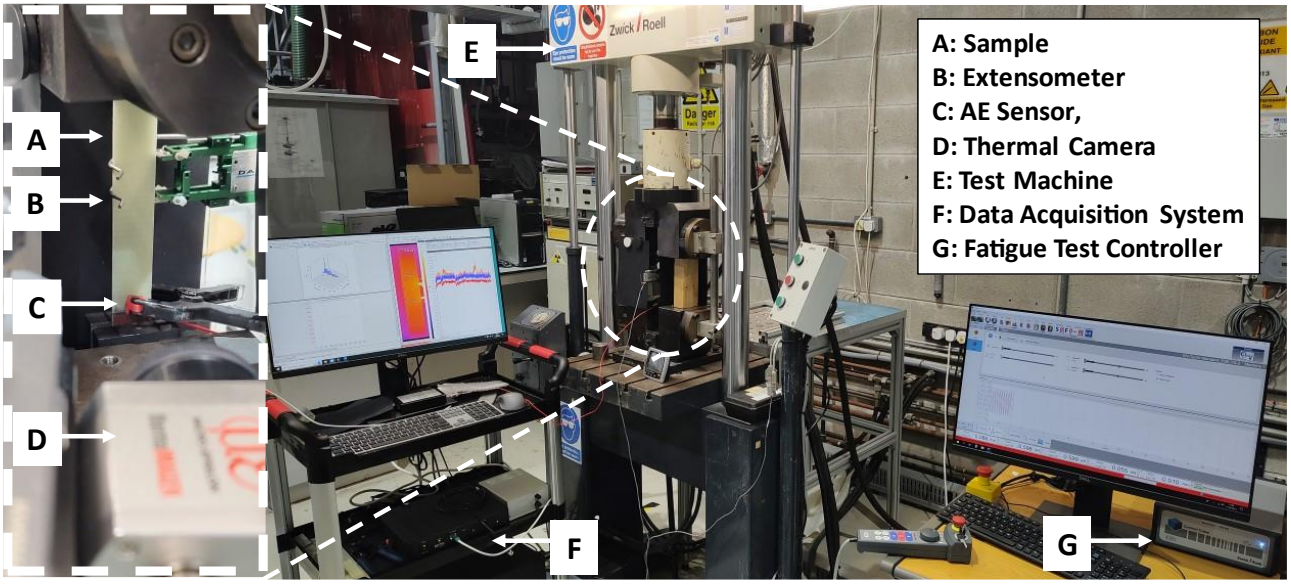

Figure 3. 2 Setup showing instrumentation used for tension-tension fatigue tests.

This project has received funding from the European Union's Horizon 2020 research and innovation programme under grant agreement No 952966.

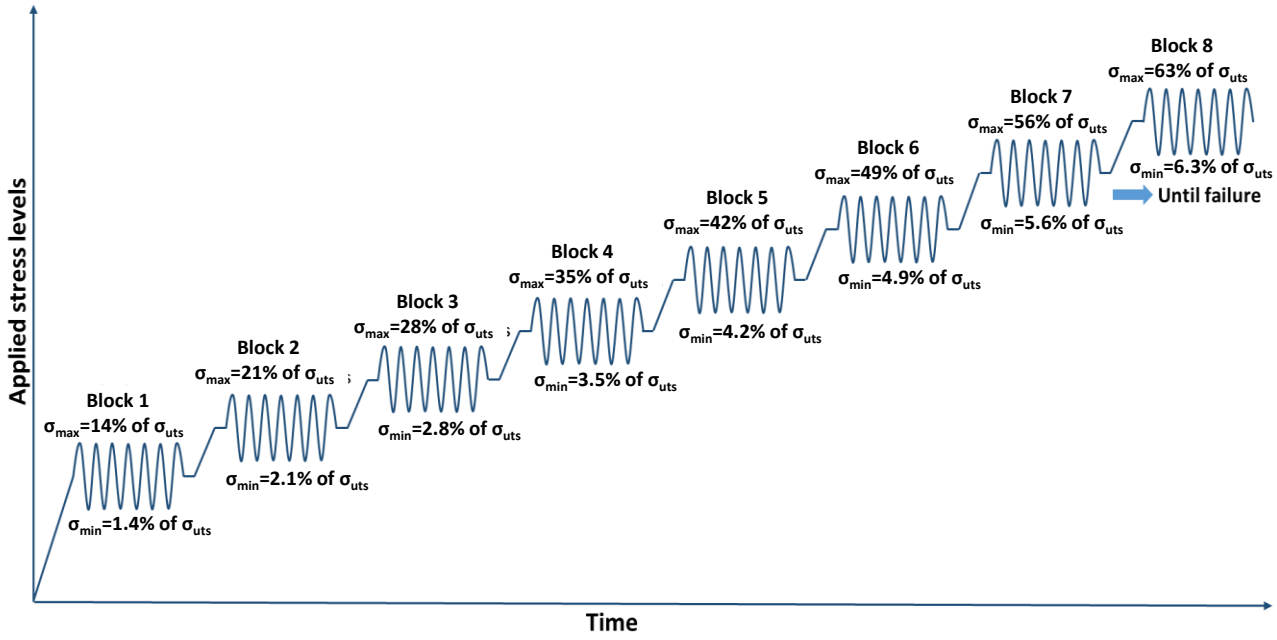

Figure 3. 3 Tension-tension fatigue test loading protocol with R = 0.1 and Frequency = 5 Hz / 8 Hz. Tests were conducted at room temperature for the step wise tests to find the critical stress limit.

3.3. Failure Analysis using Scanning Electron Microscopy (SEM)

With the objective of studying the fracture features of fatigue tested specimens and identifying the underlying failure mechanisms, fractography analysis was performed using Scanning Electron Microscopy (SEM) technique. For this purpose, select test specimens drawn from the laminates of different configurations tested were chosen. For each laminate configuration considered, a specimen each from the low cycle and high cycle regimes were identified to study the fracture features using SEM. A Hitachi SU-70 high-resolution SEM was used for the analysis. Prior to specimen examination, the specimens are required to be prepared. Figure 3. 4 illustrates the different stages of sample preparation before their examination. The region of interest in the tested specimen such as the fracture surface is extracted carefully by machining the required region using a high-speed precision cutter. The orientation of the fracture plane varies based on the laminate configuration. In some cases, the region of interest can be a section further away from the fracture plane. Even in this case, the region of interest is carefully extracted using a precision cutter. If the fracture surface is to be observed using SEM (sample 1 in Figure 3. 4) , then the sample is mounted onto a sample holder and is then subjected to gold sputtering to improve the electrical conductivity of the sample. This case is specifically for ±45°, ±30°, 90° and Quasi-Isotropic configuration where the fracture surfaces are directly exposed. The direction of viewing is depicted in Figure 3. 5 (a). In the case of sample 2, it is carefully placed in a plastic mould (coated with a release agent) such that the surface of interest is facing downwards in the mould. A two-part epoxy system (Epoxicure resin-hardener; resin: hardener ratio 100:23 by weight), to which conductive filler is added (125 grams of filler for every 100 grams of resin system) is then poured into the mould and cured at ambient temperature. After curing, the sample (sample 2) is released from the mould. This step is referred to as Sample casting in Figure 3. 4. The sample surface of interest (in sample 2) is then subjected to a step-wise grinding process followed by polishing. The polished sample is thoroughly

This project has received funding from the European Union's Horizon 2020 research and innovation programme under grant agreement No 952966.

cleaned initially using water and then using Iso Propyl Alcohol (IPA) to remove the abrasive particles adhering to the polished surface. These steps are illustrated in Figure 3. 4 for reference. The sample thus obtained is heated in a hot air oven at ≈ 50° C for two hours to remove moisture. The sample is then sputter coated. Sputter coating is employed for all the sample types required to be examined using SEM. The sample surfaces to be examined are sputter coated with gold for 90 seconds using an Emitech K550 sputter coater. The samples prepared are mounted onto suitable specimen holders and then examined using SEM. Typical viewing directions for SEM analysis are depicted in Figure 3. 5. For some configurations, pristine untested coupons were also subjected to SEM analysis to understand the fibre architecture and resin distribution.

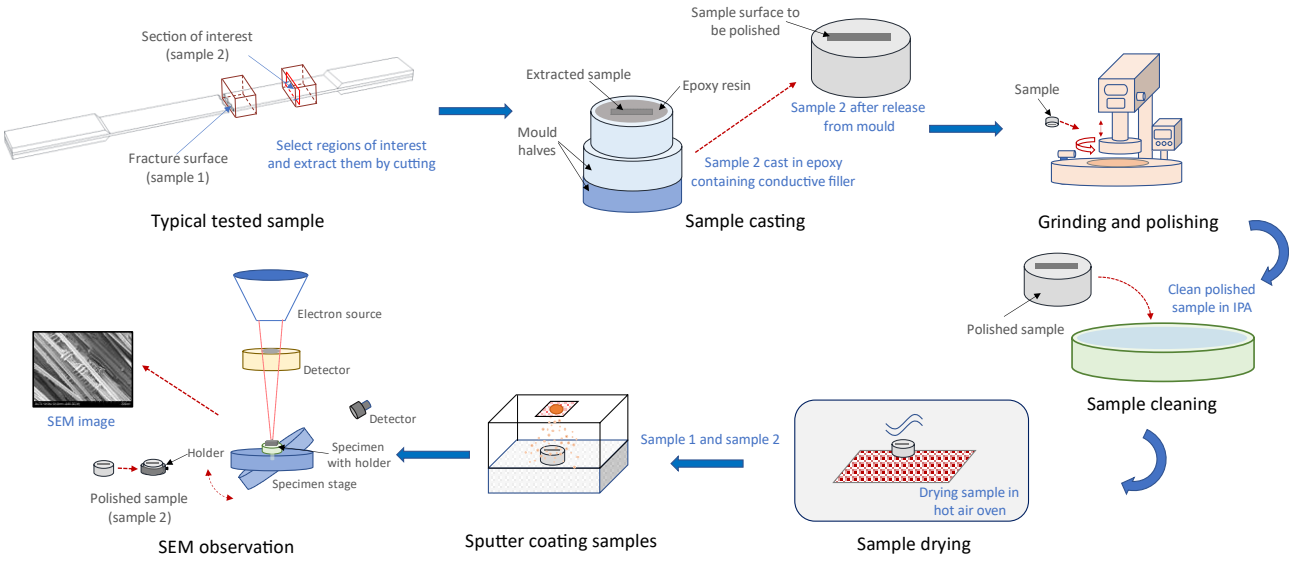

Figure 3. 4 Schematic showing various stages of sample preparation for SEM observation.

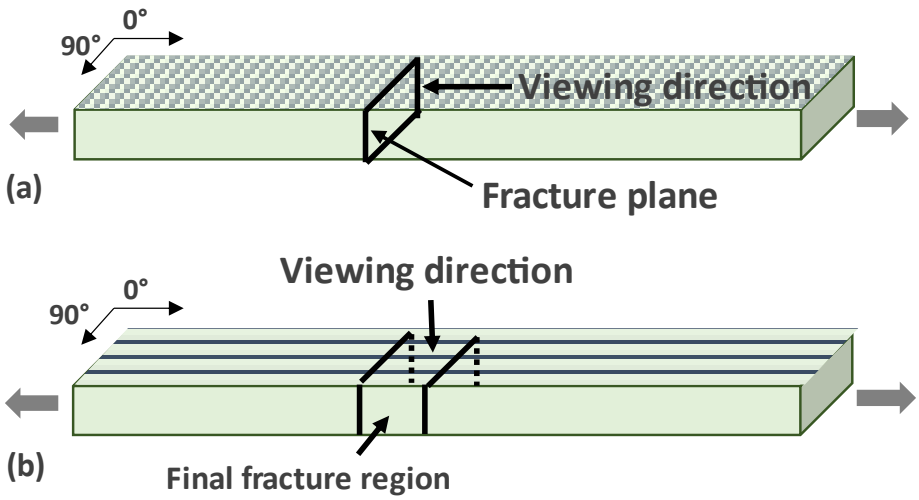

Figure 3. 5 Schematic showing the regions subjected to SEM analysis in (a) failed 90˚ test coupons and (b) failed ±45˚ and quasi-isotropic coupons.

This project has received funding from the European Union's Horizon 2020 research and innovation programme under grant agreement No 952966.

3.4. Adhesive bonded joints (Manufactured at INEGI, Porto)

The procedure for preparing the bonding specimens is presented in this section. The substrates , i.e., carbon fiber reinforced polymer (CFRP) composite coupons were cut from vacuum-infused CFRP laminates. The CFRP laminates were manufactured at INEGI's facility in Porto and shipped for testing to the University of Limerick.

The substrate laminate was made of CFRP multidirectional fabrics (ZOLTEK PX35 50K +/-45° and 0/90°, both with 600 gr/m^2) and SR InfuGreen 810 resin with the SD 4771 hardener. The stacking sequence of the laminate was $[0°, 90°, +45°, -45°]_{2S}$. After curing, coupons of size 36 mm x 160 mm were cut from the laminate using abrasive diamond cutting. The overlap area for the lap joint was 36 mm x 36 mm. The final coupon geometry is illustrated in Figure 3. 6. The bonded test coupons were prepared according to the geometry recommended in ASTM D5961. Steel end tabs (100 mm in length and about the same thickness as the CFRP coupons) were bonded to reduce the eccentricity of the load path which causes out-of-plane bending moments and consequently high peel stresses and non-uniform shear stresses in the adhesive layer. Two holes were made in the gripping region (refer Figure 3. 6) to facilitate coupon holding during the ageing process.

The adhesives selected for fatigue testing was Araldite® 2015-1 and a reversible adhesive developed by Corso Magenta. The Araldite 2015-1 is a two-component paste structural adhesive, thixotropic and non-sagging up to 10 mm thickness which can be cured at room temperature. It has a good resistance to weathering, which is why it is commonly used in marine construction (such as in hull-to-deck bonding in ship building). The reversible adhesive from Corso is a 3-component epoxy. No further details of its composition are available at this moment due to intellectual property restrictions. These adhesives were used for preparing and testing bonded joints under quasi-static loading in Task 2.3. The lap shear strength of Araldite® 2015-1 and reversible adhesively bonded joint was approximately 13 MPa and 3 MPa under quasi-static loading as reported in Task 2.3. However, it was also observed by INEGI that most reversible adhesive specimens failed at lower values, possibly due to the difficult preparation of the bonded joint.

This project has received funding from the European Union's Horizon 2020 research and innovation programme under grant agreement No 952966.

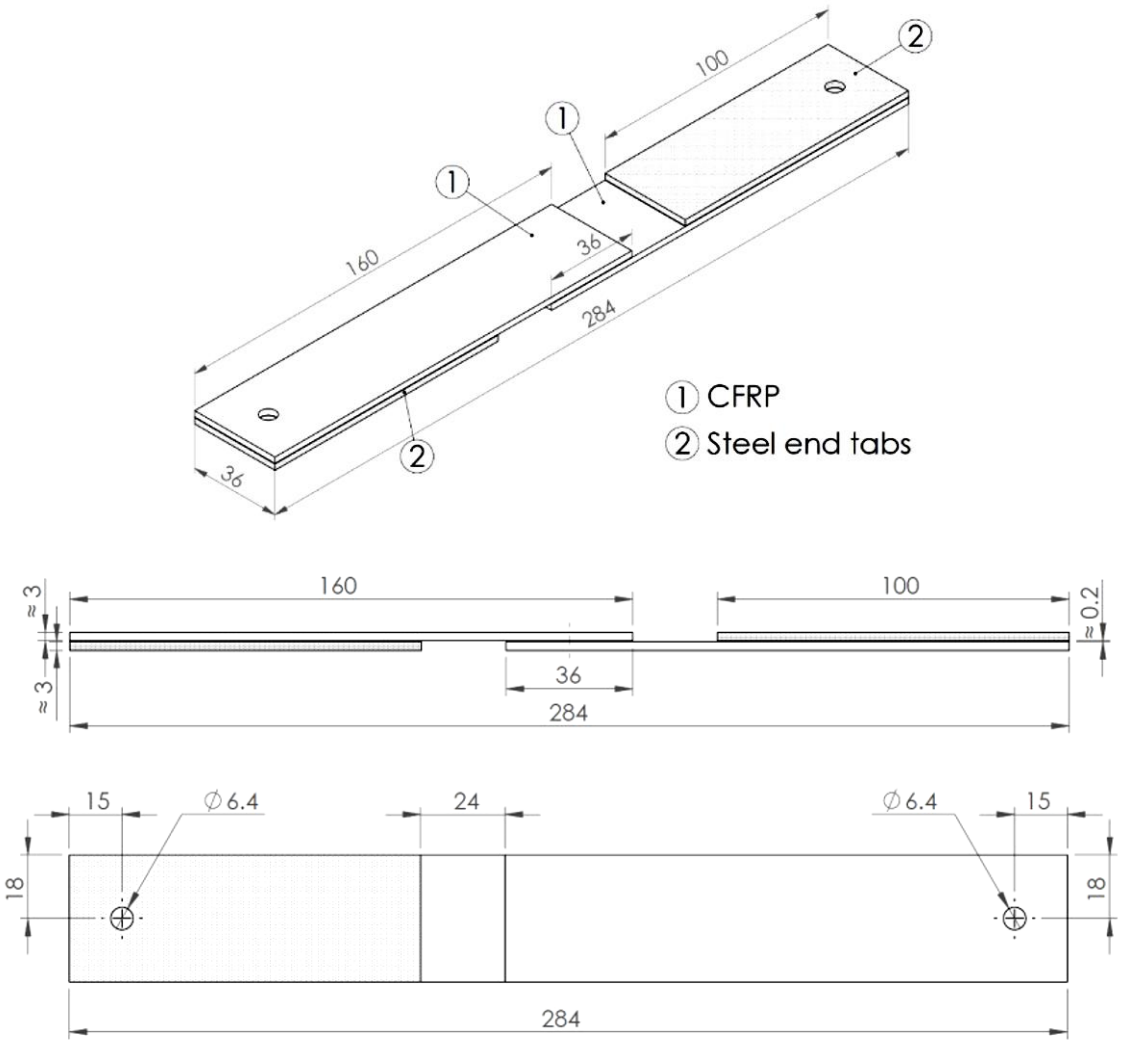

Figure 3. 6 Coupon geometry according to ASTM D5961 showing CFRP substrate, single lap joint and steel spacers (Dimensions in mm).

The peel ply on the surface of the CFRP laminate was left intact after manufacturing and cutting the coupons for preparing bonded joints. The peel ply was removed just before the application of the adhesive. This way, the surface obtained was fresh, contaminant free and rough for obtaining satisfactory bond quality. The two component Araldite 2015-1 adhesive was applied directly on to the surface using an adhesive dispensing gun with a suitable mixing nozzle which ensured that the recommended mixing ratio was obtained. However, preparing the bonded joints with the 3 component reversible adhesive was challenging. The mass ratio for mixing the components was A:B = 6:20 and C = 20% wt * (A+B). Component A had to be mixed with other components at 50° C. A slight fall in temperature led to hardening of the adhesive which made its application to the surface difficult. The container with the mixed paste (A+B+C) was maintained at 50° C on a hot plate until the adhesive was applied to all specimens. However, this process was still very challenging due to the difficulty in applying the adhesive after cooling and being nearly impossible to do repeatable adhesive applications. Airtech *Flashbreaker*® blue adhesive tape was used to limit the bonding. After application of adhesive, the two substrate surface were held in pressure using a jig set up as shown in Figure 3. 7. This setup was made using 3 mm steel plates and shim tapes, assuring that the gap between the bottom and upper adherends is constant at 0.2 mm. The alignment of the adherends was assured

This project has received funding from the European Union's Horizon 2020 research and innovation programme under grant agreement No 952966.

visually and by using blue adhesive tape (Airtech *Flashbreaker*®) to fix them, as illustrated in Figure 3. 8. The specimens were cured at 40° C for 24 hours inside Venticell 404 laboratory oven and left to cool down naturally to ambient temperature.

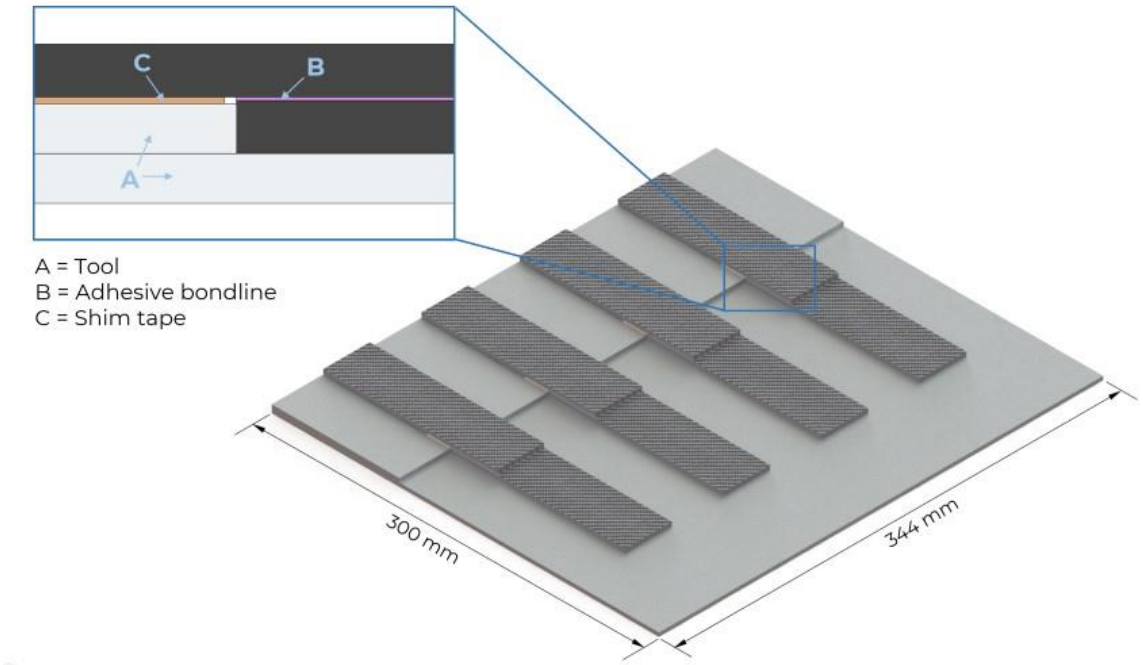

Figure 3. 7 Jig setup used for preparing bonded joints.

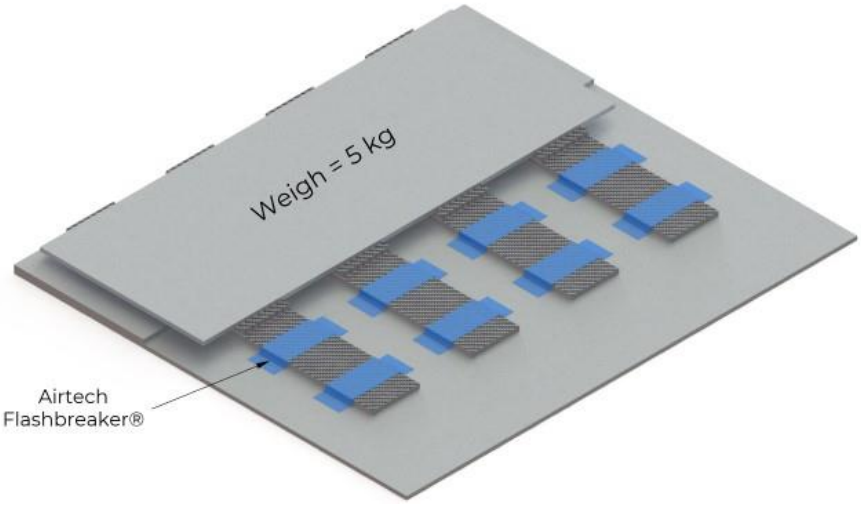

Figure 3. 8 Jig setup during curing in oven.

This project has received funding from the European Union's Horizon 2020 research and innovation programme under grant agreement No 952966.

4. FATIGUE CHARACTERIZATION RESULTS

4.1. Unidirectional 90° (Relative to loading direction)

The tension-tension fatigue tests to establish the S-N curve for the glass fibre composites with fibres oriented transverse to the loading direction (90˚) were conducted at a frequency of 8 Hz with an R ratio of 0.1. Static tensile tests were performed beforehand to obtain the tensile failure strength/ultimate tensile strength (σ_{uts}). It was found that the ultimate tensile strength of $[90^{\circ}]_{9s}$ GF/Elium and GF/ Infugreen composites was 38.79 MPa and 49.92 MPa respectively. The stress levels for tension-tension fatigue tests were decided based on these values.

4.1.1. S-N Curve

Figure 4. 1 presents the S-N curves for $[90^{\circ}]_{9s}$ GF/Elium and GF/ Infugreen composites. The maximum cycle stress and cycles to failure (S-N) data obtained was plotted on a semi-log plot. Regression analysis was done by fitting a curve following logarithmic equation. Table 4. 1 summarises the obtained regression equations and R^2 values. It was seen that the data fitted well with the logarithmic equation, which is evident from the variance (R^2) value. This is in accordance with the findings of Mandell *et al*. They observed that the composites made of unidirectional fibres where all plies are aligned at some orientation to the loading direction, tend to follow a logarithmic trend which in a semi-log plot yields a linear S-N curve [6]. Additionally, it is seen that the S-N curve of GF/Elium has a steeper slope than that of the GF/Infugreen. This may indicate that the GF/Infugreen composite exhibits a better high-cycle fatigue performance.

Table 4. 1 Regression analysis of S-N data for 90˚ GF/Infugreen and GF/Elium composites.

Laminate configuration	**GF/Infugreen**	**GF/Elium**
	Logarithmic	**Logarithmic**
[90°]	y = -2.11 ln(x) + 53.77 R^2 = 0.9508	y = -2.26 ln(x) + 48.09 R^2 = 0.9352

This project has received funding from the European Union's Horizon 2020 research and innovation programme under grant agreement No 952966.

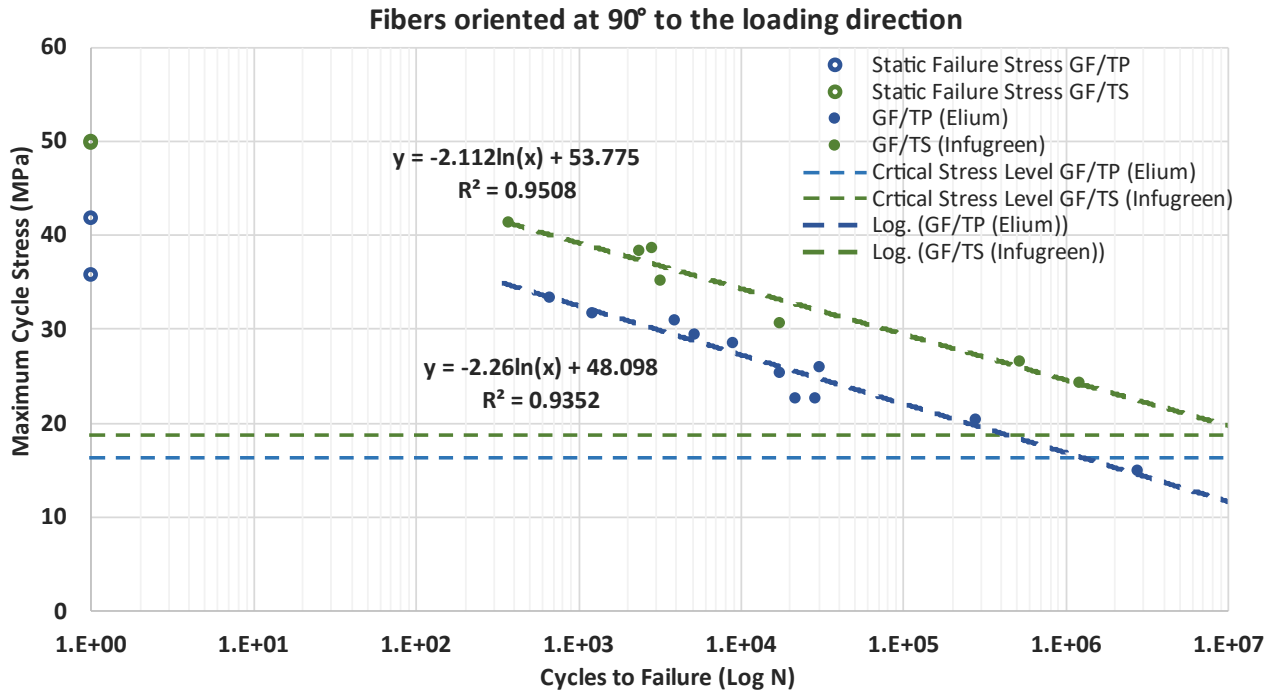

Figure 4. 1 S-N Curve for GF/Infugreen and GF/Elium with fibres oriented transverse to the loading direction including critical stress limit obtained from thermography test.

4.1.2. Thermography

Temperature stabilisation fatigue tests were performed to obtain the critical stress limit of the composites in a time efficient approach. To achieve this, step-wise constant load amplitude fatigue tests were performed according to the protocol described in the test methods section. Figure 4. 2 and Figure 4. 3 presents the evolution of the damage and specimen temperature during the stepwise fatigue testing of 90˚ GF/Elium and GF/Infugreen respectively. Damage is presented as damage factor (D) which is the loss in stiffness is obtained using the Equation Damage factor (D) = 1- Ei/E0 . The damage accumulation in GF/Elium is marginal in the first few steps, then there is significant increase in damage as test progresses (Refer Figure 4. 2(a)). The same is observed for the evolution of specimen temperature (refer Figure 4. 2(b)). When this rise in temperature is plotted along with corresponding stress levels, a bilinear curve is obtained as shown in Figure 4. 4 and Figure 4. 5 for GF/Elium and GF/Infugreen respectively. The point of intersection of this bi-linear curve indicates that, the rate accumulation of damage due to fatigue loading at stress levels beyond the intersection point is significantly higher compared to rate of damage accumulation below the intersection point. This indicates that, at the stress levels below the intersection point damage accumulation is quite small, thus giving us the critical stress limit. The Critical stress limit obtained for GF/Elium and GF/Infugreen is 16.36 MPa and 18.81 MPa respectively. This stress limit is indicated as a critical level on the S-N curve as a straight line as shown in Figure 4. 1. It can be seen from the S-N curve that, at the critical stress level, GF/Infugreen can last beyond 10 million cycles where as GF/Elium can last beyond 2 million cycles. The thermography result validates the prediction from the S-N curve that GF/Infugreen exhibits better high cycle performance. It is to be noted that this method relies on accurate measurement of the coupon temperature during the fatigue test. The rise in coupon temperature for 90° coupons is quite small. Hence,

This project has received funding from the European Union's Horizon 2020 research and innovation programme under grant agreement No 952966.

the accuracy of estimation of critical stress limit would be comparatively low. This can be improved by making more accurate temperature measurements.

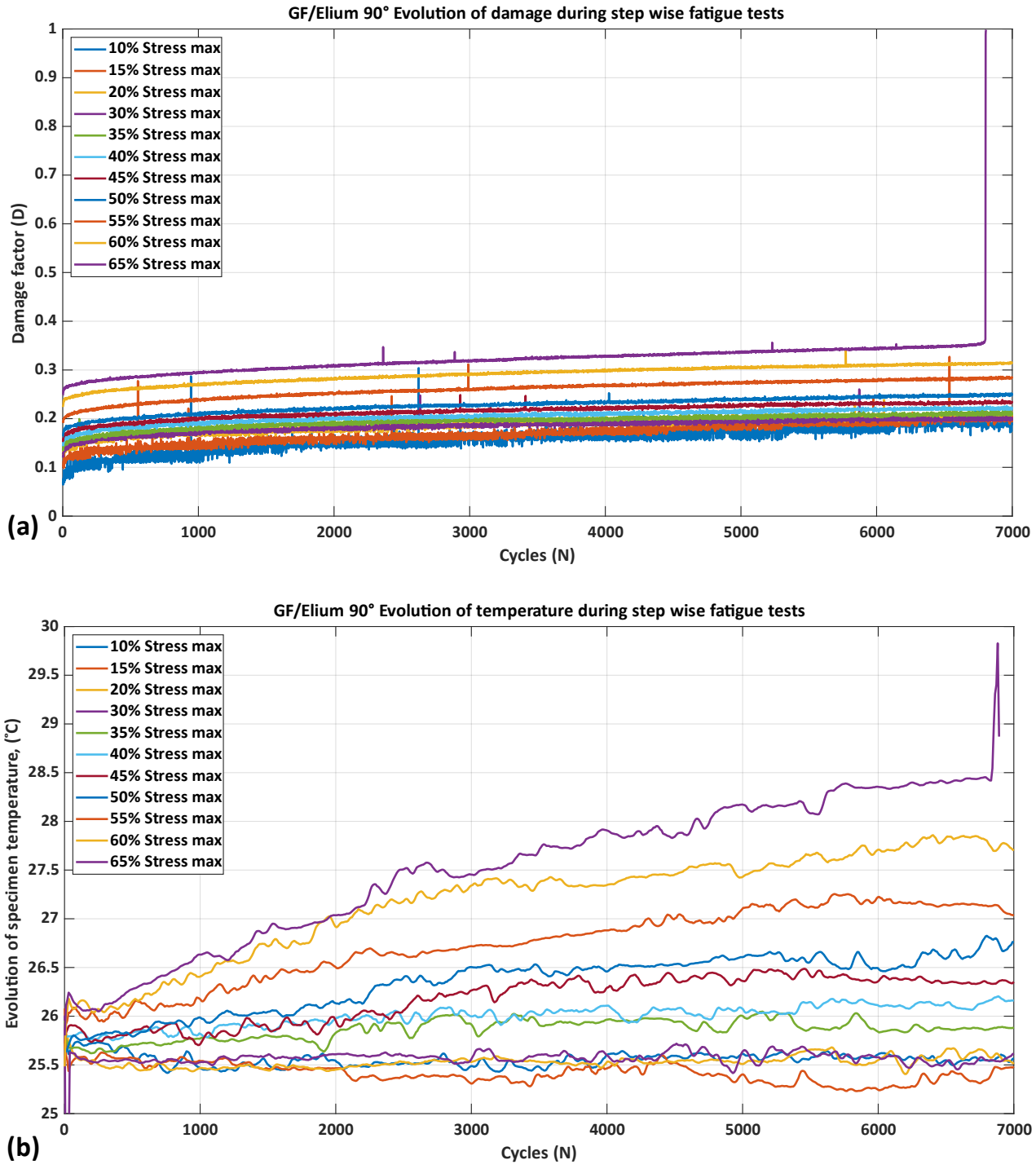

Figure 4. 2 Evolution of (a) Damage and (b) Temperature in 90° GF/Elium composite during stepwise tests.

This project has received funding from the European Union's Horizon 2020 research and innovation programme under grant agreement No 952966.

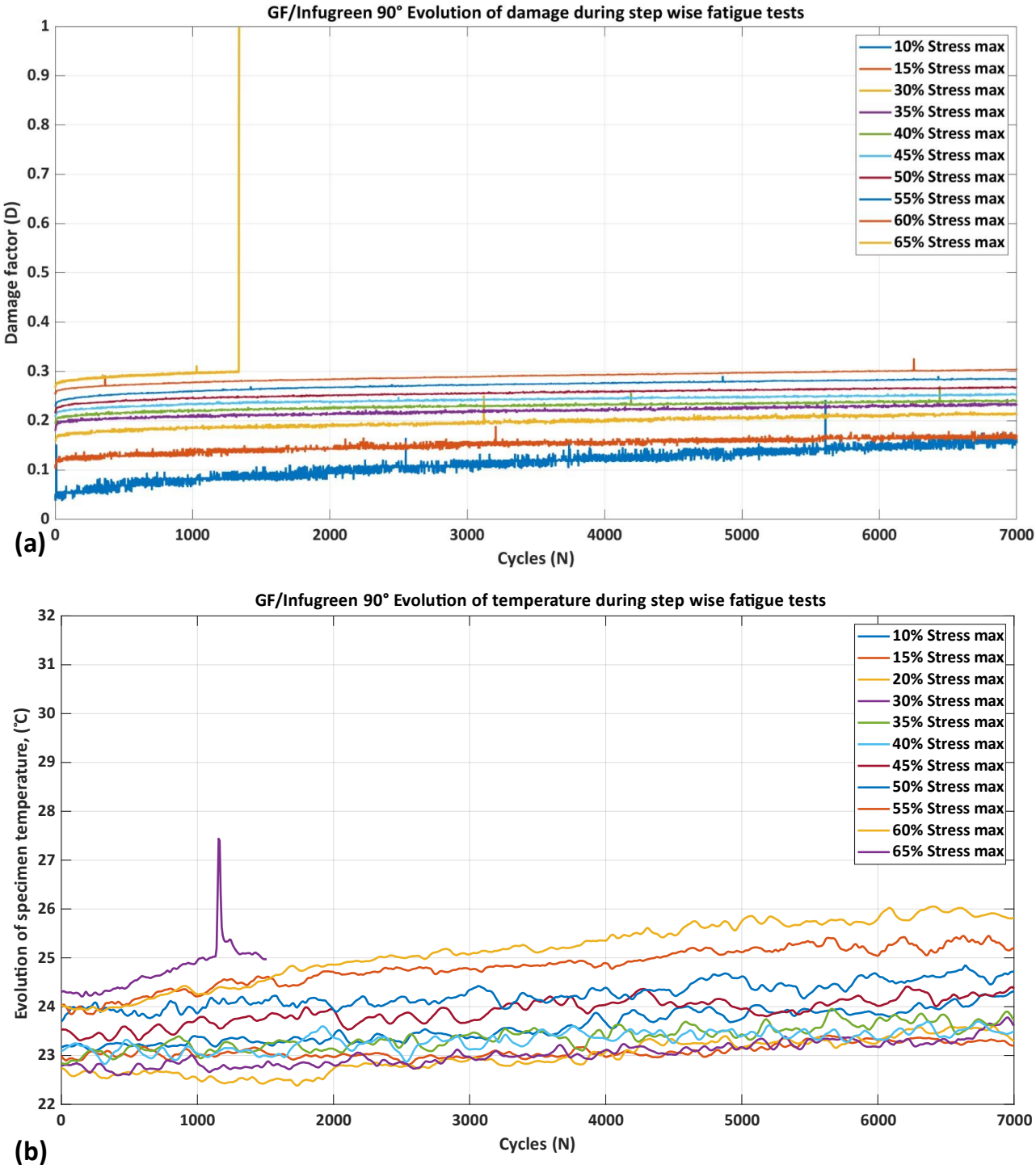

Figure 4. 3 Evolution of (a) Damage and (b) Temperature in 90° GF/Infugreen composite during stepwise tests.

This project has received funding from the European Union's Horizon 2020 research and innovation programme under grant agreement No 952966.

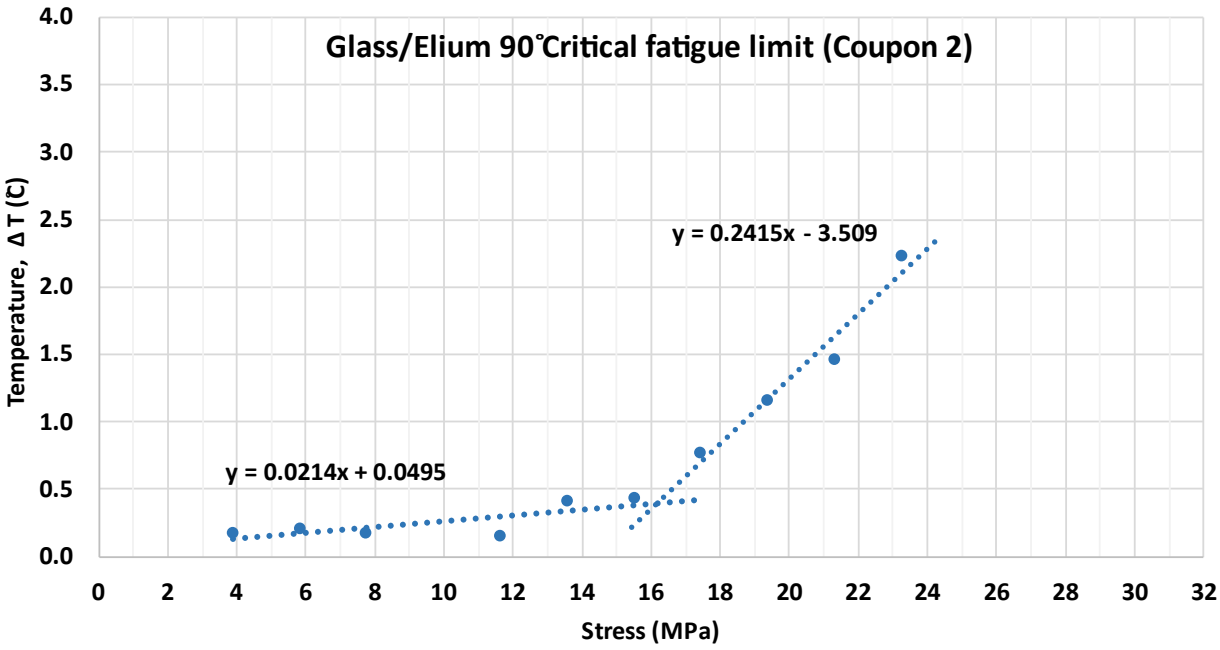

Figure 4. 4 Change in specimen temperature at the end of each load block as a function of the maximum stress applied for 90˚ GF/Elium to determine the critical stress limit.

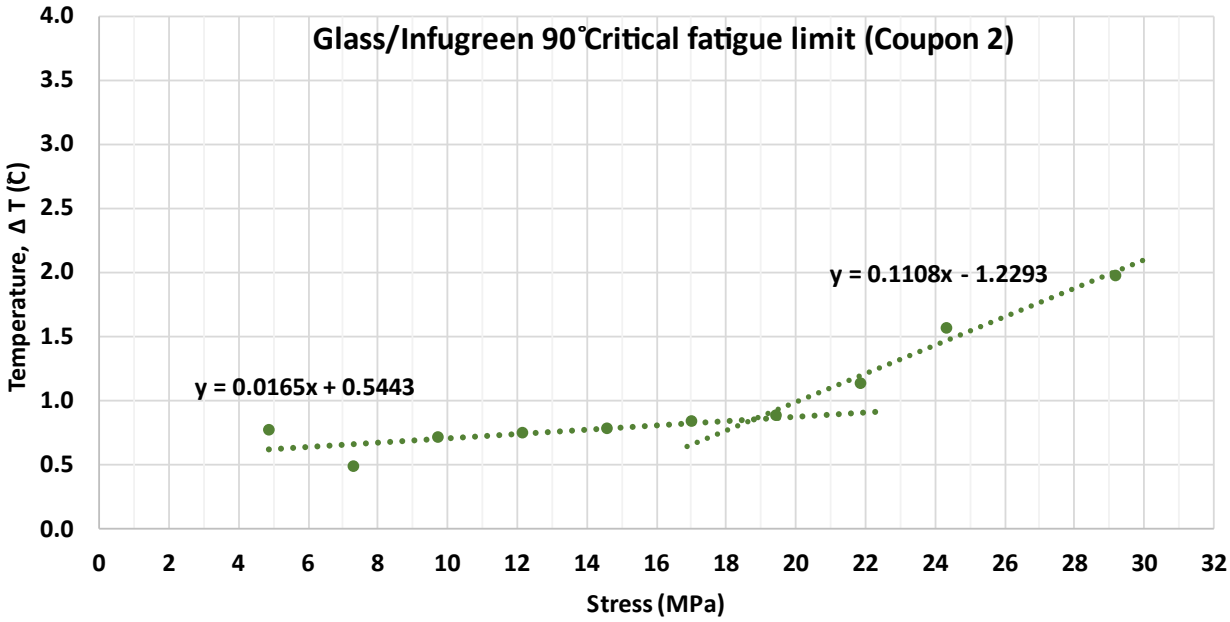

Figure 4. 5 Change in specimen temperature at the end of each load block as a function of the maximum stress applied for 90˚ GF/Infugreen to determine the critical stress limit.

4.1.3. Fractography and failure analysis

The untested tensile 90° laminate section was subjected to SEM analysis to study the features of the cross section. These SEM images served as a reference for analysing the fracture surfaces of the failed test specimens. Figure 4. 6 (a)-(c) presents the SEM images showing cross-sectional details of untested GF/Elium

This project has received funding from the European Union's Horizon 2020 research and innovation programme under grant agreement No 952966.

specimen at various magnifications. The images show the presence of polyester yarns used for stitching (construction fibres) in the interlaminar regions. In some locations, the construction fibres were observed to be grouped, possibly displaced by the evolving resin flow front during laminate fabrication. This displacement of construction fibres leads to an uneven distribution of resin-rich segments within the composite. A similar observation was made in case of GF/Infugreen composite as shown in Figure 4. 6 (d)-(f).

The tension-tension fatigue tested specimens of GF/Elium composite after failure are presented in Figure 4. 7. The specimens were loaded at a direction 90° to the fibre axis. The location of final failure of the specimens is indicated in each case. Final failure was seen to occur in the gauge section with fibre-matrix debonding being observed. Failure was localized and in some cases fibre bridging was observed. The fracture surfaces of the specimens were observed using SEM.

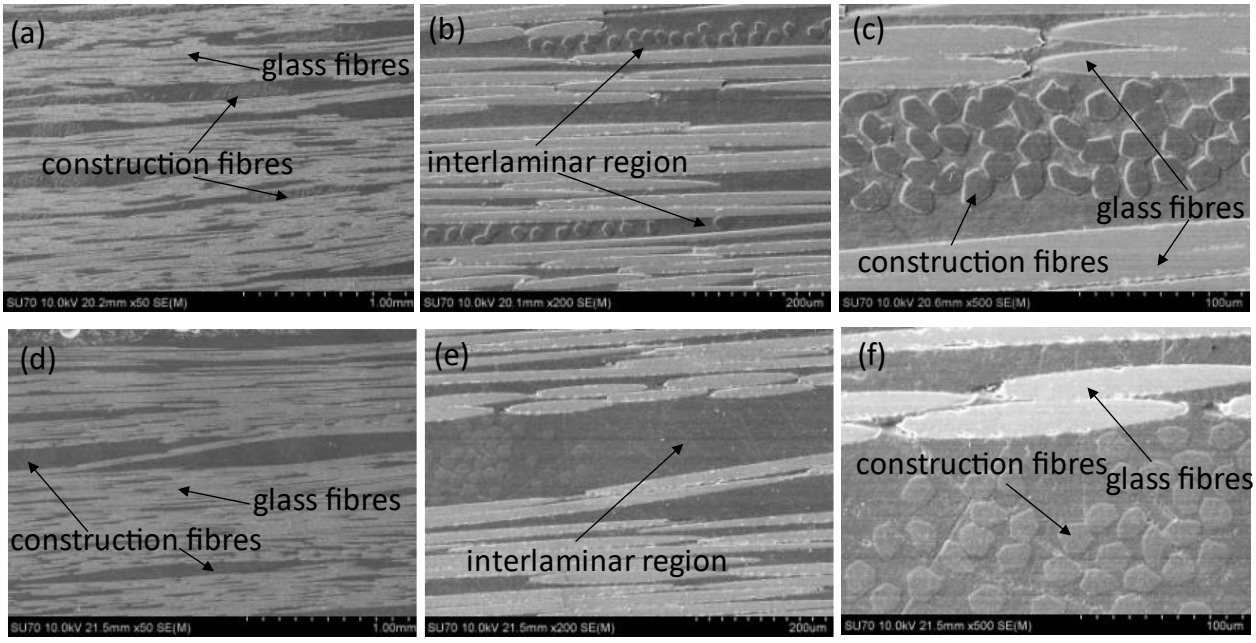

Figure 4. 6 SEM images showing cross-sectional details of untested Tensile 90° fatigue specimens, (a) to (c) GF/Elium specimen, (d) to (f) GF/Infugreen specimen.

This project has received funding from the European Union's Horizon 2020 research and innovation programme under grant agreement No 952966.

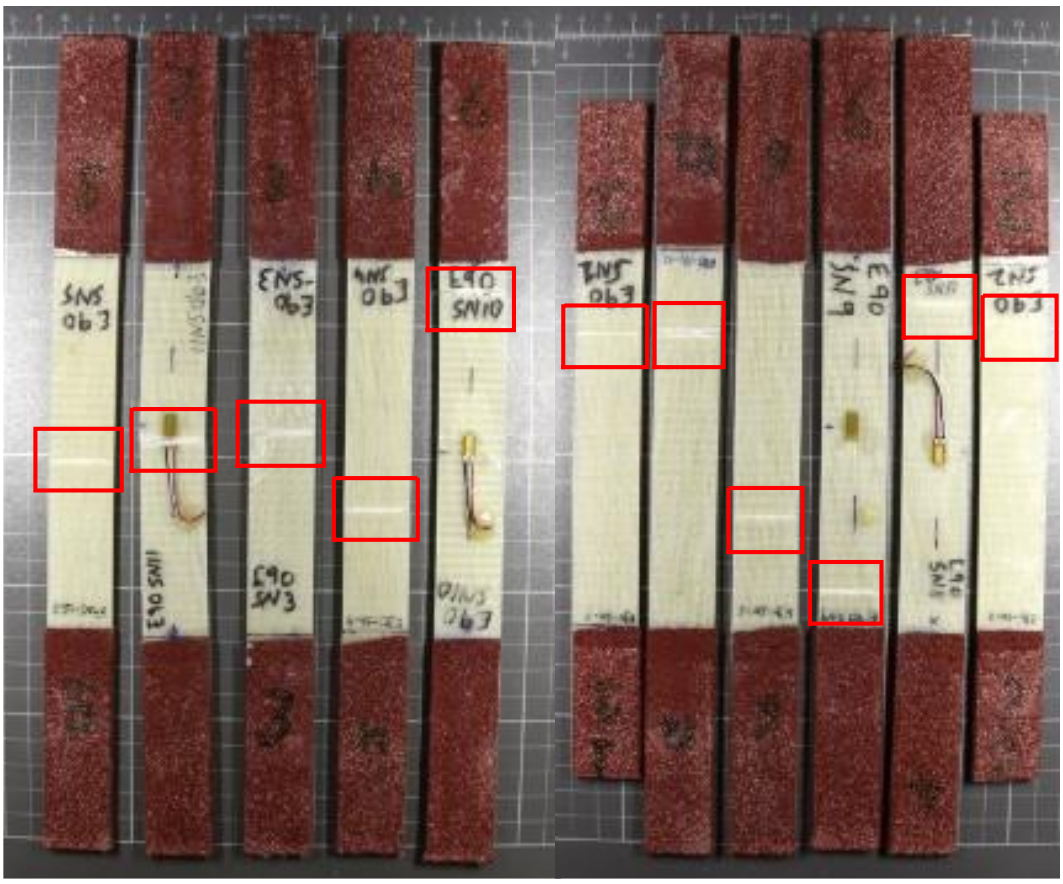

Figure 4. 7 GF/Elium 90° fatigue test specimens after failure with location of final failure indicated on the specimens.

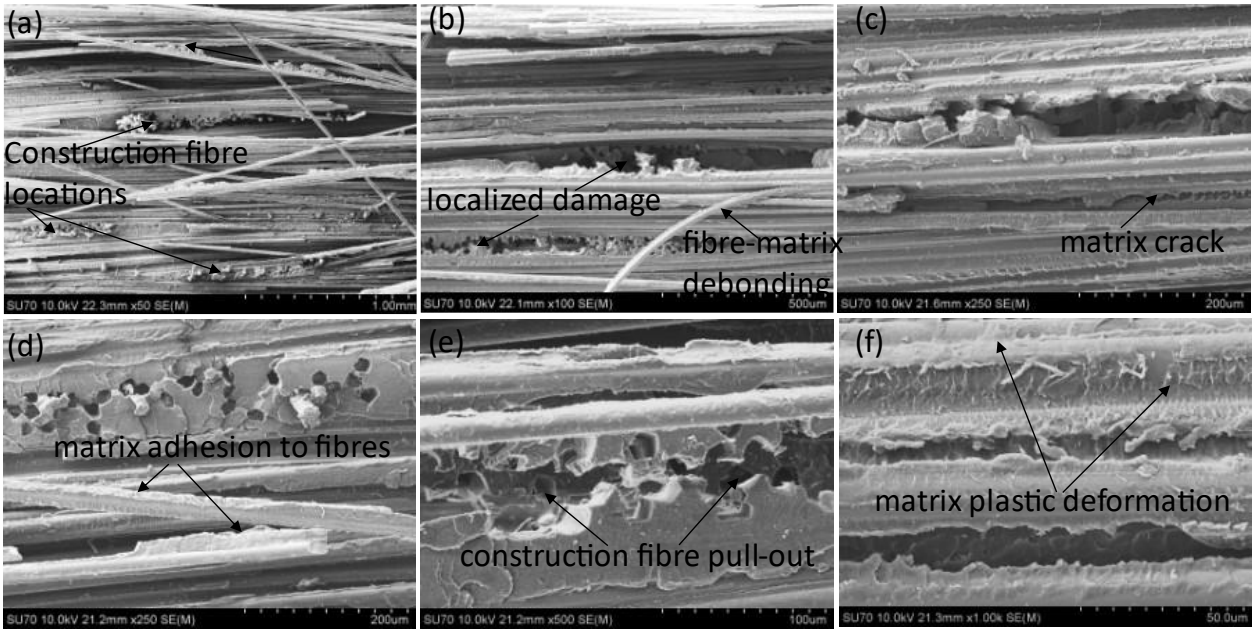

Figure 4. 8 SEM images of the fracture surface of low-cycle fatigue tested GF/Elium 90° specimen showing the failure mechanisms observed.

This project has received funding from the European Union's Horizon 2020 research and innovation programme under grant agreement No 952966.

SEM images of the fracture surface of a low-cycle fatigue tested GF/Elium composite is presented in Figure 4. 8. Figure 4. 8(a) shows the fracture features of the specimen at a low magnification. The location of construction fibres is highlighted. Localized damage at the regions of the construction fibres was seen with fibre pull-out evident. Pore-like structure caused due to pull-out of the construction fibres during fatigue loading was observed at several locations in the specimen cross-section. Evidence of matrix cracks and fibre-matrix debonding was seen. Adhesion of matrix material to debonded and broken fibres were also seen pointing to strong fibre-matrix bonding. River marks indicative of matrix plastic deformation was observed. The pull-out of construction fibres indicates a weaker bonding with the matrix and likely to have served as crack initiation points and damage propagation subsequently. The presence of localized damage areas at the location of construction fibres is indicative of this observation.

SEM images of the fracture surfaces of the high-cycle fatigue tested specimens are shown in Figure 4. 9. Unlike the low-cycle fatigue specimen, matrix damage was limited. However, fibre pull-out as in previous case was seen. Fibre-matrix debonding and fibre breakage were observed. The interfacial characteristics indicated a strong fibre-matrix bonding. Matrix cracking leading to separation of fibres was evident. The presence of a thick layers of resin adhering to the fibres was seen at several locations. Unlike the low-cycle fatigue case, evidence of matrix plastic deformation was limited. Overall, the fibre bundles remained intact, and their separation was lower as compared to the previous case.

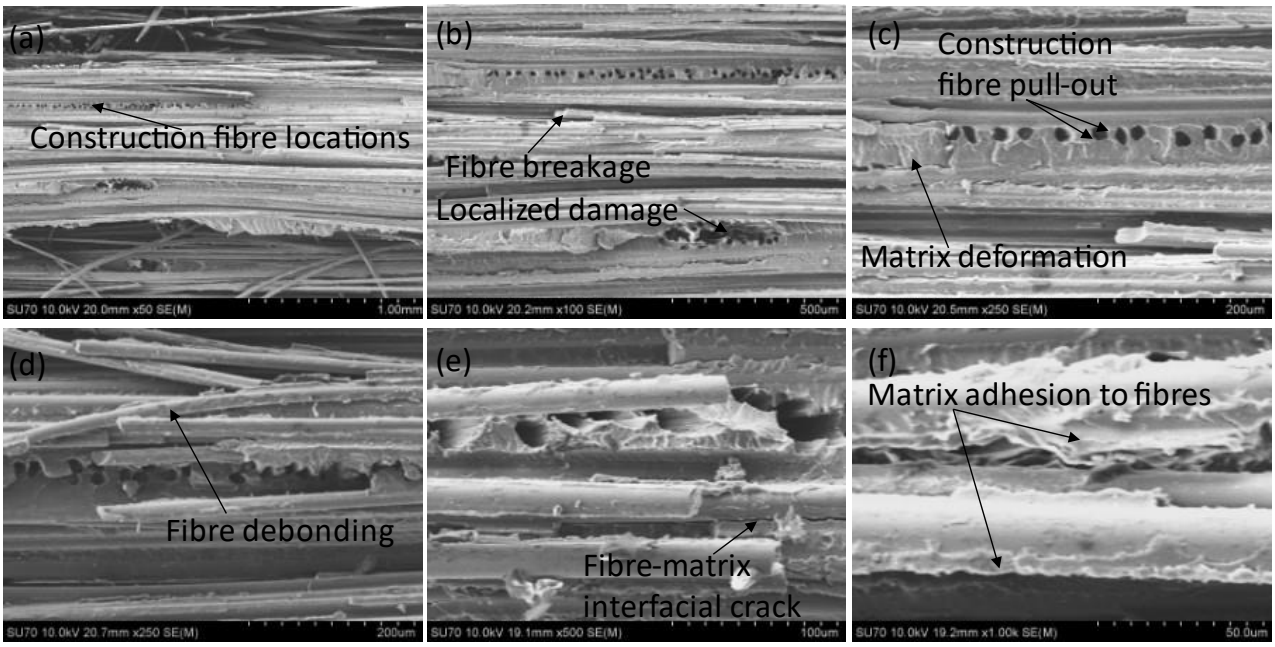

Figure 4. 9 SEM images of the fracture surface of high-cycle fatigue tested GF/Elium 90° specimen showing the failure mechanisms observed.

This project has received funding from the European Union's Horizon 2020 research and innovation programme under grant agreement No 952966.

The fatigue tested specimens of GF/Infugreen composite are shown in Figure 4. 10. The final failure locations in each specimen are shown. In case of run-out specimen, testing was ceased after 1.2 million cycles. Localised failure in the gage region was reported for the specimens tested. Fracture surface images of the low-cycle fatigue tested specimen is given in Figure 4. 11. The Infugreen matrix was observed to hold the fibres intact and very limited evidence of matrix plastic deformation was observed. The fracture surface was characterized by matrix-rich regions. The construction fibres were also seen to be mostly intact with only a few fibres displaced from their position leaving voids in the cross-section. Unlike the Elium composite, matrix adhesion to the separated fibres was less pronounced with clean fibre surfaces visible at several locations. Figure 4. 12 shows the images taken from the fracture surface of a high-cycle fatigue tested GF/Infugreen specimen. The fracture surface appeared similar to that of the low-cycle fatigue specimen. Matrix-rich regions were seen at several locations restricting fibre separation. However, matrix deformation was more pronounced and localized damage areas were seen. The construction fibres were however mostly intact in their position as seen in the figure. Fibre-matrix adhesion characteristics were similar to that of the low-cycle fatigue specimen. These observations are consistent with those made during the static tests of the GF/Infugreen composites. The failure surfaces indicate higher work required for fibre-matrix separation and final failure. This is also supported by the fatigue strength values reported in case of GF/Infugreen composites.

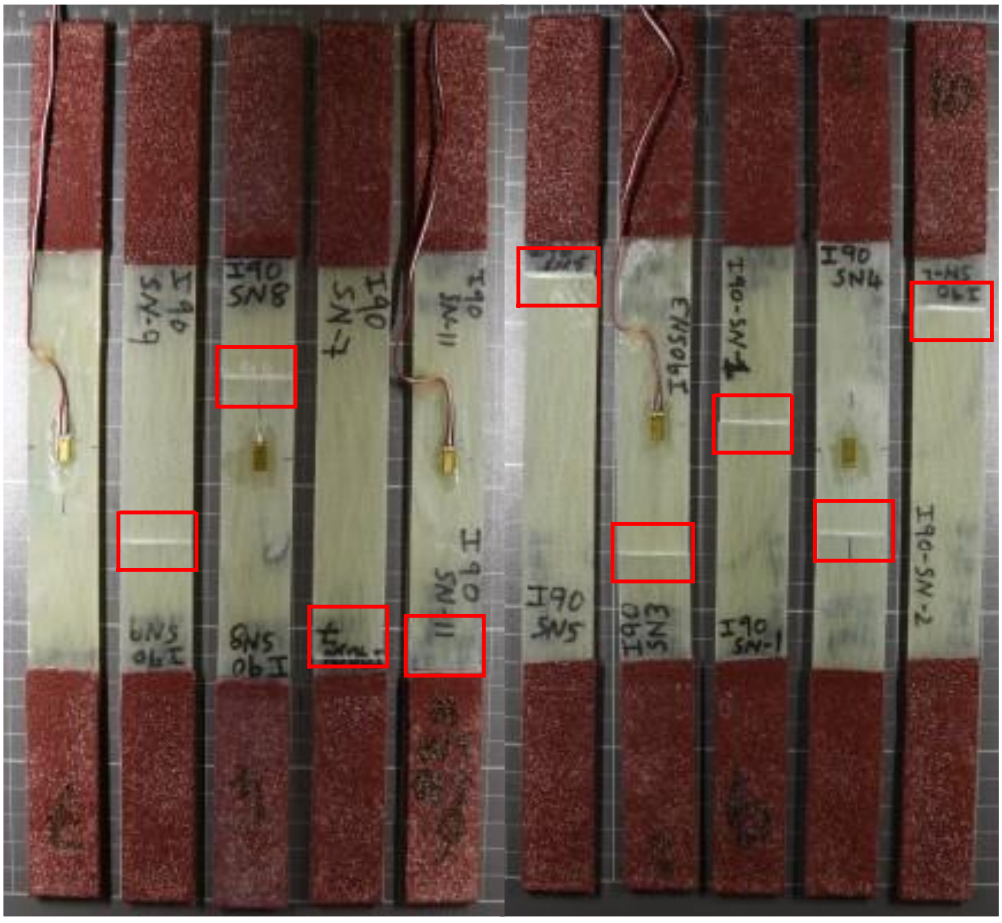

Figure 4. 10 GF/Infugreen 90° fatigue test specimens after failure with location of final failure indicated on the specimens.

This project has received funding from the European Union's Horizon 2020 research and innovation programme under grant agreement No 952966.

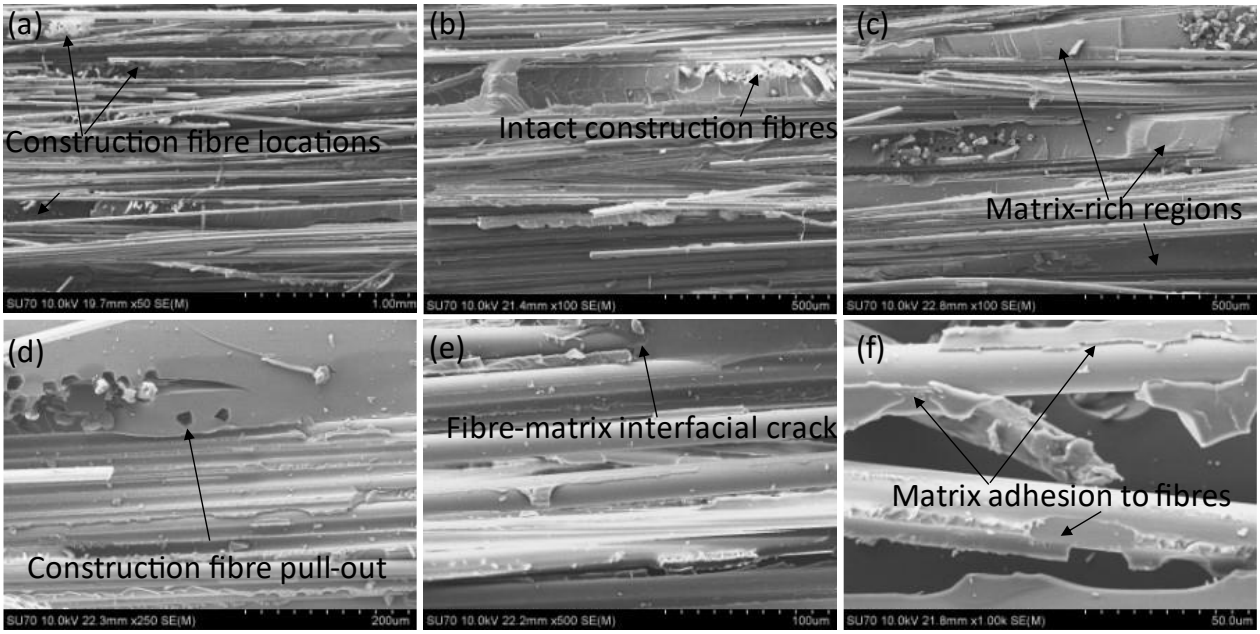

Figure 4. 11 SEM images of the fracture surface of low-cycle fatigue tested GF/Infugreen 90° specimen showing the failure mechanisms observed.

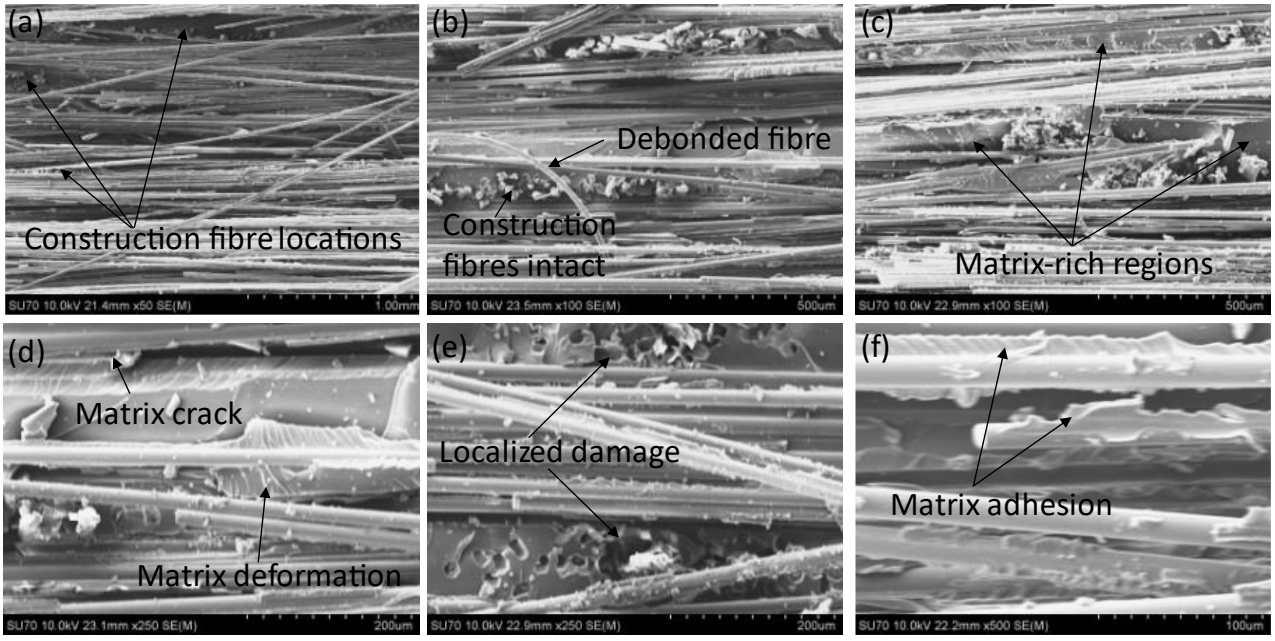

Figure 4. 12. SEM images of the fracture surface of high-cycle fatigue tested GF/Infugreen 90° specimen showing the failure mechanisms observed.

This project has received funding from the European Union's Horizon 2020 research and innovation programme under grant agreement No 952966.

4.2. ±45° (Relative to loading direction)

In-plane shear fatigue tests to establish the S-N curve for the glass fibre composites were achieved by conducting tension-tension fatigue loading tests on composite coupons with fibres oriented [±45˚] to the loading direction. The tests were conducted at a frequency of 5 Hz with an R ratio of 0.1. Static tensile test was conducted on the coupons to obtain the in-plane shear strength (τ_{uts}). It was found that the ultimate shear strength of $[\pm 45^{\circ}]_{2S}$ was 42.07 MPa and 53.83 MPa for GF/Infugreen and GF/Elium composites respectively. The stress values for tension-tension fatigue tests were defined based on these values.

4.2.1. S-N Curve

Figure 4. 13 presents the S-N curves for $[\pm 45^{\circ}]_{2S}$ GF/Infugreen and GF/Elium composites. The data obtained was plotted on a semi-log plot. Regression analysis was done by fitting a curve following logarithmic and power law. Table 4. 2 summarises the obtained curve equations and R^2 values. It is seen that the data fit well with the power law equation, which is evident from the variance (R^2) value. This is again in agreement with the findings of Mandell et al. They observed that in some complex composite material systems like oblique oriented fibres with no dominant orientation, woven fabrics and short fibre composites the S-N curve tend to follow a non-linear trend in semi-log plot [6,16,17]. This observation is clearly seen from the variance values in the regression analysis present in the Table 4. 2. However, closer observation of the low cycle fatigue data show that there is a linear relationship (logarithmic function) in the low cycle fatigue regime which is depicted with red dotted lines in the Figure 4. 13. Whereas, in the high cycle regime the curve tends to flatten out. Similar observations were made by Mandell et al. particularly for woven fabric reinforcements. They observed steep curve at low to moderate cycles which was attributed to the occurrence of delamination at the weave cross-over points and the curve would flatten in high-cycle regime [6,16,17]. Considering that, the $[\pm 45^{\circ}]_{2S}$ coupons were manufactured using Saertex fabric which has 3% of glass fibres running in the transverse direction, a similar delamination phenomenon is likely to occur at low cycle fatigue thus, explaining the steep slope of the curve observed initially. Again, it is clear from the S-N curve that GF/Elium has a better fatigue performance at high stress levels. However, the performance of GF/Elium and GF/Infugreen appear to be same in high cycle regime.

This project has received funding from the European Union's Horizon 2020 research and innovation programme under grant agreement No 952966.

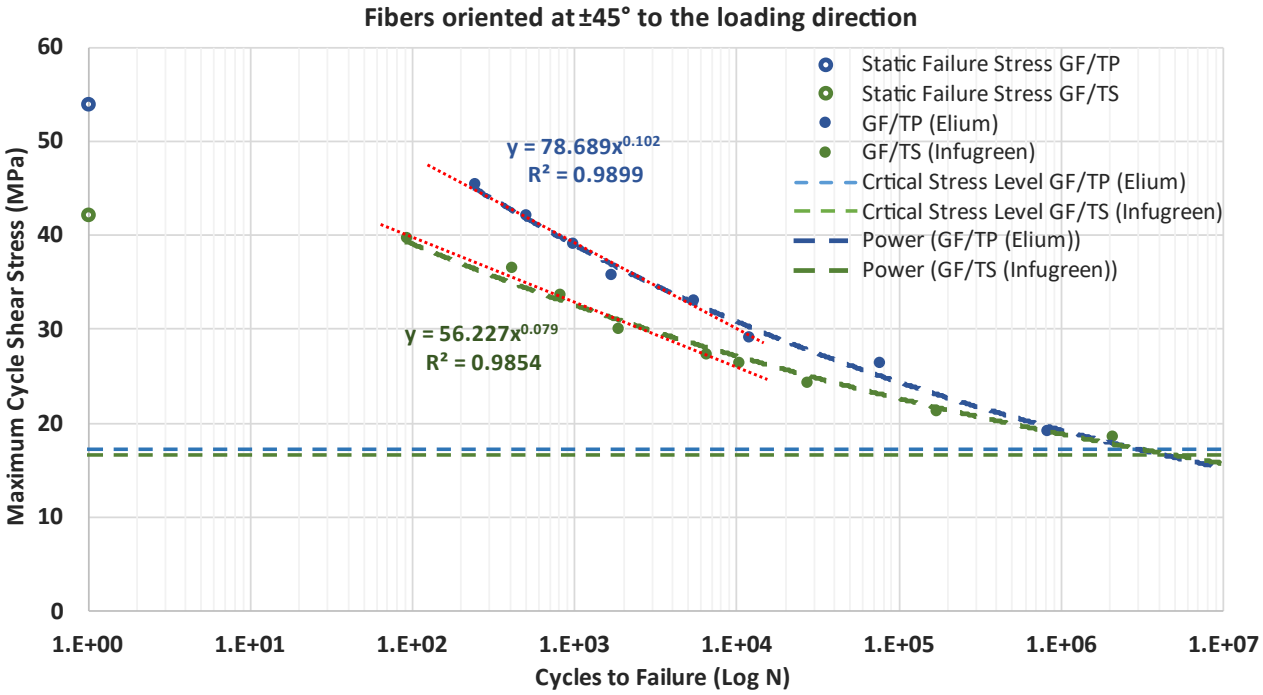

Figure 4. 13 S-N Curve (In-plane shear stress) for Glass fibre – Infugreen and Elium with fibres in the [±45˚] orientation.

Table 4. 2 Regression analysis of S-N data for ±45˚ GF/Infugreen and GF/Elium composites.

Laminate configuration	Infugreen		Elium	
	Logarithmic	Power	Logarithmic	Power
[±45°]	y = -2.186 ln(x) + 48.043 R^2 = 0.9507	**y = 56.227 $x^{-0.079}$** **R^2 = 0.9854**	y = -3.118 ln(x) + 60.679 R^2 = 0.9715	**y = 78.689 $x^{-0.102}$** **R^2 = 0.9899**

Note: Best fit highlighted in bold green font.

4.2.2. Thermography

Temperature stabilisation fatigue tests were performed to obtain the fatigue limit of the composites speedily. To achieve this step-wise constant load amplitude fatigue tests were performed according to the protocol described in the test methods section. Figure 4. 14 and Figure 4. 15 present the evolution of the damage and specimen temperature during the stepwise test for ±45˚ GF/Elium and GF/Infugreen respectively. Damage is presented as damage factor (D) which is a measure of loss in stiffness obtained using the Equation Damage factor (D) = 1- E_i/E_0 which represents the change in the ratio of dynamic stiffness (E_i) to static stiffness (E_0) [10].

This project has received funding from the European Union's Horizon 2020 research and innovation programme under grant agreement No 952966.

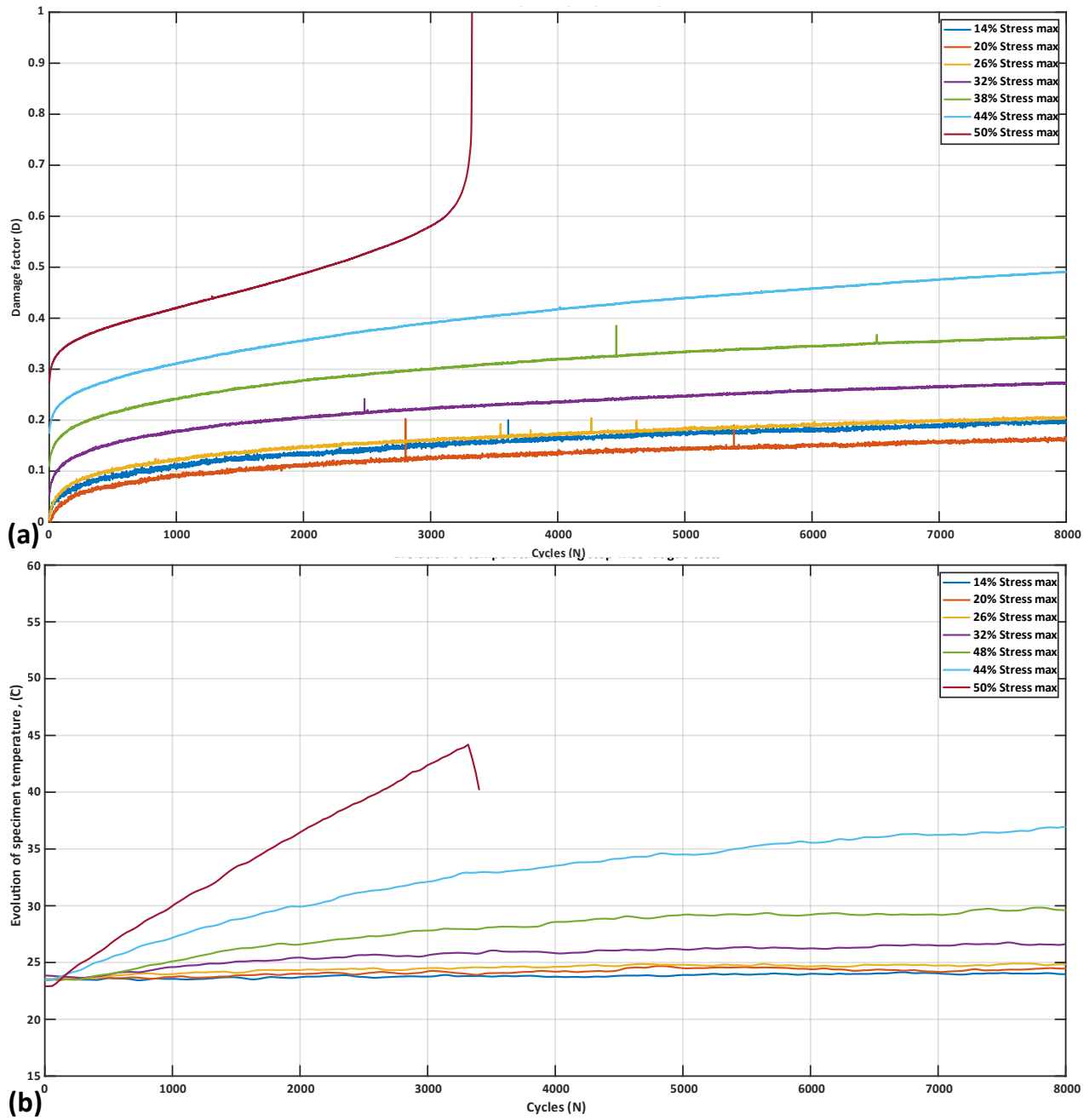

Figure 4. 14 Evolution of (a) Damage and (b) Temperature in ±45˚ GF/Elium composite during stepwise tests.

The graphs in Figure 4. 14 (a) indicates that the damage (D) in ±45˚ GF/Elium composite is marginal but consistently increasing during the low-stress cycles. The same can be observed from the temperature evolution in Figure 4. 14(b). Additionally, Figure 4. 14(a) indicates that the damage accumulation starts from the very first stress block and gradually keeps rising to a progressive failure. In comparison, the evolution of damage (D) and temperature of the specimen ±45˚ GF/Infugreen composite is presented in Figure 4. 15. It can be observed that the damage accumulation in GF/Infugreen stabilises after few initial cycles in each stress level. Whereas for GF/Elium the damage accumulation continues to happen through the end of the step as seen from Figure 4. 14.

This project has received funding from the European Union's Horizon 2020 research and innovation programme under grant agreement No 952966.

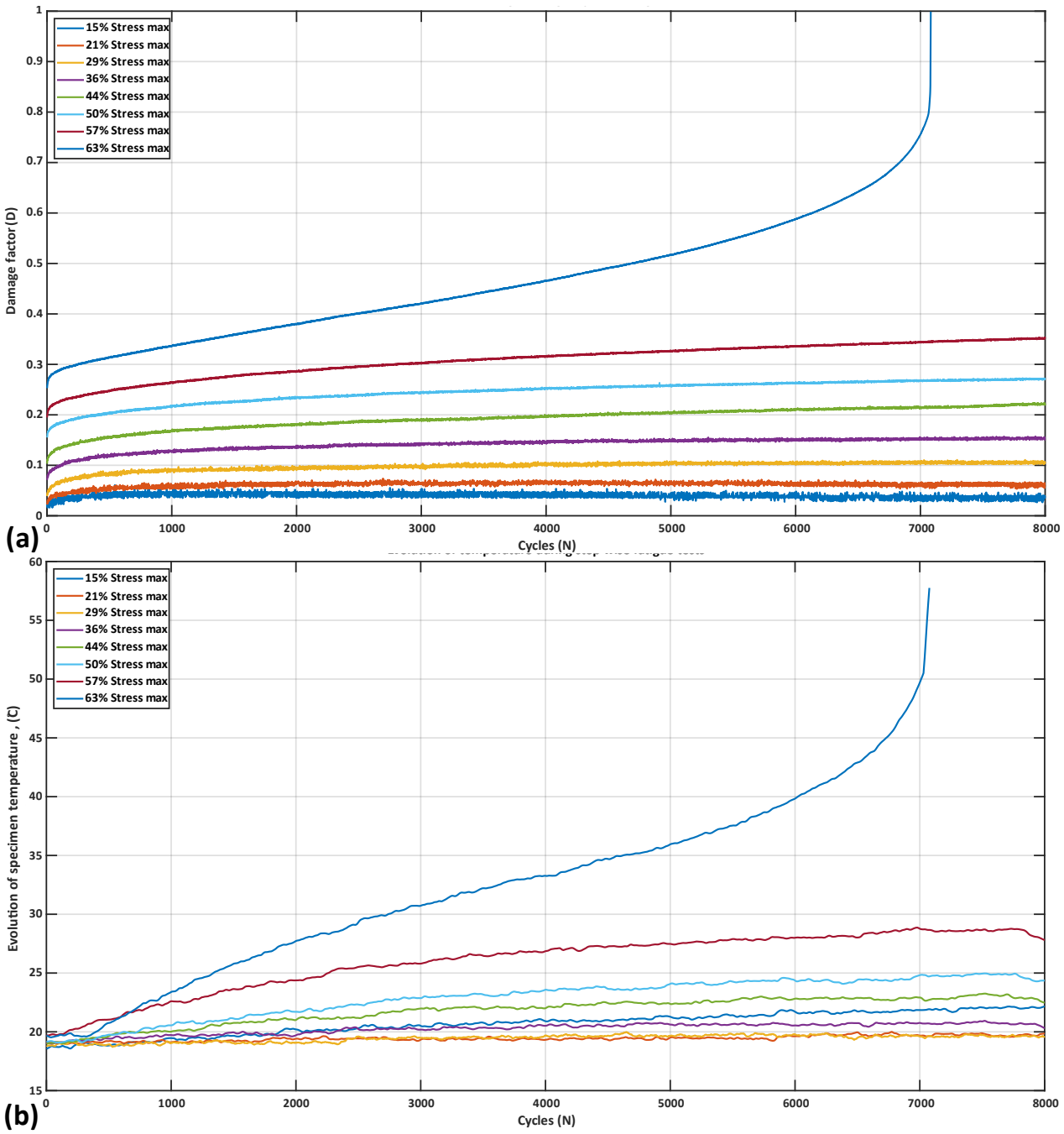

Figure 4. 15 Evolution of (a) Damage and (b) Temperature in ±45˚ GF/Infugreen composite during stepwise tests.

Additionally, the rise in specimen temperature of each block was plotted against the maximum stress level applied, as shown in Figure 4. 16 and Figure 4. 17 for GF/Elium and GF/Infugreen respectively. It is evident from the plots that the data points can fit into 2 different linear trendlines. As discussed earlier, in this graphical method the stress level at the intersection of these linear trendlines is considered to be the critical stress level. This can physically be interpreted as the stress level after with the rate of damage accumulation rises at a higher rate compared to damage accumulation below this stress level. A fatigue limit of 17.22 MPa and 16.70 MPa was obtained for GF/Elium and GF/Infugreen from three tests. This stress limit is also depicted

This project has received funding from the European Union's Horizon 2020 research and innovation programme under grant agreement No 952966.

in Figure 4. 13 on the S-N curve indicating that both GF/Elium and GF/Infugreen can with stand approximately 10 million cycles at this stress level.

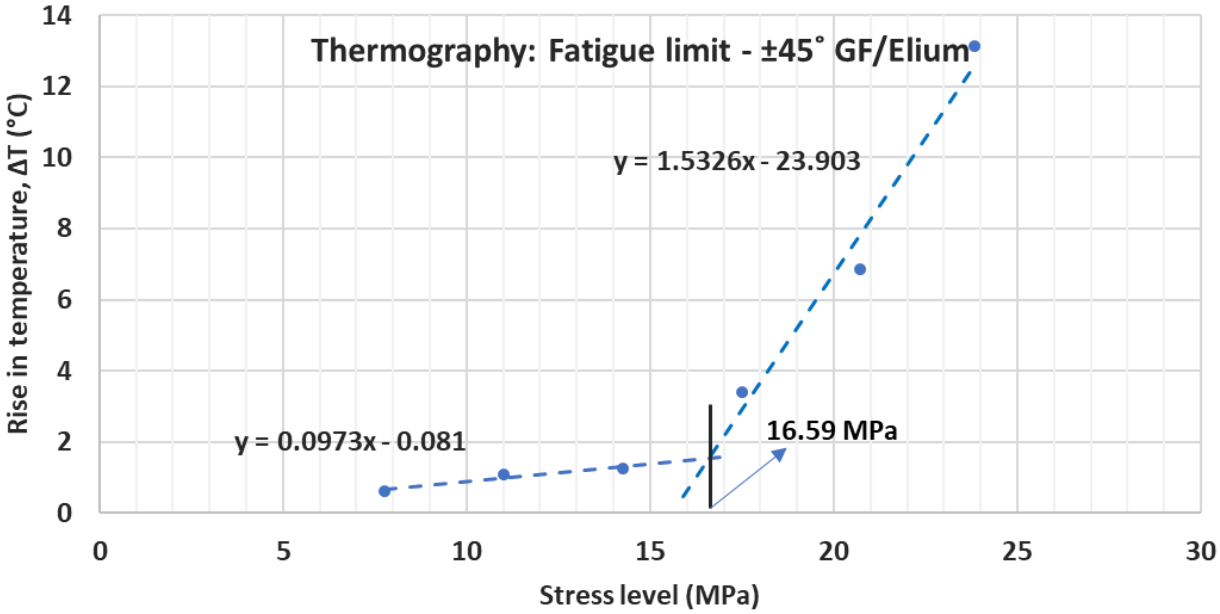

Figure 4. 16 Change in specimen temperature at the end of each load block as a function of the maximum stress applied for ±45˚ GF/Elium to determine the critical stress limit.

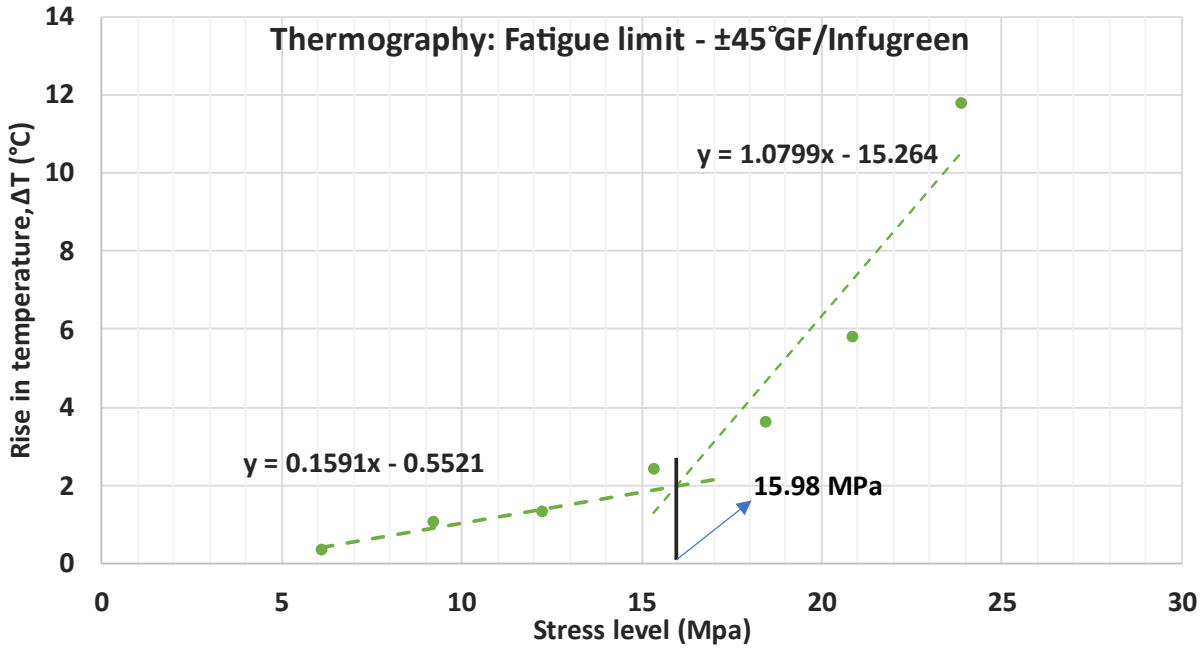

Figure 4. 17 Change in specimen temperature at the end of each load block as a function of the maximum stress applied for ±45˚ GF/Infugreen to determine the critical stress limit.

This project has received funding from the European Union's Horizon 2020 research and innovation programme under grant agreement No 952966.

4.2.3. Fractography and failure analysis

Figure 4. 18(a) and Figure 4. 18(b) shows images of the typical fatigue tested GF/Elium and GF/Infugreen composite specimens, respectively along with marked failure locations. The failures were similar in case of both the material systems and was seen to occur in the gage section of the specimens tested. Localized failure on account of matrix shear was seen. Figure 4. 19 shows SEM images of cross section of untested 45° GF/Elium and GF/Infugreen composite specimens. While Figure 4. 19 (a) to (c) correspond to GF/Elium specimen, Figure 4. 19 (d) to (f) shows the cross-sectional features of a GF/Infugreen composite specimen. The images indicate the presence of construction fibres between the individual plies. However, bundling of the construction fibres was observed in both the composites examined. The images also indicate the absence of any damage induced during the fabrication or machining process prior to specimen testing. The presence of resin-rich areas in the specimen cross-section was also seen. Failure was seen to occur within the gage length, and it was similar across the specimens as can be seen from Figure 4. 18. Closer examination of specimens showed evidence of delamination between the individual plies. Figure 4. 20 shows the SEM images corresponding to a low-cycle fatigue tested GF/Elium composite specimen. Fibre splitting was clearly observed. However, large regions of fibres in the same ply remained intact indicating the dominance of ply delamination during the failure process. Although matrix adhesion to fibres was seen, there was also evidence of fibre debonding. The bundling of construction fibres was seen in the SEM images. Figure 4. 21 shows the images taken from a GF/Elium high-cycle fatigue tested specimen. Evidence of matrix plastic deformation could be seen. Fibre-matrix debonding, fibre splitting and breakage was also observed. As compared to low-cycle fatigue tested specimen, matrix deformation was found to be slightly pronounced. However, overall, similar failure behavior was observed in the composites.

The failure in the case of GF/Infugreen specimens was seen to be similar to that observed in case of GF/Elium specimens. Evidence of ply delamination, fibre breakage was seen. Figure 4. 22 shows the failure surfaces of a low-cycle fatigue tested GF/Infugreen composite specimen. The delaminated regions show the fibres to be intact in the plies. Therefore, as in the case of GF/Elium composites, it is likely that delamination failure was initiated prior to the observation of other failure modes. Fibre-debonding and fibre splitting was also observed. Matrix adhesion to fibres was seen at several locations. The SEM images of the high-cycle fatigue tested specimen is presented in Figure 4. 23. In this case, fibre breakage in localized regions was seen. As compared to GF/Elium composite, fibre-matrix adhesion was observed to be higher. The adhesion of matrix to the fibres was also clearly seen. The fibre surfaces were observed to be smoother in the case of GF/Elium composites as compared to GF/Infugreen composites. This was in contrast to previous observations in the case of specimens of other configurations and will be investigated further. A comparison of low-cycle and high-cycle fatigue tested GF/Infugreen composites showed similar behavior with no significant difference in fracture characteristics observed.

This project has received funding from the European Union's Horizon 2020 research and innovation programme under grant agreement No 952966.

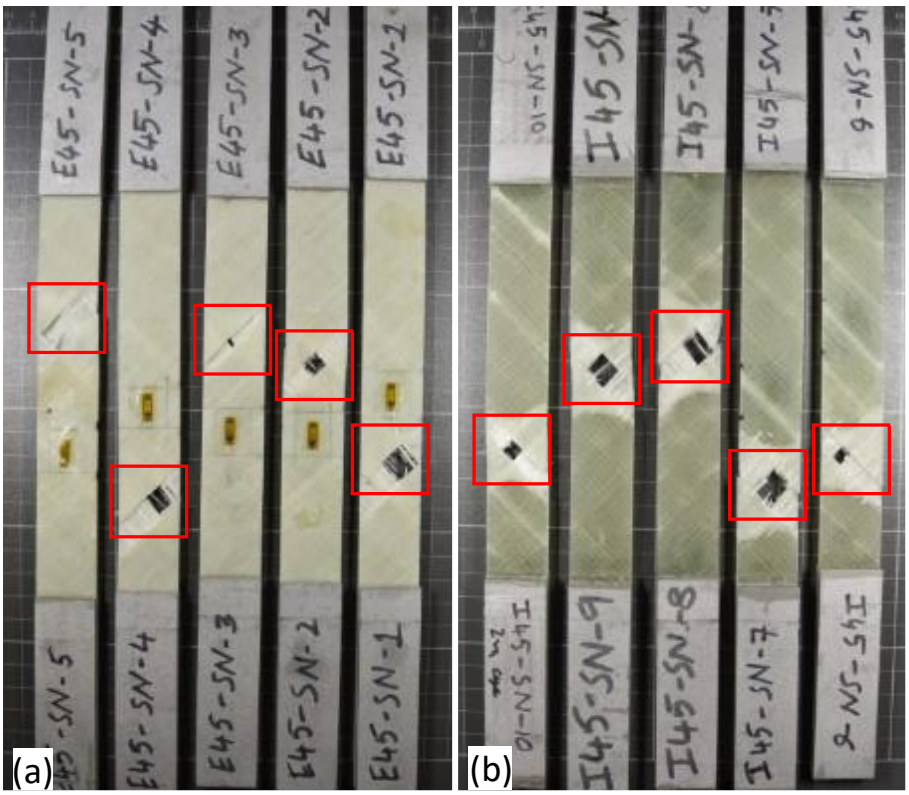

Figure 4. 18 ±45° fatigue test specimens after failure with location of final failure indicated on the specimens (a) GF/Elium specimens, (b) GF/Infugreen specimens.

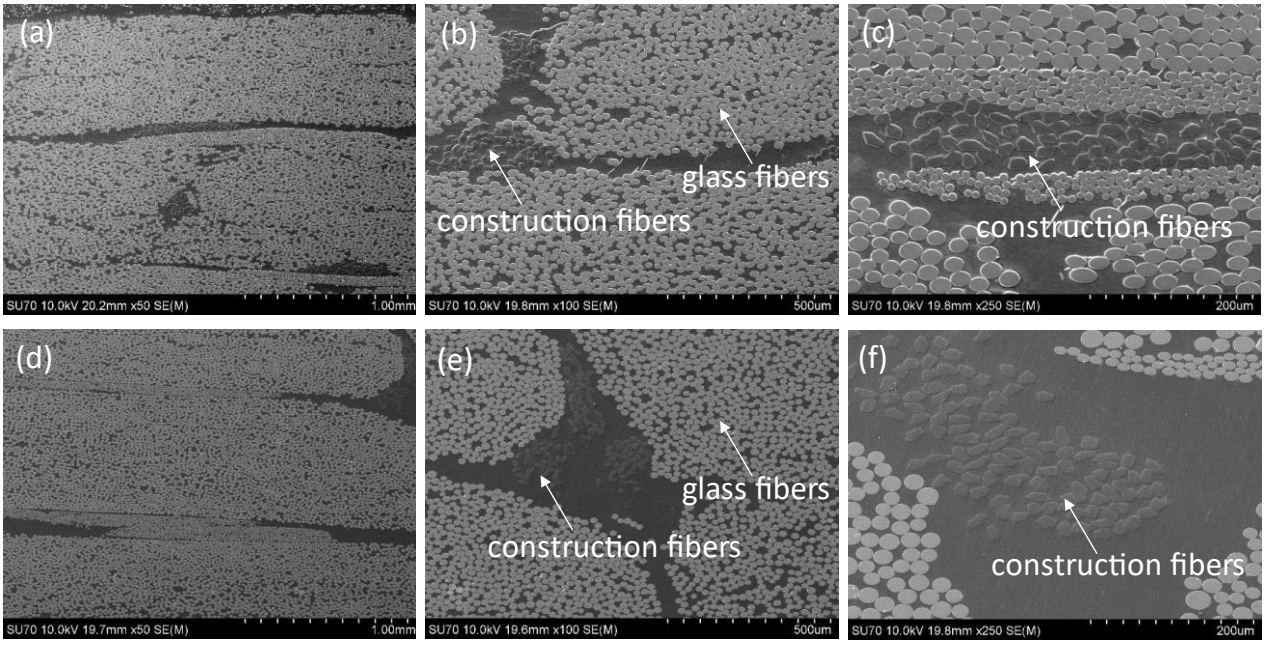

Figure 4. 19 Untested Tensile ±45° fatigue specimens, (a) to (c) GF/Elium specimen, (d) to (f) GF/Infugreen specimen.

This project has received funding from the European Union's Horizon 2020 research and innovation programme under grant agreement No 952966.

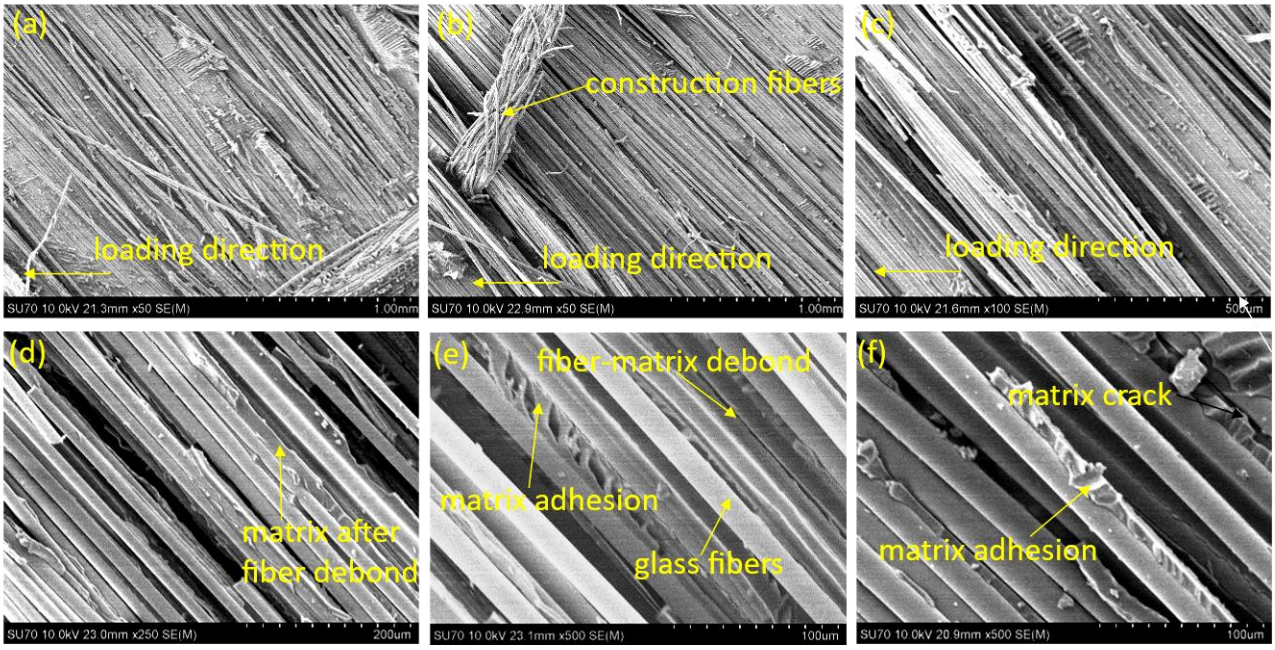

Figure 4. 20 SEM images from a low-cycle fatigue tested GF/Elium ±45° specimen.

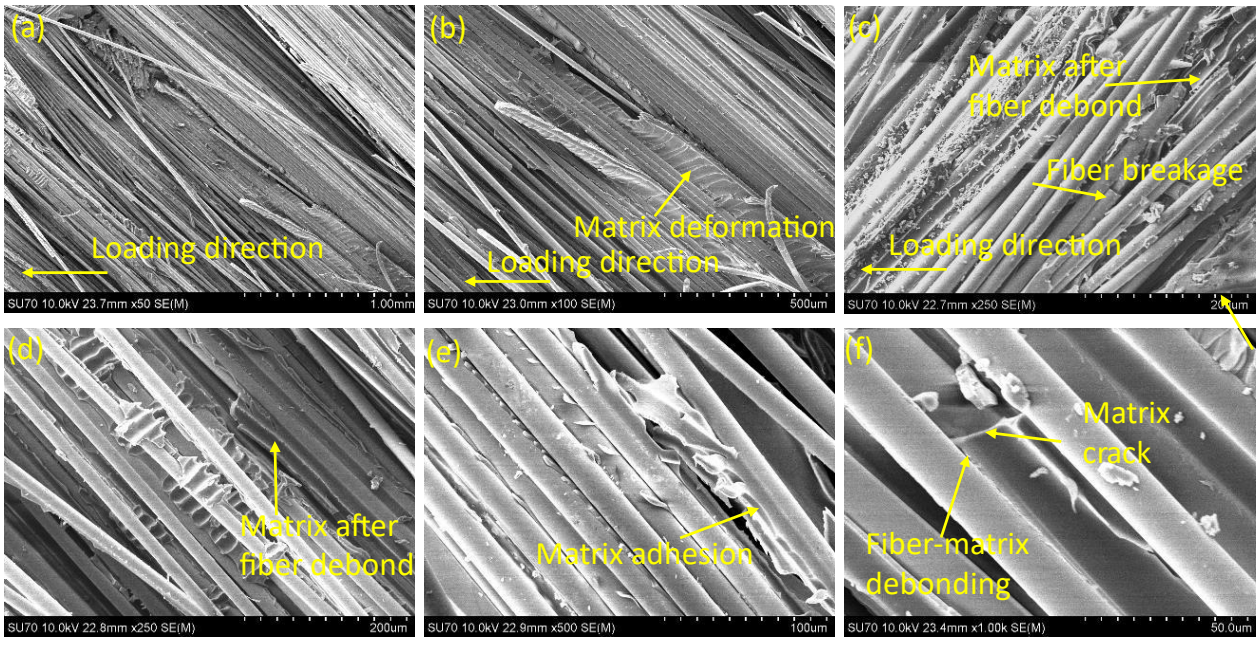

Figure 4. 21 SEM images from a high-cycle fatigue tested GF/Elium ±45° specimen.

This project has received funding from the European Union's Horizon 2020 research and innovation programme under grant agreement No 952966.

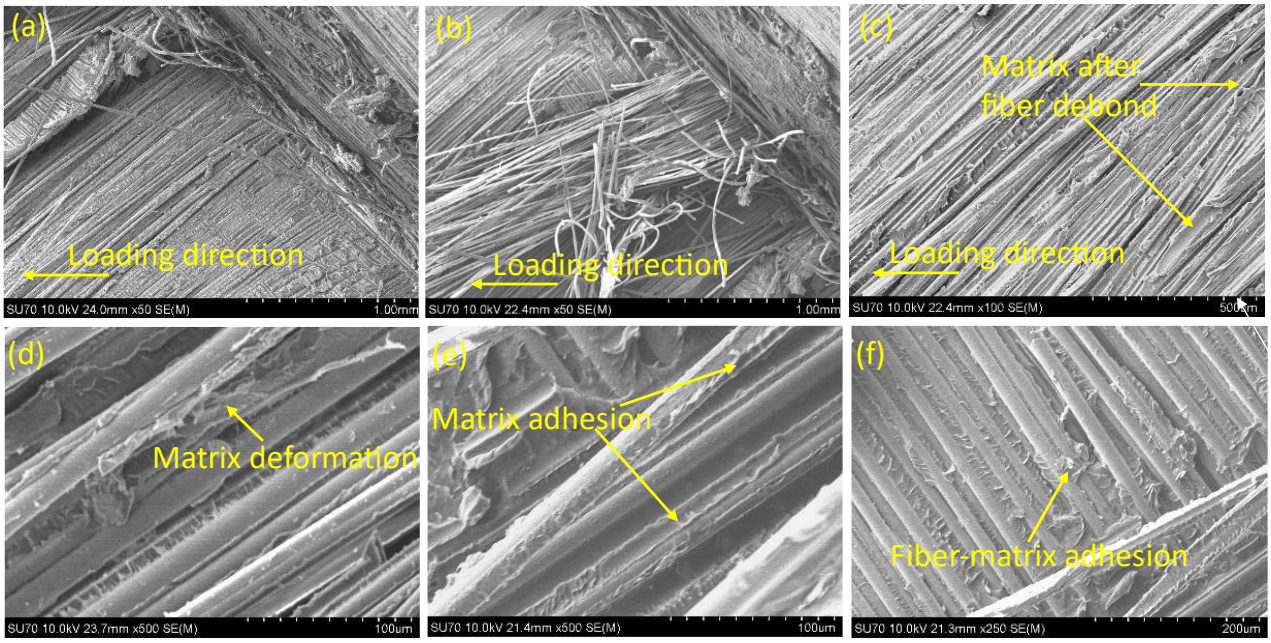

Figure 4. 22 SEM images from a low-cycle fatigue tested GF/Infugreen ±45° specimen.

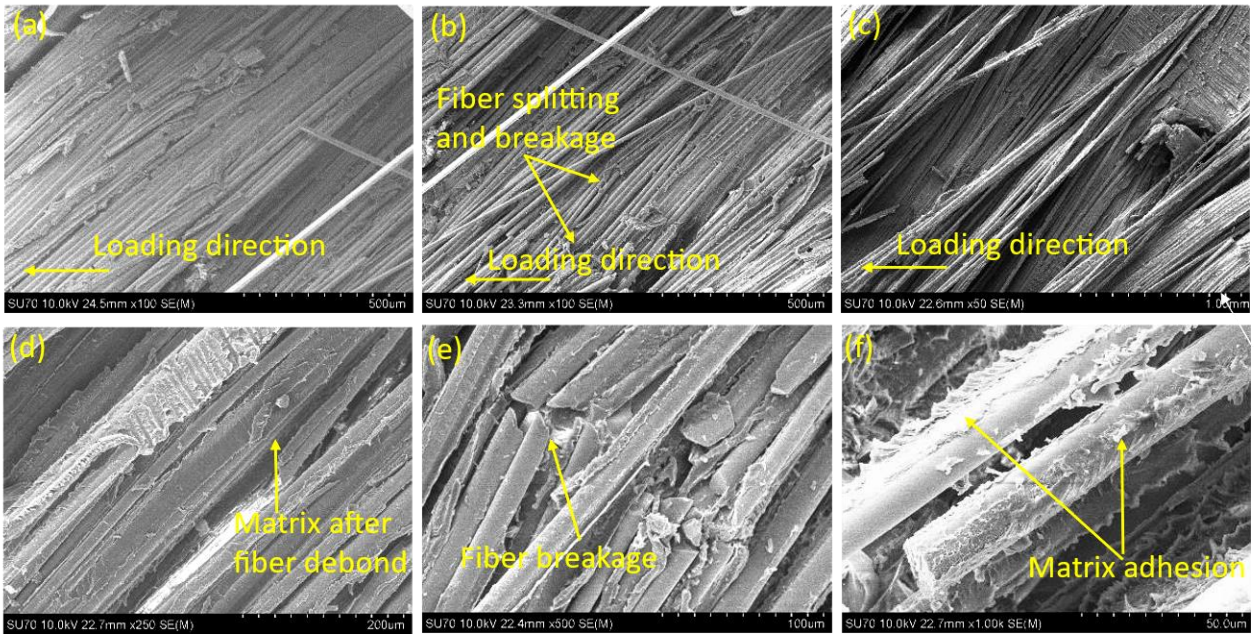

Figure 4. 23 SEM images from a high-cycle fatigue tested GF/Infugreen ±45° specimen.

This project has received funding from the European Union's Horizon 2020 research and innovation programme under grant agreement No 952966.

4.3. Quasi-isotropic

The tension-tension fatigue tests to establish the S-N curve for the glass fibre composites in the quasi-isotropic configuration ($[0^\circ, +45^\circ, 90^\circ, -45^\circ]_{2S}$) was achieved by conducting constant amplitude loading tests on composite coupons at a frequency of 5 Hz with an R ratio of 0.1. Static tensile tests was conducted on the coupons to obtain the ultimate tensile failure strength (σ_{uts}). It was found that the ultimate tensile strength of the quasi-isotropic composite coupons was 341.44 MPa and 313.85 MPa for GF/Infugreen and GF/Elium composites respectively. The stress values for tension-tension fatigue tests were decided based on these values.

4.3.1. S-N Curve

The Figure 4. 24 presents the S-N curves for quasi-isotropic GF/Infugreen and GF/Elium composites. The data obtained was plotted in the semi-log plot. Regression analysis was done by fitting a curve following logarithmic and power law. The Table 4. 1 summarises the obtained line equations and R^2 values. It was seen that the data fit well with the logarithmic equation, which is evident from the variance (R^2) value. This is accordance with the findings of Mandell *et al*. They observed that the composites made of multidirectional reinforcements where the lifetime is clearly dominated by one fibre orientation, tend to follow logarithmic trend in a semi-log plot which yields a linear S-N curve [6,16,17]. In this case the lifetime of the quasi-isotropic composites is clearly dominated by [0°] plies. Additionally, the S-N curve of GF/Infugreen has a lower slope than that of the GF/Elium. This may signify that the GF/Infugreen composite exhibits a better high-cycle fatigue performance.

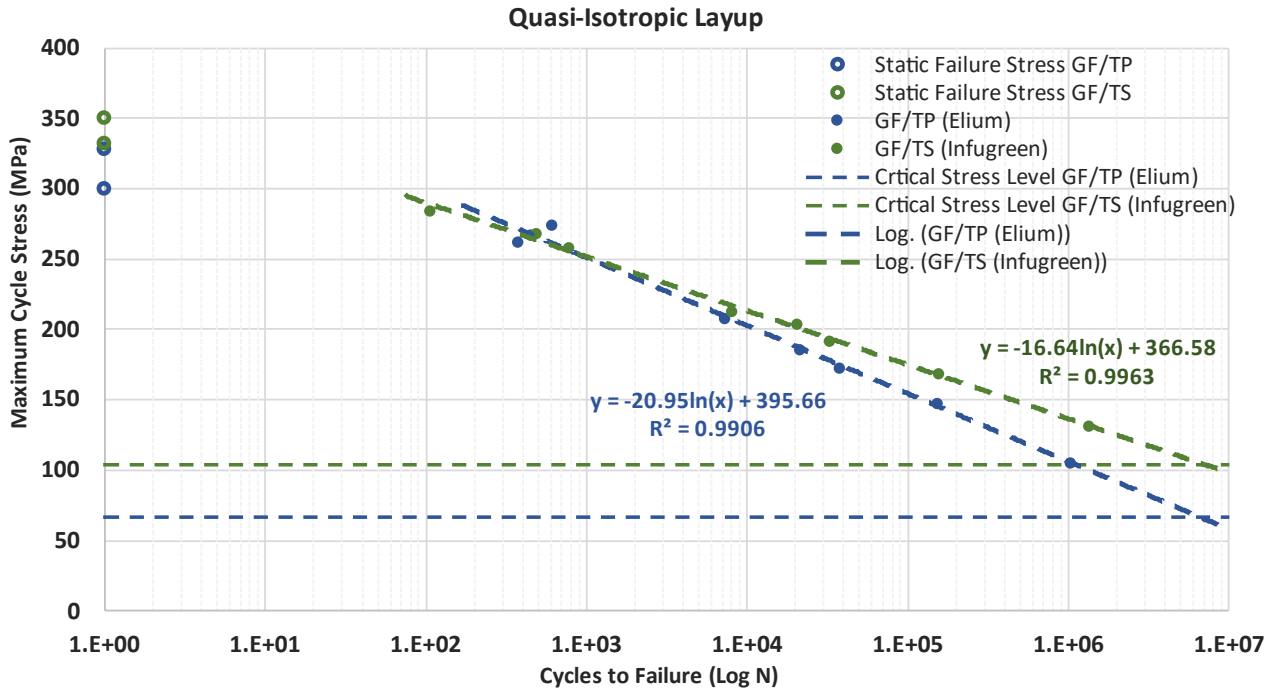

Figure 4. 24 S-N Curve for GF/Infugreen and GF/Elium in quasi-isotropic configuration.

This project has received funding from the European Union's Horizon 2020 research and innovation programme under grant agreement No 952966.

Table 4. 3 Regression analysis of S-N data for quasi-isotropic GF/Infugreen and GF/Elium composites.

Laminate configuration	Infugreen		Elium	
	Logarithmic	**Power**	**Logarithmic**	**Power**
Quasi-isotropic	**$y = -16.64 \ln(x) + 366.58$** **$R^2 = 0.9963$**	$y = 441.91\, x^{-0.083}$ $R^2 = 0.9780$	**$y = -20.95 \ln(x) + 395.66$** **$R^2 = 0.9906$**	$y = 554.57\, x^{-0.114}$ $R^2 = 0.9702$

Note: Best fit highlighted in bold green font.

4.3.2. Thermography

Temperature stabilisation fatigue tests were performed to obtain the critical stress limit of the composites in time efficient manner. To achieve this step-wise constant load amplitude fatigue tests were performed according to the protocol described in the test methods section. Figure 4. 25 and Figure 4. 26 presents the evolution of the damage and specimen temperature during the stepwise testing of quasi-isotropic GF/Elium and GF/Infugreen respectively. Damage is presented as damage factor (D) which is the lost in stiffness obtained using the 1Equation Damage factor (D) = 1- Ei/E0 . Additionally, the rise in specimen temperature of each block was plotted against the maximum stress level applied, as shown in Figure 4. 27 and Figure 4. 28 for GF/Elium and GF/Infugreen respectively. It is evident from the plot that the data points can be fit into 2 different linear trendlines. In this graphical method the stress level at the intersection of these linear trendlines is considered the critical stress limit. This can physically be interpreted as the stress level after with the rate of damage accumulation rises at a hight rate compared to damage accumulation below this stress level. A critical stress limit of 66.76 MPa and 104.33 MPa was obtained for GF/Elium and GF/Infugreen respectively. This critical stress limits are depicted in Figure 4. 24 on the S-N curve indicating that quasi-isotropic GF/Infugreen can with stand approximately 10 million cycles at this stress level.

This project has received funding from the European Union's Horizon 2020 research and innovation programme under grant agreement No 952966.

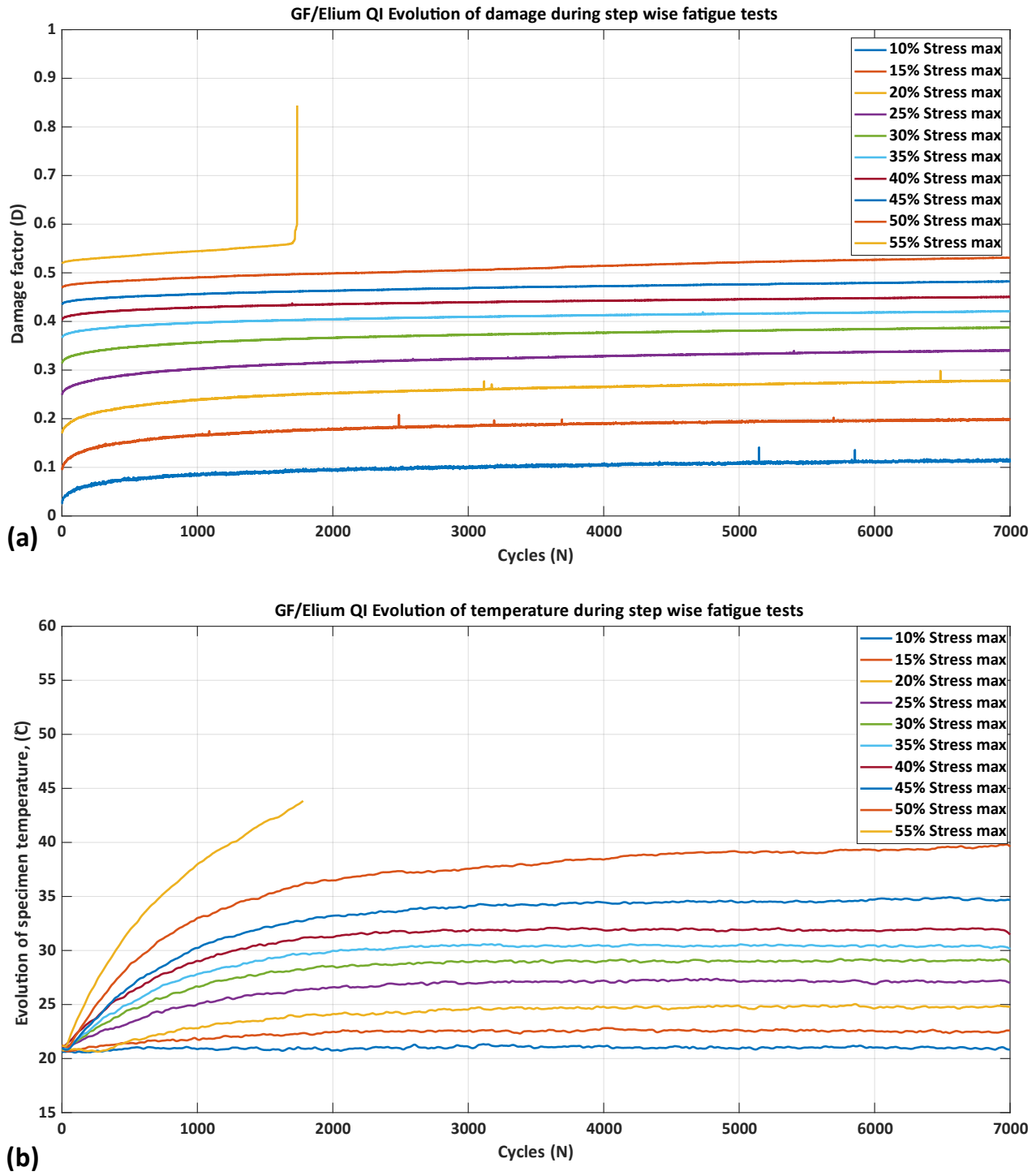

Figure 4. 25 Evolution of (a) Damage and (b) Temperature in quasi-isotropic GF/Elium composite during stepwise tests.

This project has received funding from the European Union's Horizon 2020 research and innovation programme under grant agreement No 952966.

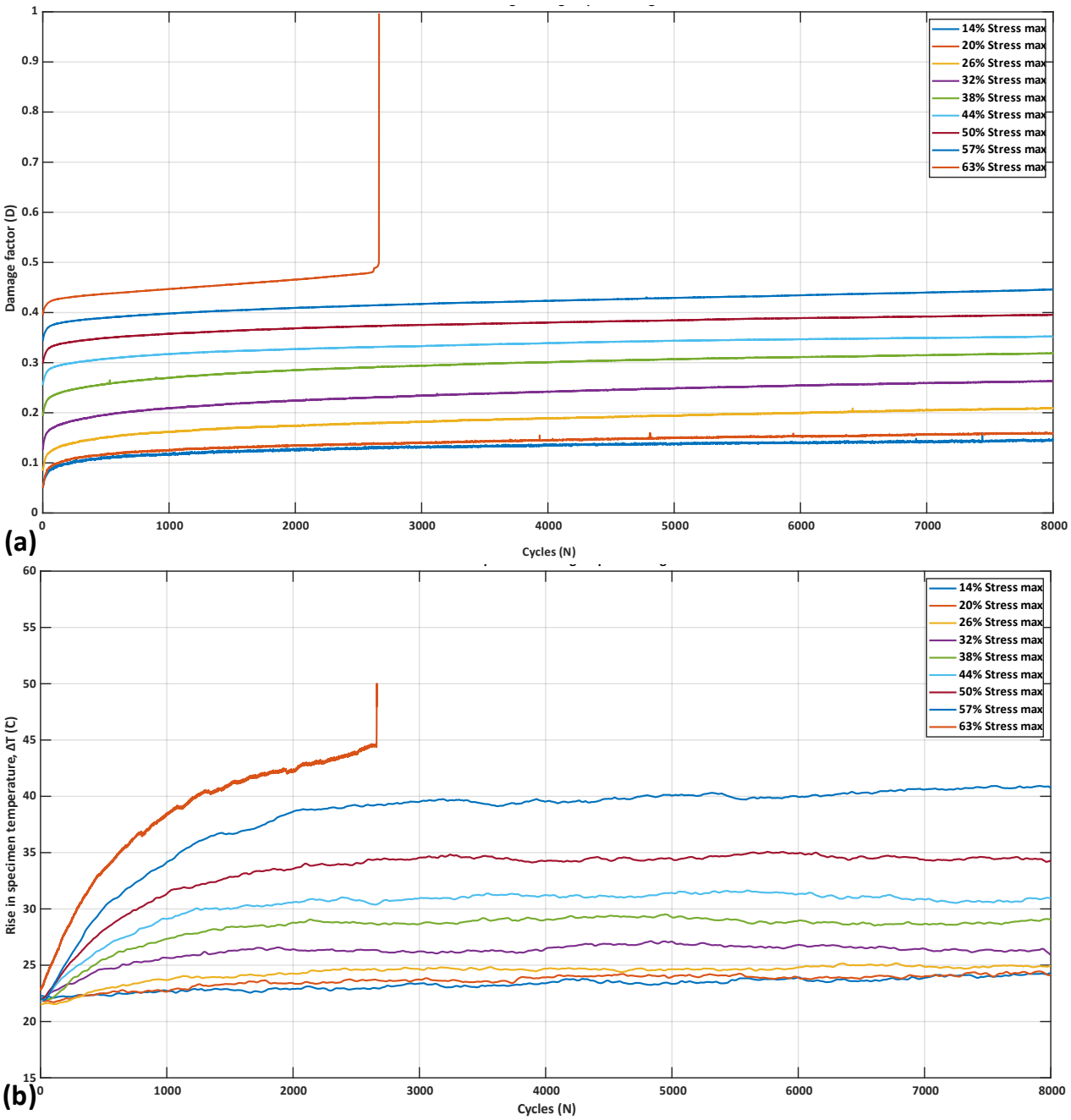

Figure 4. 26 Evolution of (a) Damage and (b) Temperature in quasi-isotropic GF/Infugreen composite during stepwise tests.

This project has received funding from the European Union's Horizon 2020 research and innovation programme under grant agreement No 952966.

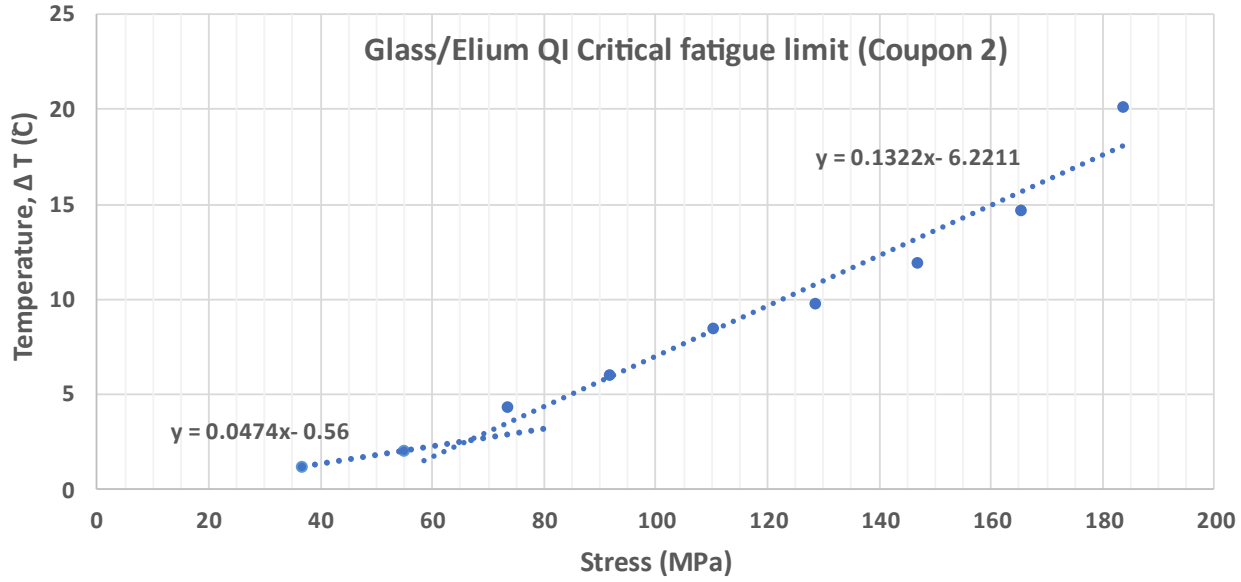

Figure 4. 27 Change in specimen temperature at the end of each load block as a function of the maximum stress applied for quasi-isotropic GF/Infugreen to determine the critical stress limit.

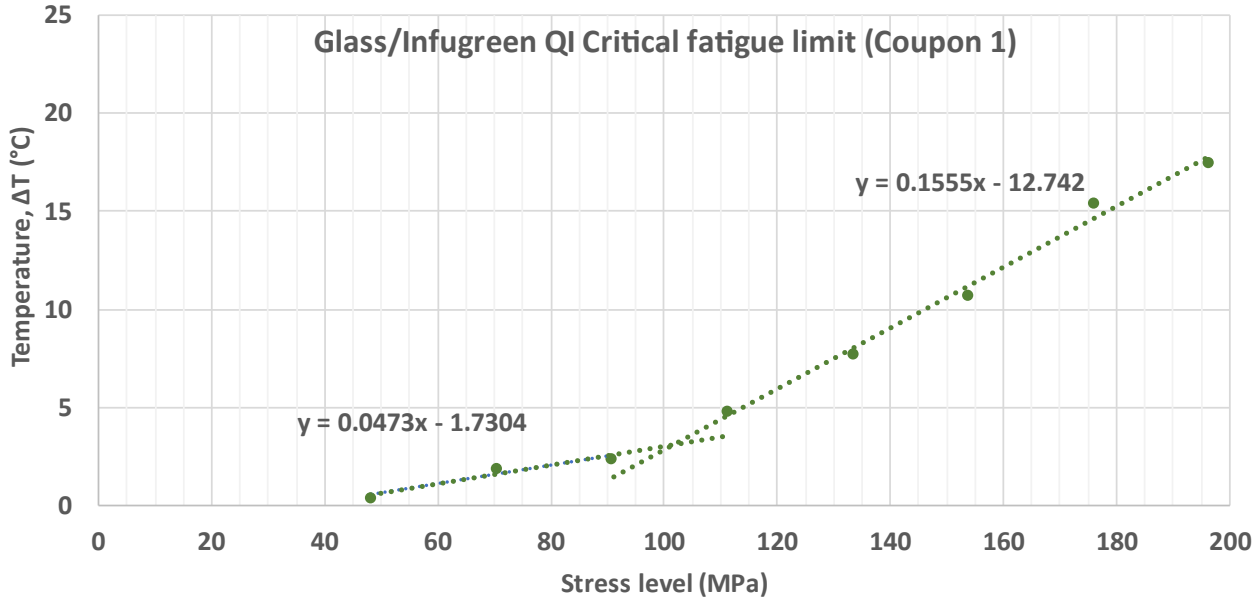

Figure 4. 28 Change in specimen temperature at the end of each load block as a function of the maximum stress applied for quasi-isotropic GF/Infugreen to determine the critical stress limit.

This project has received funding from the European Union's Horizon 2020 research and innovation programme under grant agreement No 952966.

4.3.3. Fractography and failure analysis

The GF/Elium fatigue tested specimens of QI configuration can be seen in Figure 4. 29. The location of final failure in the specimens is indicated in the figure. Observation of the coupons during tests revealed that the failure initiated in the 90° and ±45° plies, which was evident from the whitening of the test coupon. Additionally significant edge delamination was observed during the test progress. In addition, splitting of the 0˚ fibres in the outer plies was observed, which occurred from the cut edges of the coupon. Figure 4. 30 shows the SEM images of the fracture surface of a low-cycle fatigue tested GF/Elium specimen. Fibre splitting, fibre-breakage, fibre-matrix debonding was observed in the plies of different orientations as seen. Evidence of matrix deformation was seen in the plies oriented at different angles to the loading direction. The presence of fatigue cracks was also observed on the fracture surface. For comparison, fracture surface images from the high-cycle fatigue tested GF/Elium specimen is included in Figure 4. 31. As in the case of low-cycle fatigue specimen, fibre breakage in plies oriented at different angles were seen. Evidence of matrix cracks in a direction perpendicular to the loading direction was recorded. A comparison of the low-cycle and high-cycle test specimens indicated a difference in the extent of matrix plastic deformation. Extensive fibre debonding from the matrix in the 45° ply was observed. The presence of matrix cracks between adjacent fibres leading to final fibre splitting and eventual breakage was evidenced from the images.

Figure 4. 29 GF/Elium Quasi-Isotropic (QI) fatigue test specimens after failure with location of final failure indicated on the specimens.

This project has received funding from the European Union's Horizon 2020 research and innovation programme under grant agreement No 952966.

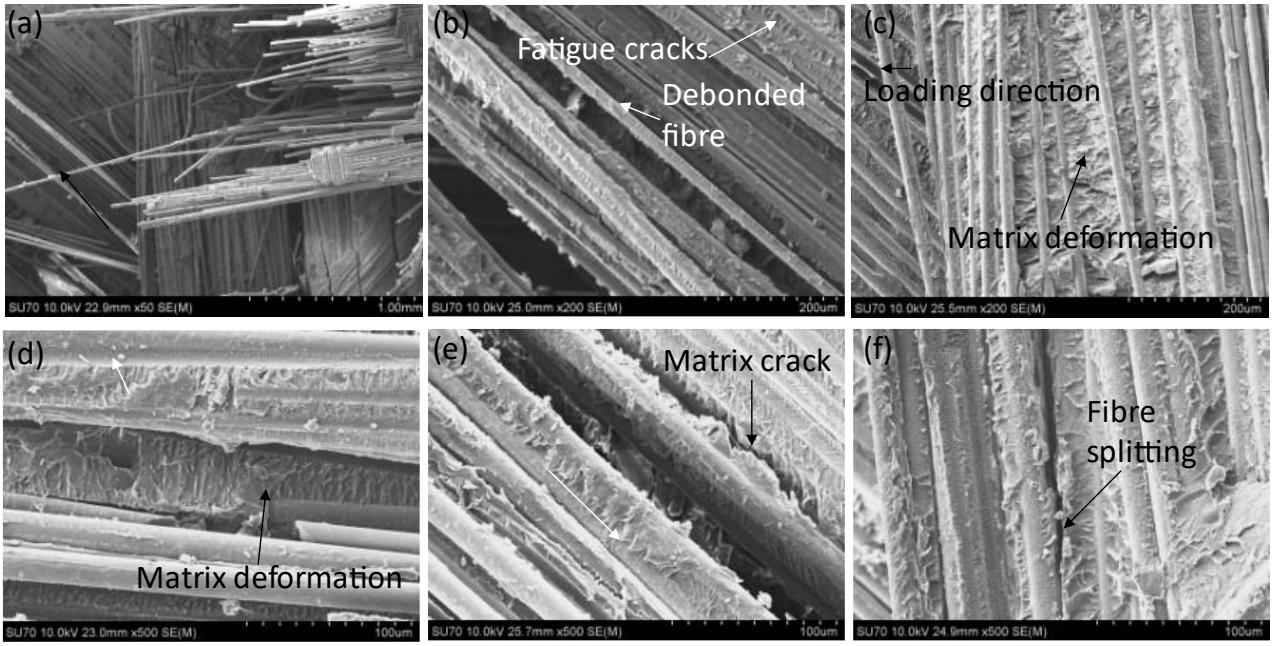

Figure 4. 30 SEM images of the fracture surface of low-cycle fatigue tested GF/Elium QI specimen showing the failure mechanisms observed.

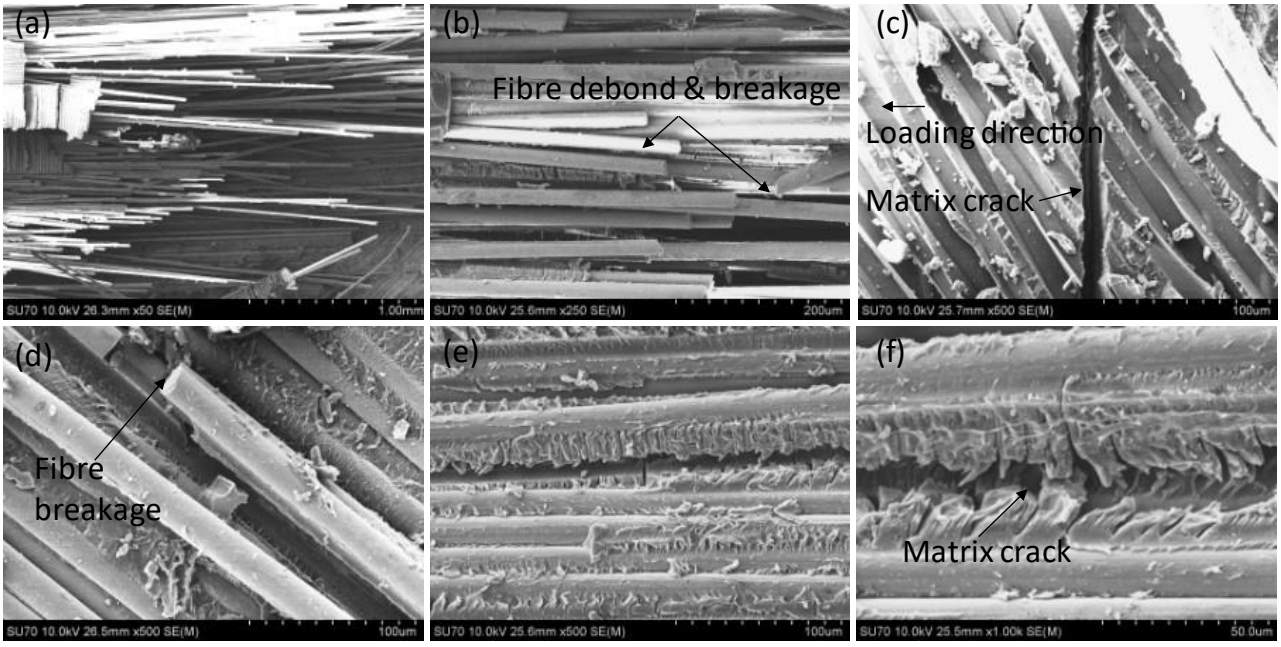

Figure 4. 31 SEM images of the fracture surface of high-cycle fatigue tested GF/Elium QI specimen showing the failure mechanisms observed.

This project has received funding from the European Union's Horizon 2020 research and innovation programme under grant agreement No 952966.

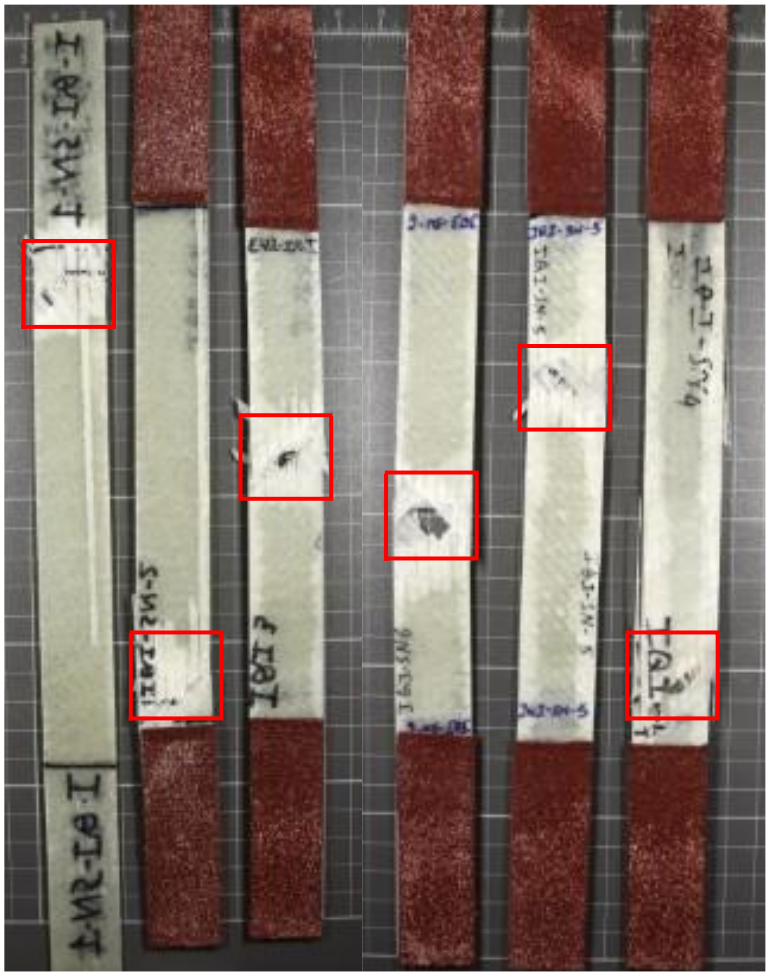

Figure 4. 32 GF/Infugreen Quasi-Isotropic (QI) fatigue test specimens after failure with location of final failure indicated on the specimens.

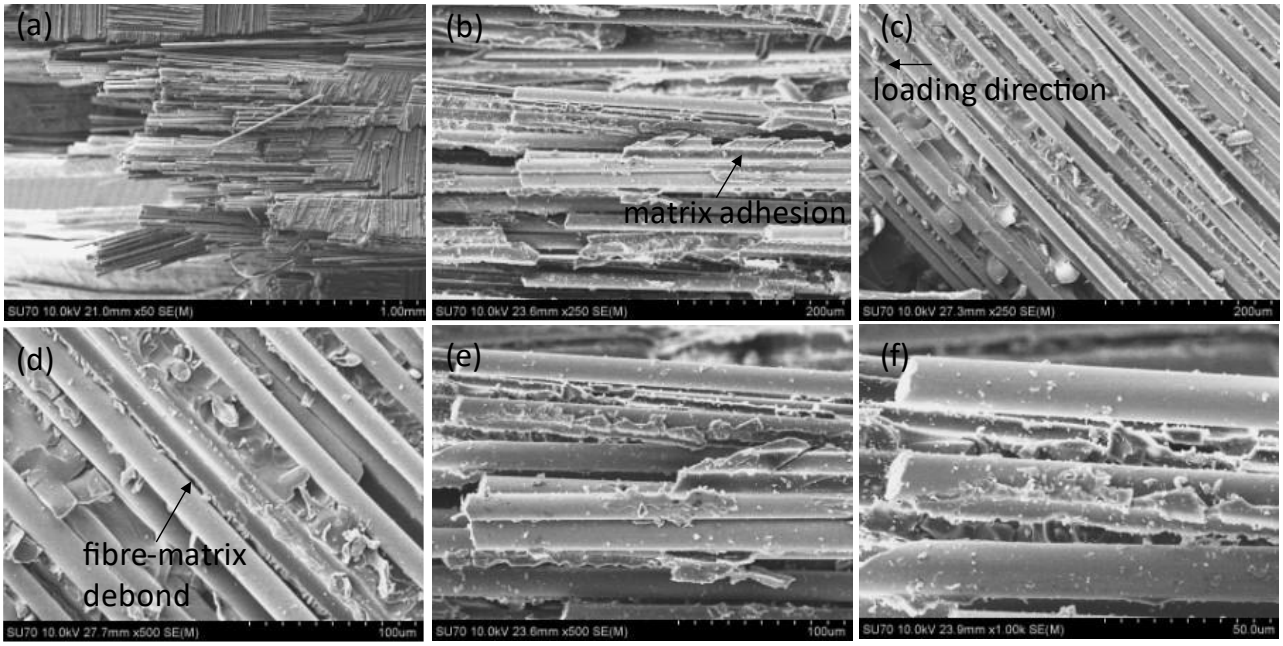

Figure 4. 33 SEM images of the fracture surface of low-cycle fatigue tested GF/Infugreen QI specimen showing the failure mechanisms observed.

This project has received funding from the European Union's Horizon 2020 research and innovation programme under grant agreement No 952966.

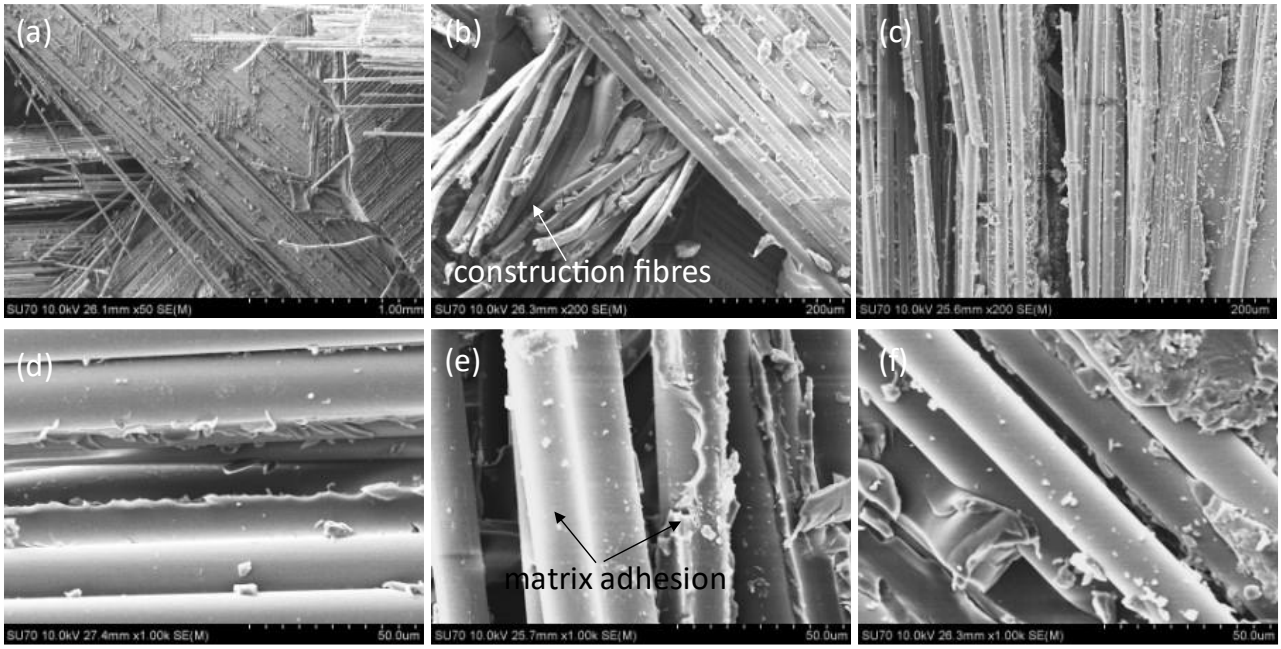

Figure 4. 34 SEM images of the fracture surface of high-cycle fatigue tested GF/Infugreen QI specimen showing the failure mechanisms observed.

The fatigue tested GF/Infugreen specimen fracture surfaces were also examined using SEM. Figure 4. 32 presents the typical GF/Infugreen specimens after testing highlighting the location of final failure in specimens. As in the case of GF/Elium specimens, final failure in the specimens indicated failure in the off-axis plies in the specimens. However, fibre splitting in the 0° plies in specimens was not as pronounced as in the case GF/Elium specimens. Damage was more localized as seen in Figure 4. 32. Figure 4. 33 shows the fracture surface of the GF/Infugreen specimen subjected to low-cycle fatigue. The fibre surfaces appeared cleaner as compared to the GF/Elium specimens. However, evidence of matrix adhesion to the fibres after failure could be observed. Mechanisms such as fibre-matrix debonding, fibre splitting, and breakage were commonly seen. Similar observations were made in case of the specimen subjected to high-cycle fatigue as seen from Figure 4. 34. As seen in Figure 4. 34, the fibre surfaces were largely smooth in case of the fibres oriented at ±45° to the loading direction. However, matrix adhesion was pronounced in case of fibres oriented along the fibre direction. As compared to GF/Elium composite, matrix deformation was lesser with the absence of river marks on the fracture surface.

This project has received funding from the European Union's Horizon 2020 research and innovation programme under grant agreement No 952966.

4.4. ±30° (Relative to loading direction)

The tension-tension fatigue tests to establish the S-N curve for the glass fibre composites in the oblique configuration was achieved by conducting fatigue loading tests on composite coupons manufactured with the layup $[+30^\circ, -30^\circ]_{6s}$ where fibres are at at ±30° with respect to the loading direction. The tests were conducted at a frequency of 5 Hz with an R ratio of 0.1. Static tensile test was conducted on the coupons to obtain the ultimate tensile failure strength (σ_{uts}). It was found that the ultimate tensile strength of the quasi-isotropic composite coupons was 335.13 MPa and 345.91 MPa for GF/Infugreen and GF/Elium composites respectively. The stress parameters & load values for tension-tension fatigue tests were decided based on these values.

4.4.1. S-N Curve

Figure 4. 35 presents the S-N curves for ±30° GF/Elium and GF/ Infugreen composites. The maximum cycle stress and cycles to failure (S-N) data obtained was plotted on a semi-log plot. Regression analysis was done by fitting a curve following power law with 2 terms. Table 4. 4 summarises the obtained regression equations and R^2 values. It was seen that the data fitted well with the power law equation, which is evident from the variance (R^2) value. The fatigue behaviour of composites is almost close to that of metals with distinct fatigue limit.

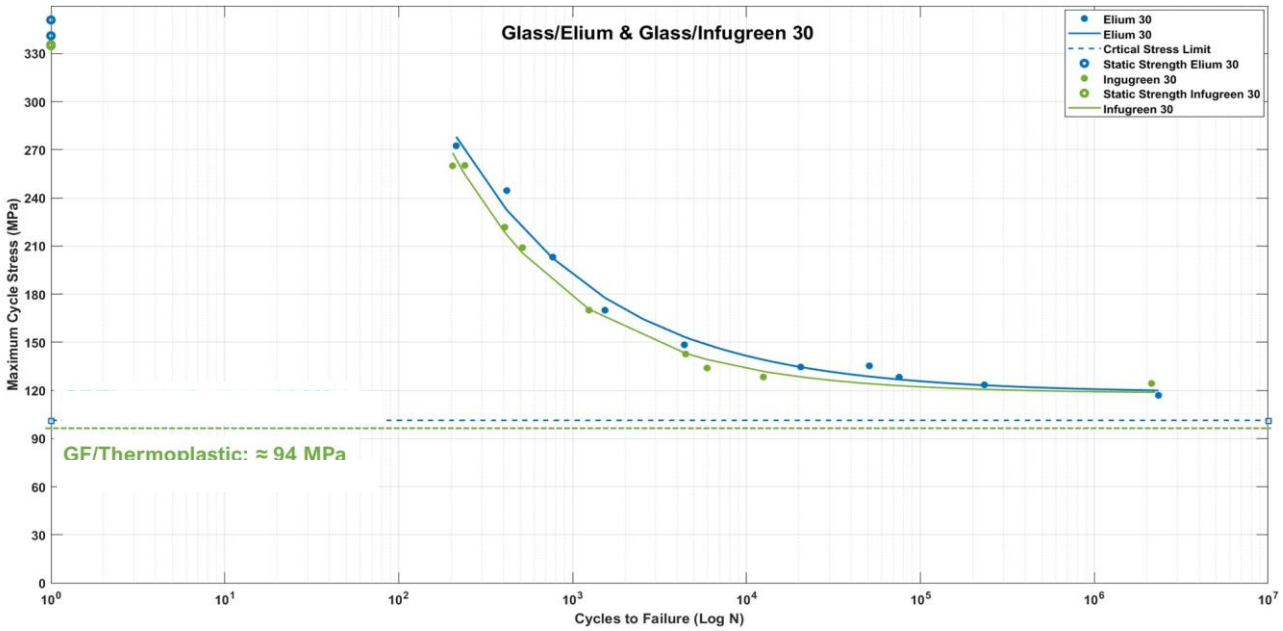

Figure 4. 35 S-N Curve for Glass fibre – Infugreen and Elium with fibres in the [±30°] orientation.

Table 4. 4 Regression analysis of S-N data for ±30° GF/Infugreen and GF/Elium composites.

Laminate configuration	GF/Infugreen	GF/Elium
	Power law (2 Terms)	Power law (2 Terms)
±30°	$y = 3304\,x^{-0.5816} + 118.1$ $R^2 = 0.9922$	$y = 3304\,x^{-0.5816} + 118.1$ $R^2 = 0.9922$

This project has received funding from the European Union's Horizon 2020 research and innovation programme under grant agreement No 952966.

4.4.2. Thermography

Temperature stabilisation fatigue tests were performed to obtain the critical stress limit of the composites in time efficient manner. To achieve this step-wise constant load amplitude fatigue tests were performed according to the protocol described in the test methods section. Figure 4. 36 and Figure 4. 37 presents the evolution of the damage and specimen temperature during the stepwise testing of ±30° GF/Elium and GF/Infugreen respectively. Damage is presented as damage factor (D) which is the lost in stiffness obtained using the 1Equation Damage factor (D) = 1- Ei/E0 . Additionally, the rise in specimen temperature of each block was plotted against the maximum stress level applied, as shown in Figure 4. 38 and Figure 4. 39 for GF/Elium and GF/Infugreen respectively. It is evident from the plot that the data points can be fit into 2 different linear trendlines. In this graphical method the stress level at the intersection of these linear trendlines is considered the critical stress limit. This can physically be interpreted as the stress level after with the rate of damage accumulation rises at a hight rate compared to damage accumulation below this stress level. A critical stress limit of 91.03 MPa and 94.84 MPa was obtained for GF/Elium and GF/Infugreen respectively. This critical stress limits are depicted in Figure 4. 35 on the S-N curve indicating that ±30° GF/Elium and GF/Infugreen can with stand approximately anything more 10 million cycles at this stress level.

This project has received funding from the European Union's Horizon 2020 research and innovation programme under grant agreement No 952966.

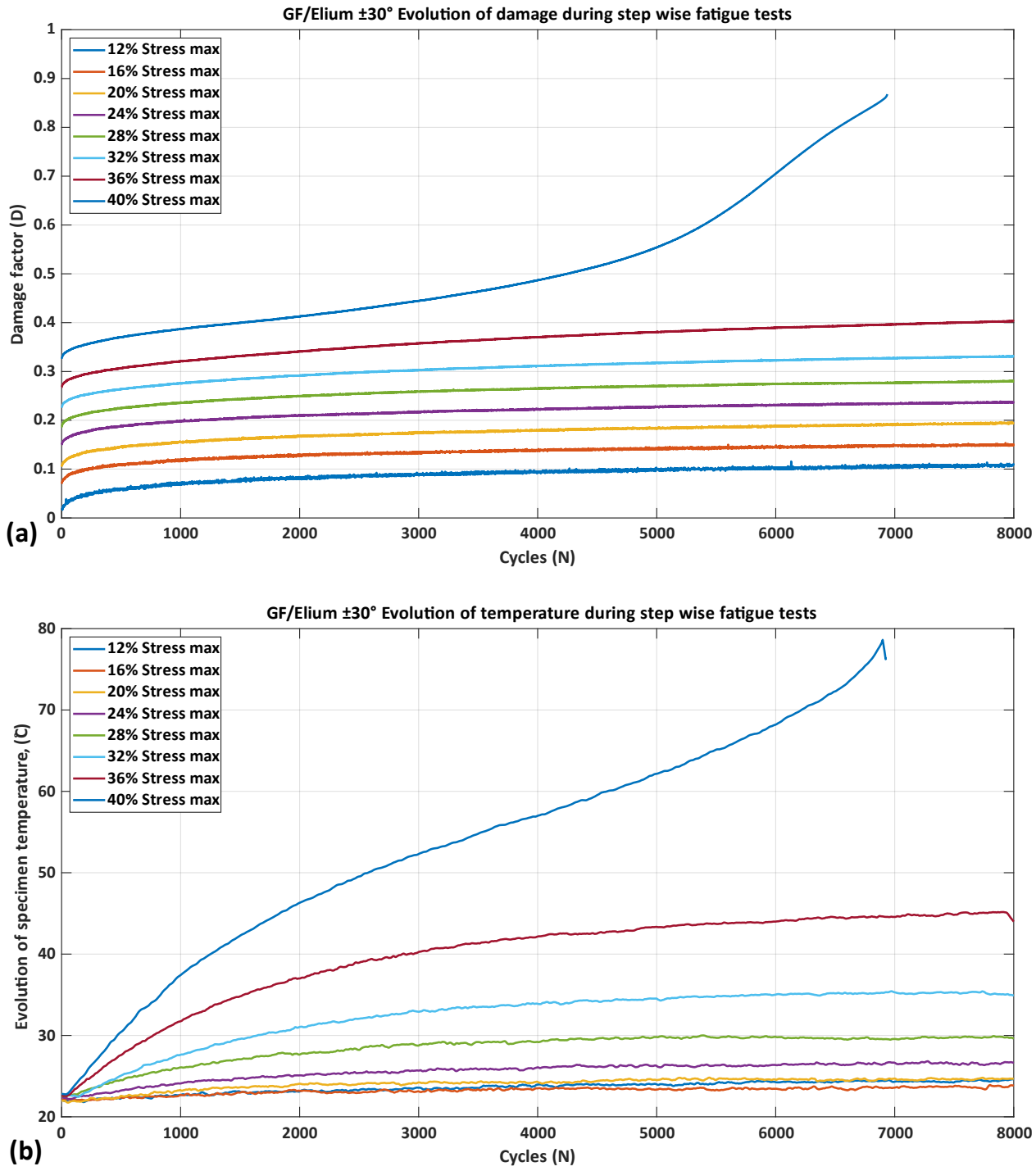

Figure 4. 36 Evolution of (a) Damage and (b) Temperature in ±30˚GF/Elium composite during stepwise tests

This project has received funding from the European Union's Horizon 2020 research and innovation programme under grant agreement No 952966.

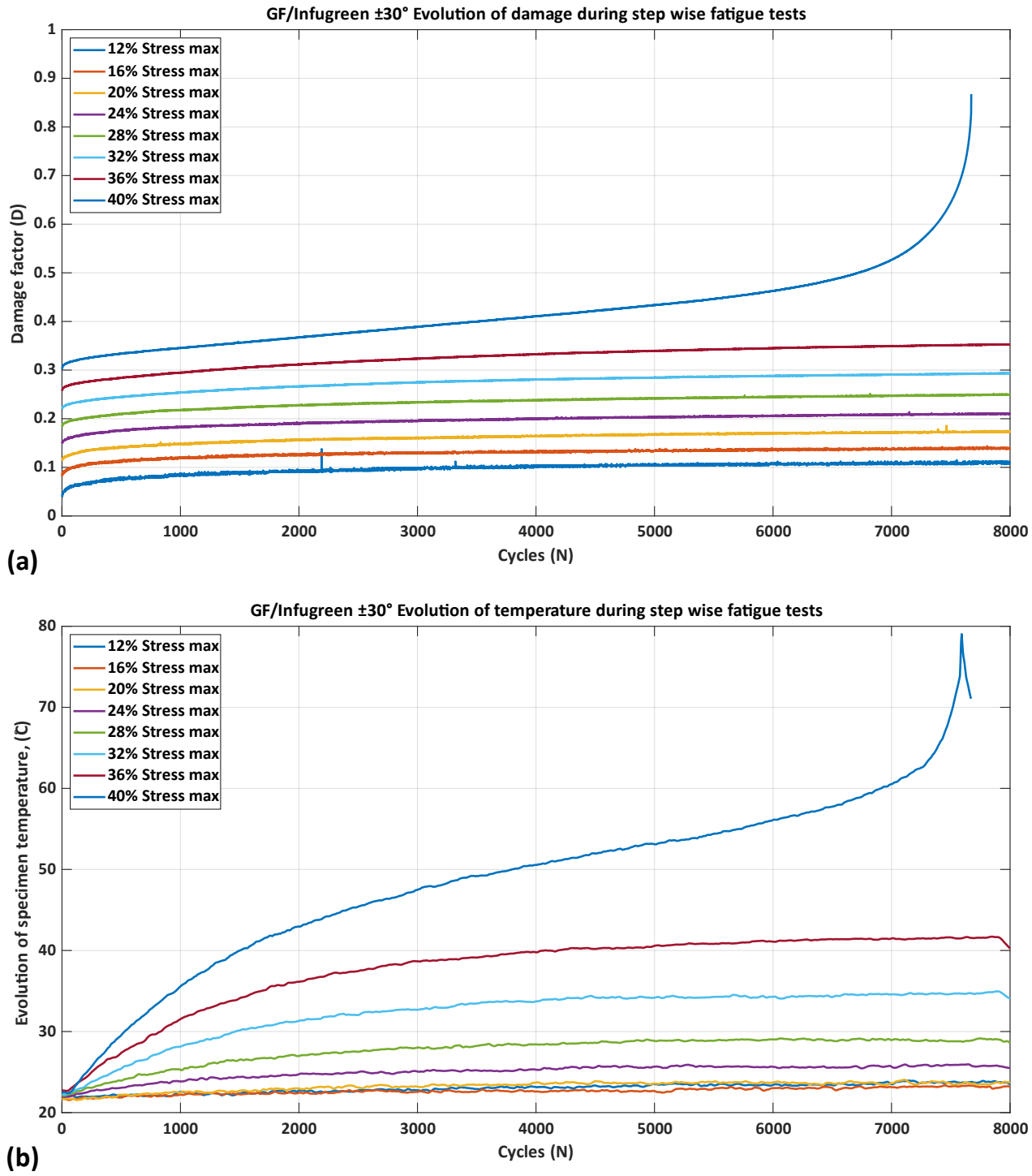

Figure 4. 37 Evolution of (a) Damage and (b) Temperature in ±30˚GF/Infugreen composite during stepwise tests

This project has received funding from the European Union's Horizon 2020 research and innovation programme under grant agreement No 952966.

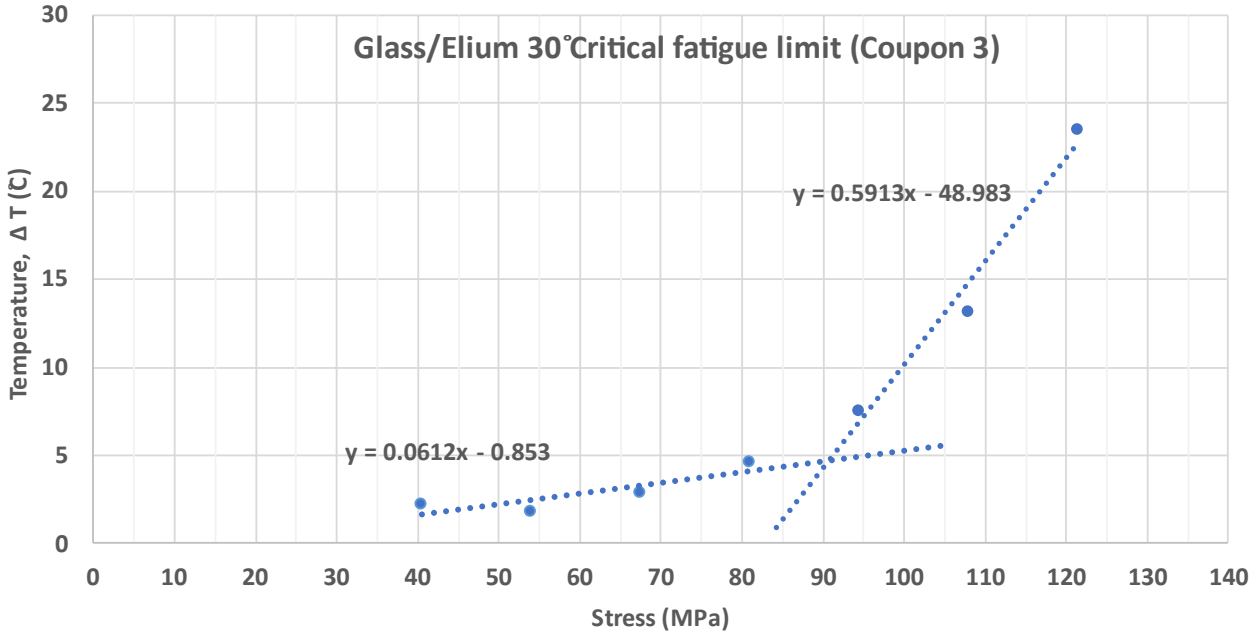

Figure 4. 38 Change in specimen temperature at the end of each load block as a function of the maximum stress applied for [±30°] GF/Elium to determine the critical stress limit.

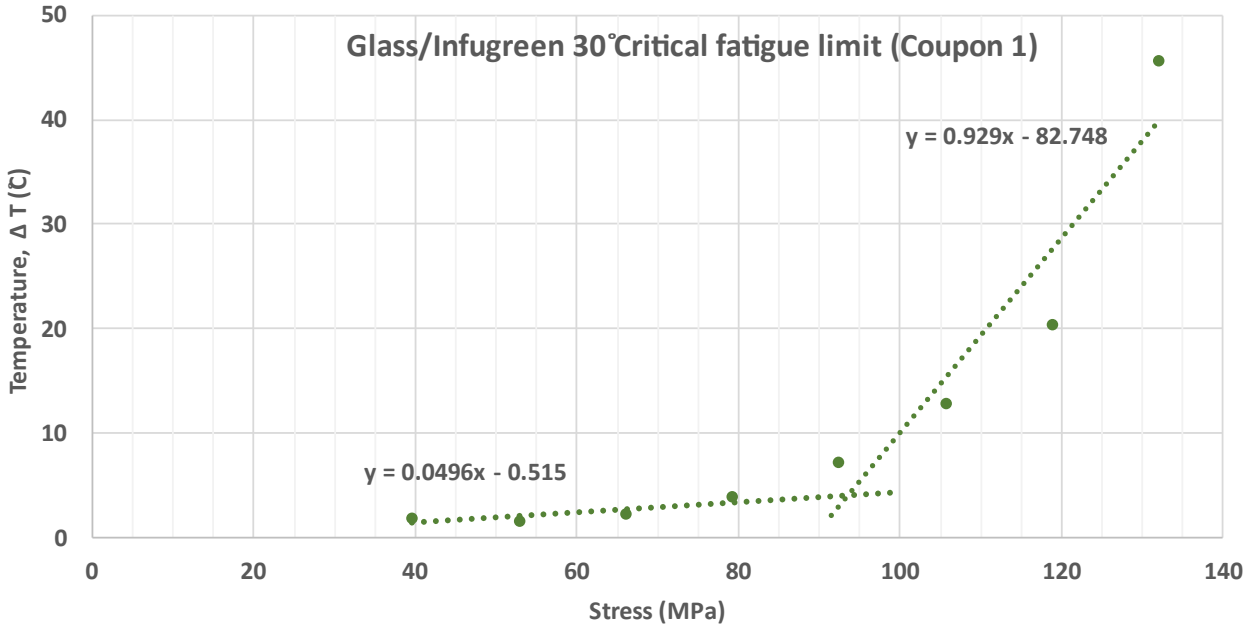

Figure 4. 39 Change in specimen temperature at the end of each load block as a function of the maximum stress applied for [±30°] GF/Infugreen to determine the critical stress limit.

This project has received funding from the European Union's Horizon 2020 research and innovation programme under grant agreement No 952966.

4.4.3. Fractography and failure analysis

Similar to other configurations, fatigue tested specimens of the ±30° lay-up configuration were examined using SEM. Prior to testing, the cross-section of untested GF/Elium and GF/Infugreen composites were also examined. The SEM images of pristine coupon is presented in Figure 4. 40. The images provide information about the fibre architecture in the specimens. Figure 4. 40 (a) to (c) correspond to GF/Elium composite and Figure 4. 40 (d) to (f) were obtained from GF/Infugreen composite specimen. As in previous cases, the construction fibres were seen to be displaced and grouped during the infusion process. This was observed in both the types of composites considered. Further, images taken at higher magnifications confirmed the absence of manufacturing defects (voids) prior to testing. However, the presence of matrix-rich areas was observed in the pristine specimen cross-sections of the composites. The GF/Elium specimens subjected to fatigue testing are shown in

Figure 4. 41. Specimen failure was seen to occur in the gage region as seen. Further, delamination between the individual plies in the specimens was observed in addition to fibre breakage. Specimen necking was observed due to rotation of the fibres aligning to the loading direction. To gain further insight, the fracture regions were examined with SEM. Figure 4. 42 presents the SEM images taken from the low-cycle fatigue tested GF/Elium specimen. Fibre splitting and breakage was commonly observed in all the plies. The fracture process led to fibre-matrix debonding with small chunks of the matrix material still adhering to the fibre surfaces. Evidence of matrix cracks in a direction along the fibre orientation that leads to fibre splitting was seen. Exposed regions on the fracture surface due to ply delamination indicated sub-surface fibres to be held intact by the matrix. However, the exposed ply surface also provided evidence of the matrix undergoing plastic deformation prior to delamination.

Figure 4. 43, shows the SEM images corresponding to high-cycle fatigue tested GF/Elium specimen. Signs of fibre breakage and delamination failure are clear from the SEM images. However, fibre splitting was not as pronounced as seen in low cycle specimens. Many fibres were seen to be held intact by the matrix. However, the fracture surfaces indicated the matrix material to have undergone plastic deformation extensively. River marks were widely seen on the exposed ply surface on account of delamination. The observations indicate that the failure process was gradual in the case of the high-cycle fatigue tested specimens.

The low-cycle and high-cycle fatigue tested GF/Infugreen specimens were also subjected to fractography assessment. Figure 4. 44 shows the tested GF/Infugreen specimens with the location of final failure indicated in the Figure.

The final failure was localized as can be seen and resulted in ply delamination failure. Fibre breakage in the plies was also observed. The overall failure was observed to be similar to the GF/Elium composites. Specimen necking due to ply rotation towards the loading axis was observed even in this case. Figure 4. 45 shows the SEM images taken from a low-cycle fatigue tested GF/Infugreen specimen. Matrix cracks leading to fibre splitting and fibre breakage was typically observed. Due to fibre splitting and subsequent breakage, adhesion of matrix material to fibre surface was seen at several locations. Matrix deformation was not as pronounced as seen in the case of GF/Elium composites tested under similar conditions. The exposed ply surface on account of delamination showed many fibres to be intact similar to that observed previously in

This project has received funding from the European Union's Horizon 2020 research and innovation programme under grant agreement No 952966.

case of GF/Elium composite. The SEM images from the high-cycle fatigue tested specimen is presented in Figure 4. 46. As in the case of GF/Elium composite, fibre breakage was observed but many fibres were seen to be held in position by the matrix material. However, the exposed fibre surfaces indicated that matrix adhesion was less pronounced in case of GF/Infugreen composite as compared to the GF/Elium composite. Therefore, fibre surfaces were relatively smoother as compared to that in case of GF/Elium specimens. The difference in fracture characteristics, especially matrix deformation during loading can result in a difference in fatigue behavior between GF/Elium and GF/Infugreen composites.

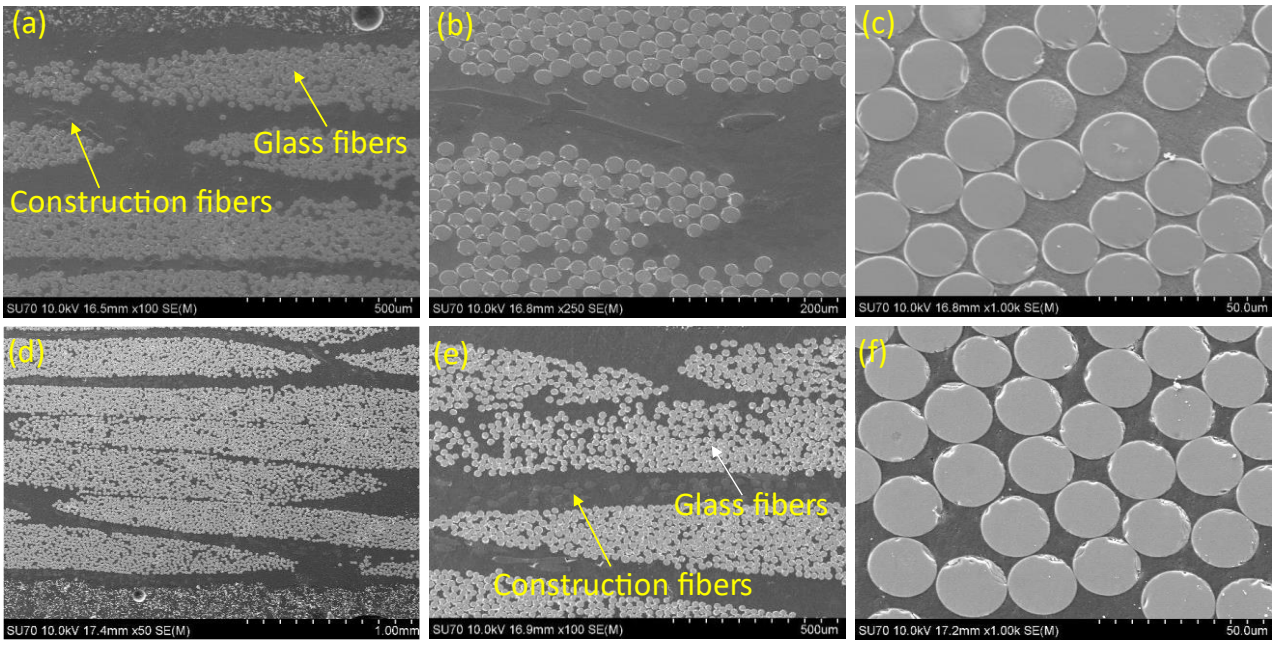

Figure 4. 40 SEM images from untested ±30° fatigue specimens, (a) to (c) GF/Elium specimen, (d) to (f) GF/Infugreen specimen.

This project has received funding from the European Union's Horizon 2020 research and innovation programme under grant agreement No 952966.

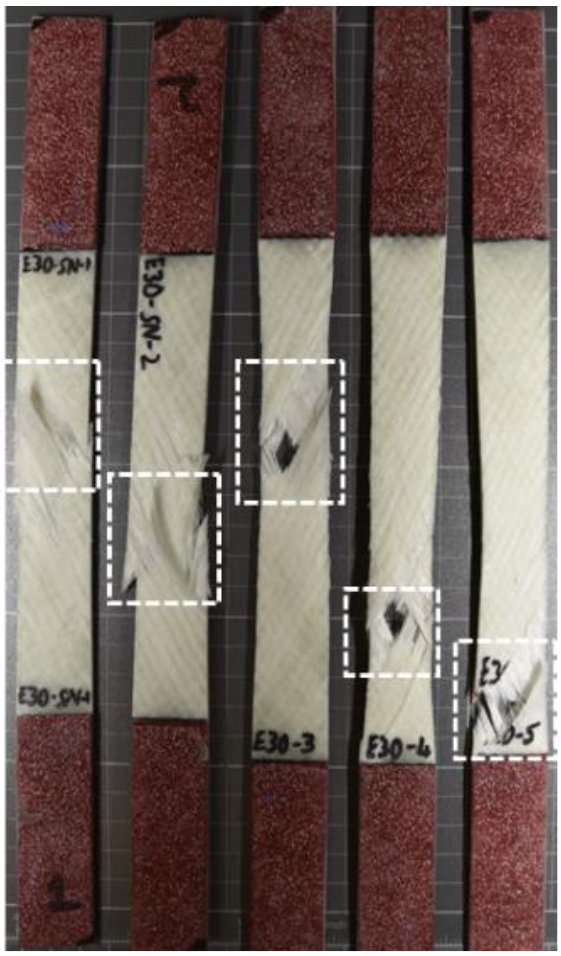

Figure 4. 41 GF/Elium ±30° fatigue test specimens after failure with location of final failure indicated on the specimens.

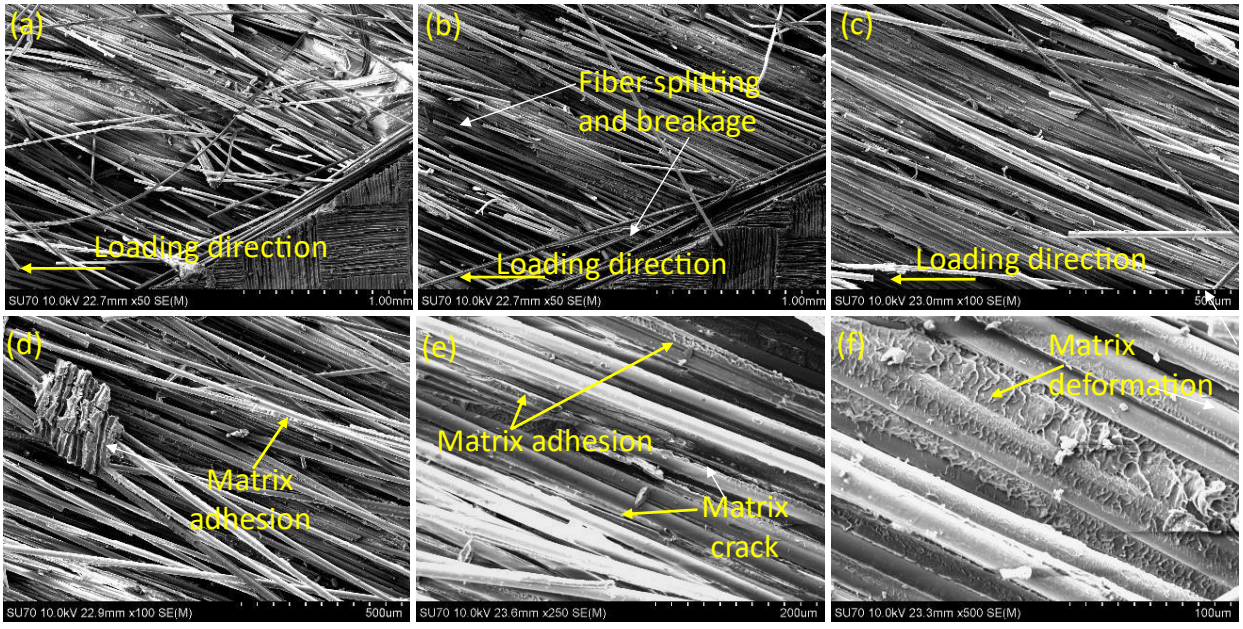

This project has received funding from the European Union's Horizon 2020 research and innovation programme under grant agreement No 952966.

Figure 4. 42 SEM images from a low-cycle fatigue tested GF/Elium ±30° specimen.

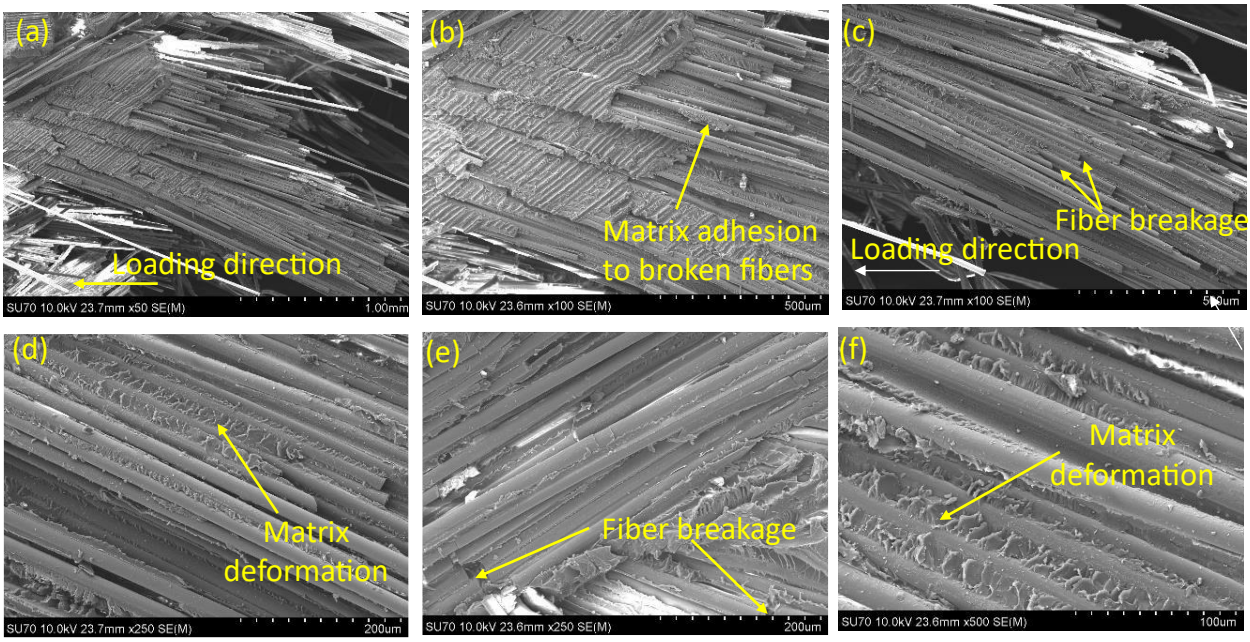

Figure 4. 43 SEM images from a high-cycle fatigue tested GF/Elium ±30° specimen.

This project has received funding from the European Union's Horizon 2020 research and innovation programme under grant agreement No 952966.

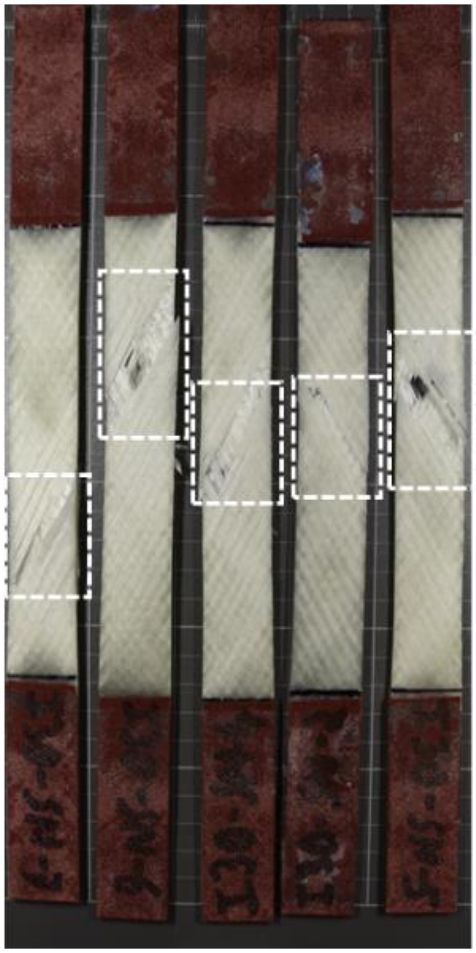

Figure 4. 44 GF/Infugreen ±30° fatigue test specimens after failure with location of final failure indicated on the specimens.

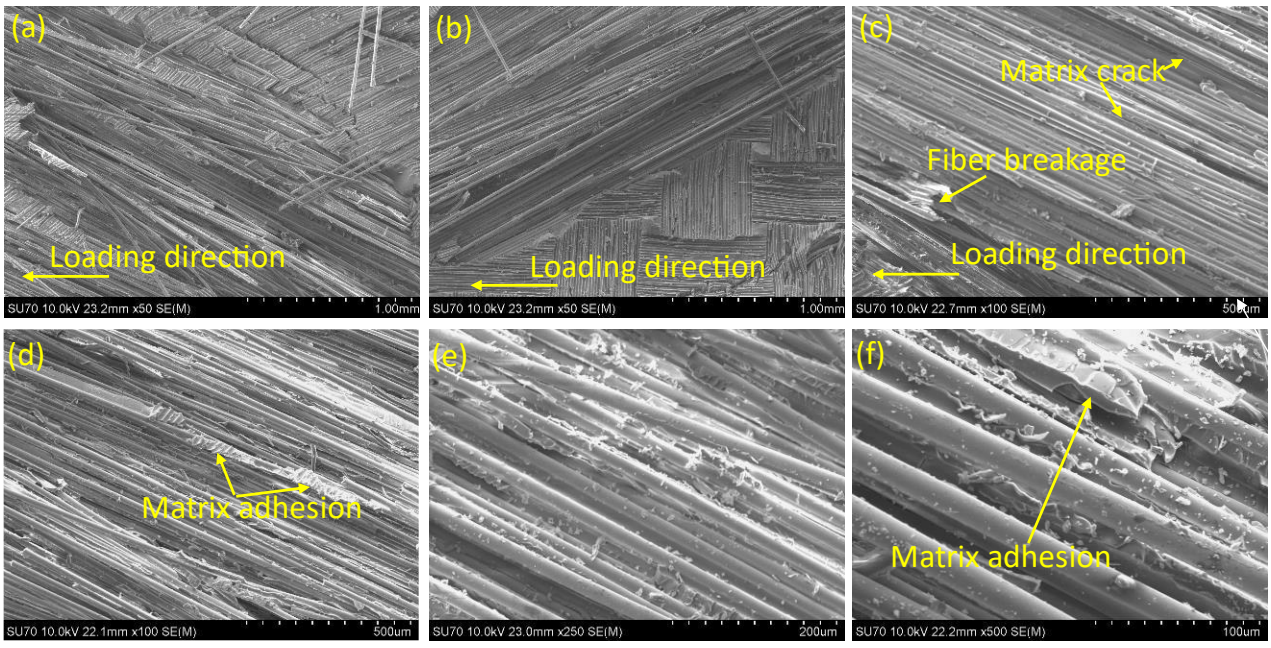

Figure 4. 45 SEM images from a low-cycle fatigue tested GF/Infugreen ±30° specimen.

This project has received funding from the European Union's Horizon 2020 research and innovation programme under grant agreement No 952966.

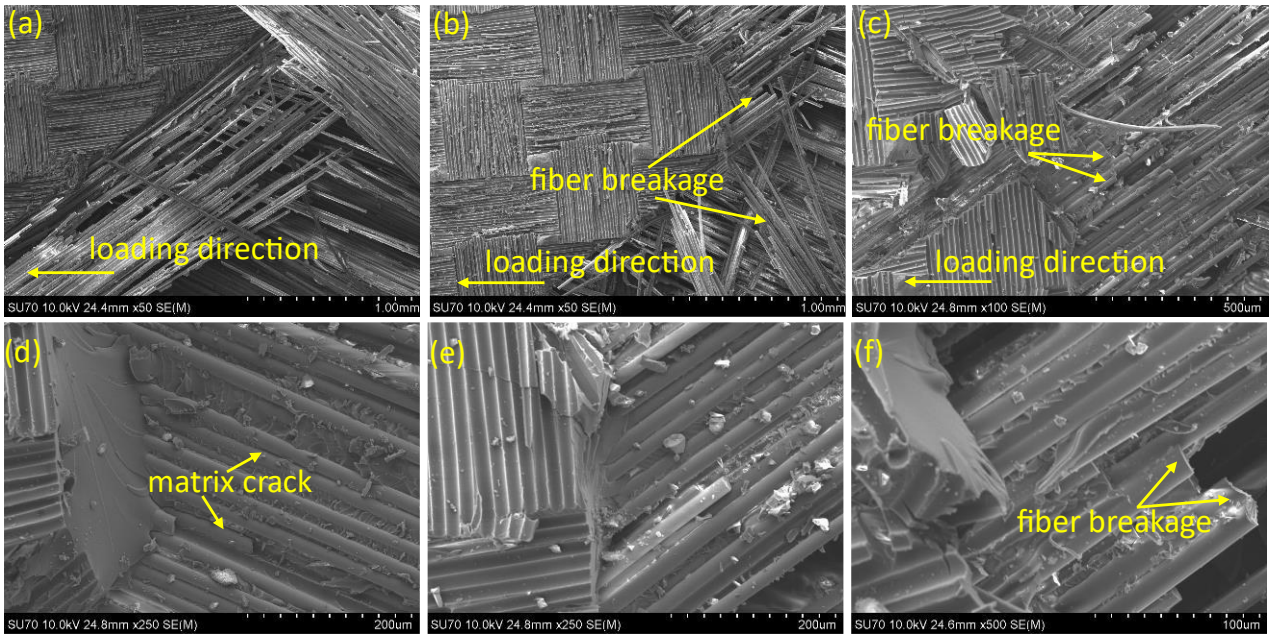

Figure 4. 46 SEM images from a high-cycle fatigue tested GF/Infugreen ±30° specimen.

This project has received funding from the European Union's Horizon 2020 research and innovation programme under grant agreement No 952966.

4.5. Unidirectional 0° (Relative to loading direction)

The tension-tension fatigue tests to establish the S-N curve for the glass fibre composites with fibres oriented parallel to the loading direction (0˚) were conducted at a frequency of 5 Hz with an R ratio of 0.1. Static tensile tests were performed beforehand to obtain the tensile failure strength/ultimate tensile strength (σ_{uts}). It was found that the ultimate tensile strength of $[0^\circ]_{2S}$ GF/Elium and GF/Infugreen composites was 938.52 MPa and 977.94 MPa respectively. The stress levels for tension-tension fatigue tests were decided based on these values.

4.5.1. S-N Curve

The fatigue tests to establish the S-N curves for Unidirectional 0˚ GF/Elium and GF/Infugreen was the most challenging. Initially, the laminates were made of Saertex GF fabric which yielded coupons of 3 mm thickness. The failure mode under fatigue loading was not acceptable as the failure initiated at the grips. To overcome this issue, a second set of Unidirectional 0° laminates were made with Gerster fabric (12 layers) which yielded coupons of thickness 2.7 mm. Again, the same issue of failure close to the grips was encountered. It was found that the issue occurred due to high failure loads which required higher grip pressures to be maintained. As a remedy for this, a thinner laminate was made from 6 layers of Gerster GF fabric (1.7 mm Thick), and the results presented in this report belong to this third set of coupons. Figure 4. 47 shows S-N curves for 0˚ GF/Elium and GF/Infugreen.

The data obtained was plotted on a semi-log plot. Regression analysis was done by fitting a curve following logarithmic and power law. The Table 4. 5 summarises the obtained line equations and R^2 values. It was seen that the data fit well with both logarithmic equation and power law, which is evident from the variance (R^2) value. However, the Y intercept which denotes quasi-static strength is very high when power law is used, which is unrealistic. Hence, logarithmic equation is considered, which yields a linear curve on semi-log plot. This is accordance with the findings of Mandell et al. They observed that the composites made of unidirectional reinforcements, tend to follow logarithmic trend in a semi-log plot which yields a linear S-N curve [5,15,16]. Additionally, S-N curve of GF/Infugreen has a higher slope than that of the GF/Elium. This may signify that the GF/Elium composite exhibits a better high-cycle fatigue performance.

Table 4. 5 Regression analysis of S-N data for 0˚ GF/Infugreen and GF/Elium composites.

Laminate configuration	**GF/Infugreen**		**GF/Elium**	
	Logarithmic	**Power**	**Logarithmic**	**Power**
0°	**$y = -60.39 \ln(x) + 1185.5$** **$R^2 = 0.9429$**	$y = 1832.4\, x^{-0.117}$ $R^2 = 0.9352$	**$y = -41.86 \ln(x) + 932.36$** **$R^2 = 0.9231$**	$y = 1115.9\, x^{-0081}$ $R^2 = 0.9517$

This project has received funding from the European Union's Horizon 2020 research and innovation programme under grant agreement No 952966.

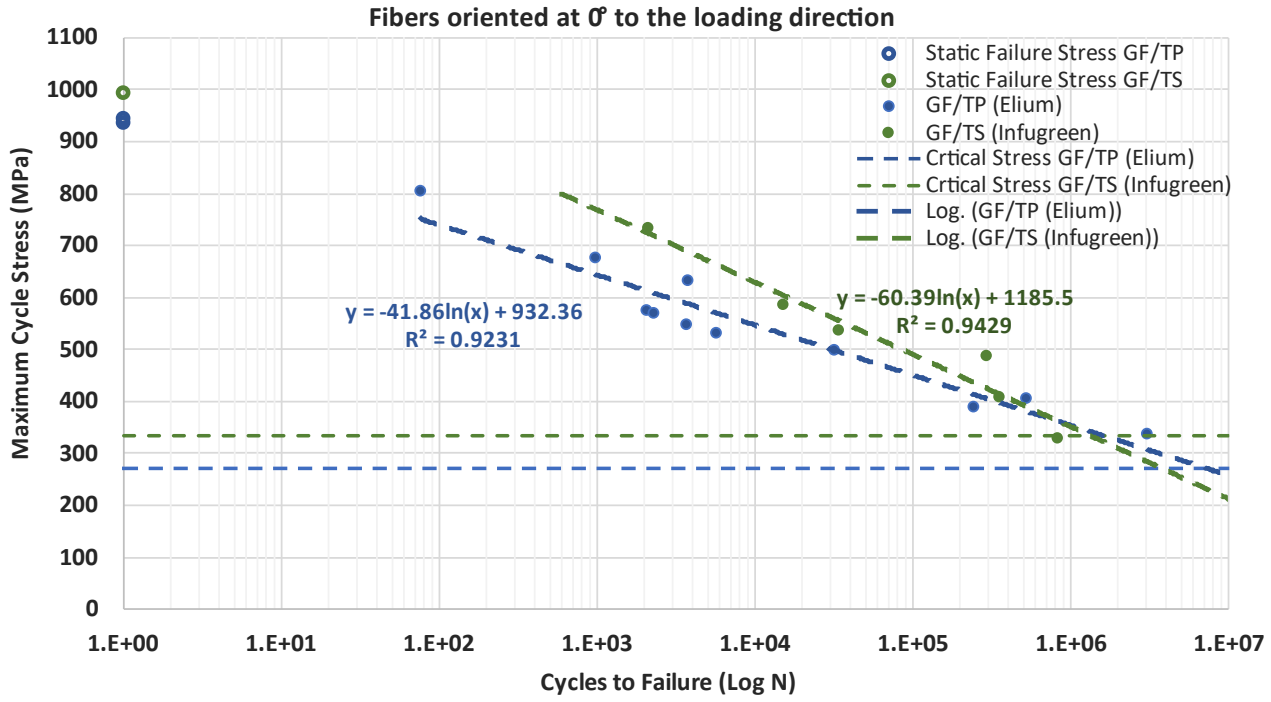

Figure 4. 47 S-N Curve for GF/Infugreen and GF/Elium with fibres oriented parallel (0°) to the loading direction.

4.5.2. Thermography

Temperature stabilisation fatigue tests were performed to obtain the critical stress limit of the composites in time efficient manner. To achieve this step-wise constant load amplitude fatigue tests were performed according to the protocol described in the test methods section. Figure 4. 48 and Figure 4. 49 presents the evolution of the damage and specimen temperature during the stepwise testing of 0° GF/Elium and GF/Infugreen respectively. Damage is presented as damage factor (D) which is the lost in stiffness obtained using the 1Equation Damage factor (D) = 1- Ei/E0 . Additionally, the rise in specimen temperature of each block was plotted against the maximum stress level applied, as shown in Figure 4. 50 and Figure 4. 51 for GF/Elium and GF/Infugreen respectively. It is evident from the plot that the data points can be fit into 2 different linear trendlines. In this graphical method the stress level at the intersection of these linear trendlines is considered the critical stress limit. This can physically be interpreted as the stress level after with the rate of damage accumulation rises at a hight rate compared to damage accumulation below this stress level. A critical stress limit of 271.05 MPa and 333.97 MPa was obtained for GF/Elium and GF/Infugreen respectively. This critical stress limits are depicted in Figure 4. 47 on the S-N curve indicating that 0° GF/Elium and GF/Infugreen can with stand approximately anything more 10 million and 2 million cycles at this stress level respectively.

This project has received funding from the European Union's Horizon 2020 research and innovation programme under grant agreement No 952966.

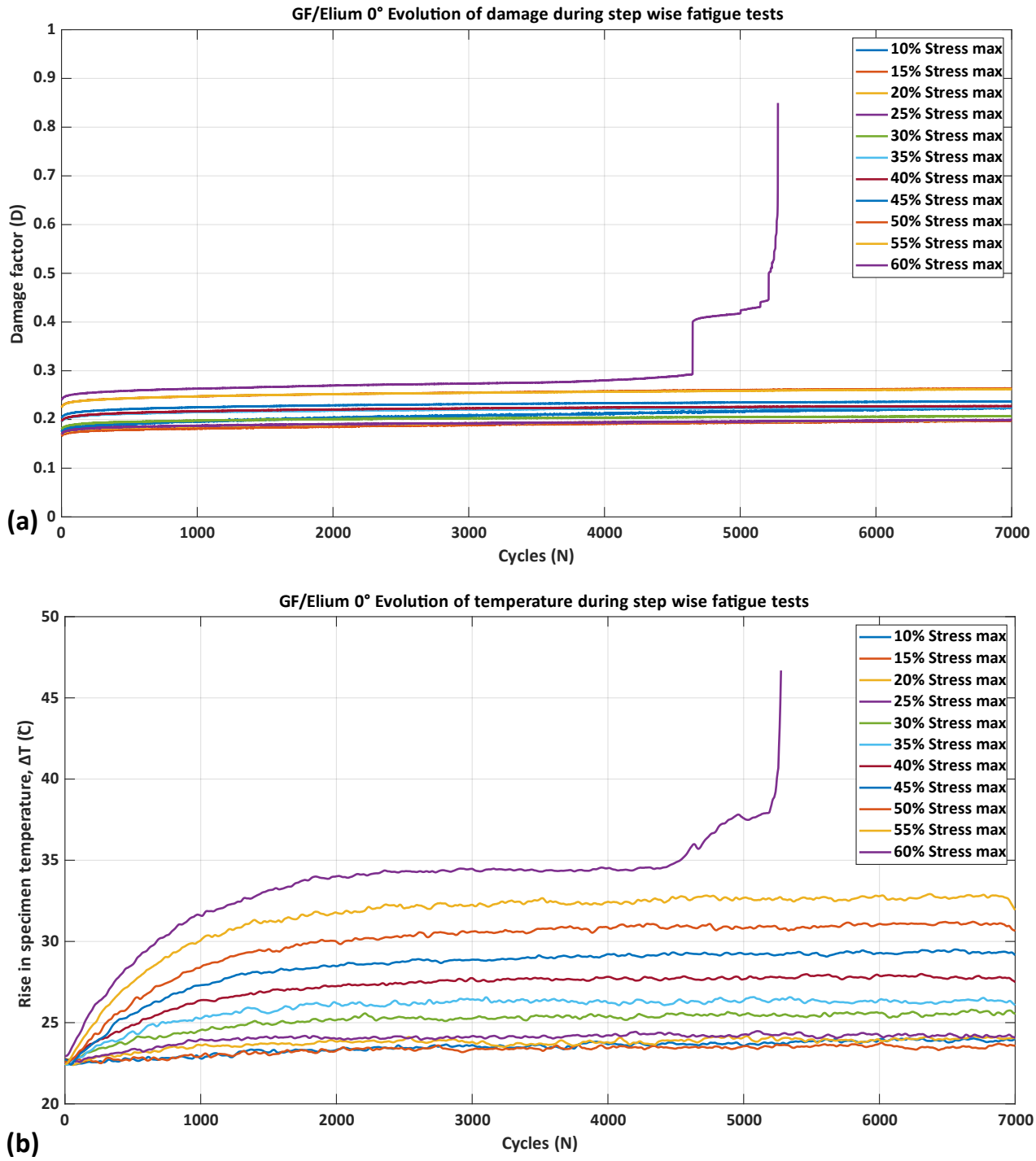

Figure 4. 48 Evolution of (a) Damage and (b) Temperature in 0˚ GF/Elium composite during stepwise tests

This project has received funding from the European Union's Horizon 2020 research and innovation programme under grant agreement No 952966.

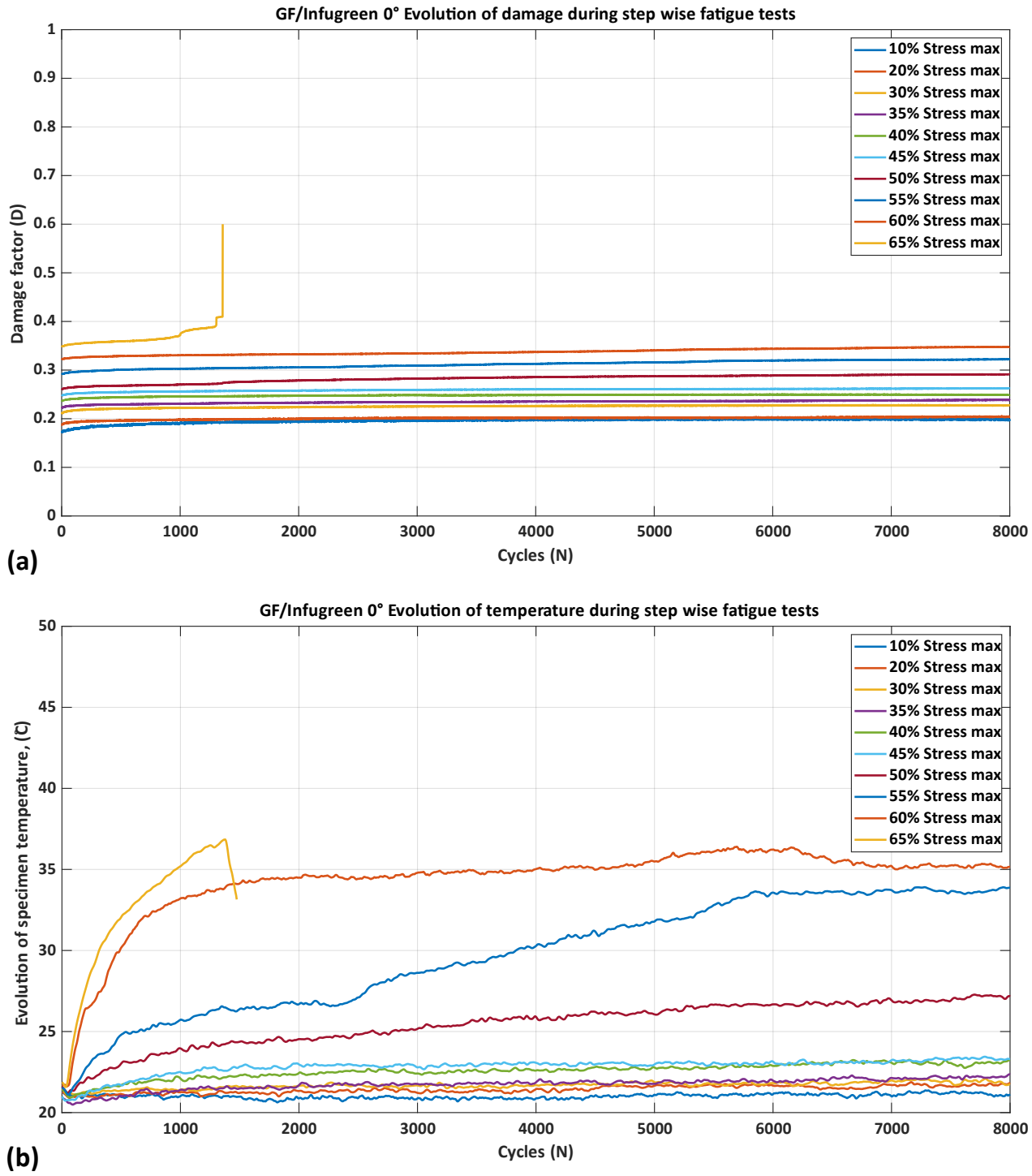

Figure 4. 49 Evolution of (a) Damage and (b) Temperature in 0˚ GF/Infugreen composite during stepwise tests

This project has received funding from the European Union's Horizon 2020 research and innovation programme under grant agreement No 952966.

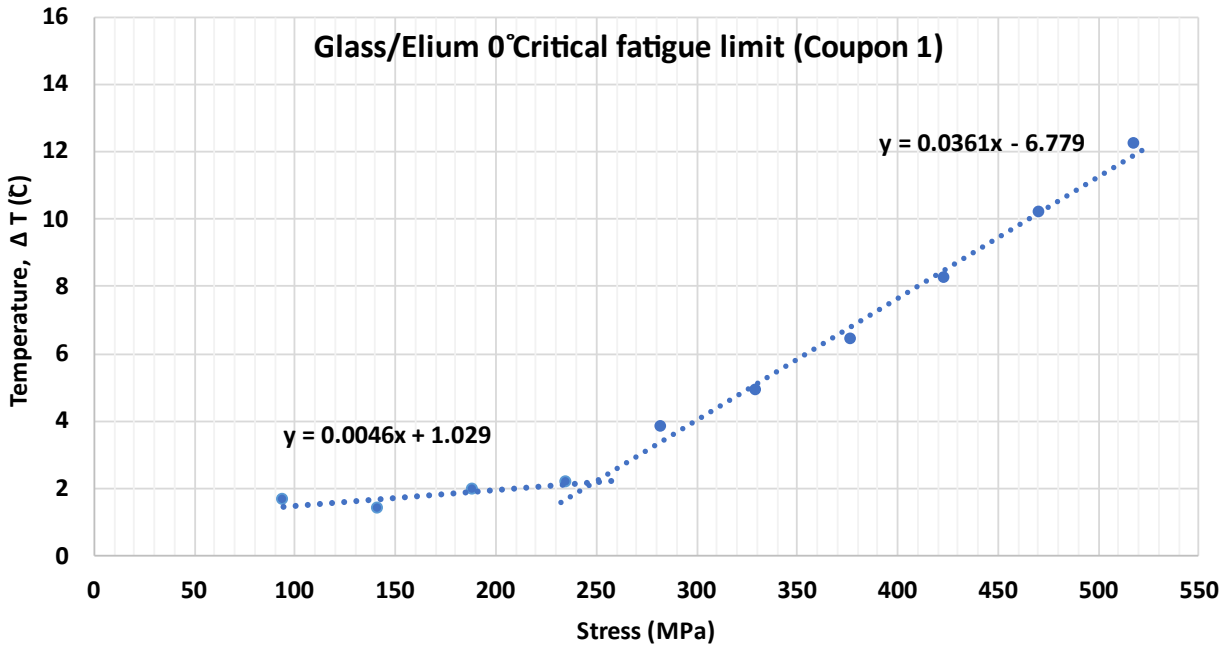

Figure 4. 50 Change in specimen temperature at the end of each load block as a function of the maximum stress applied for 0° GF/Elium to determine the critical stress limit.

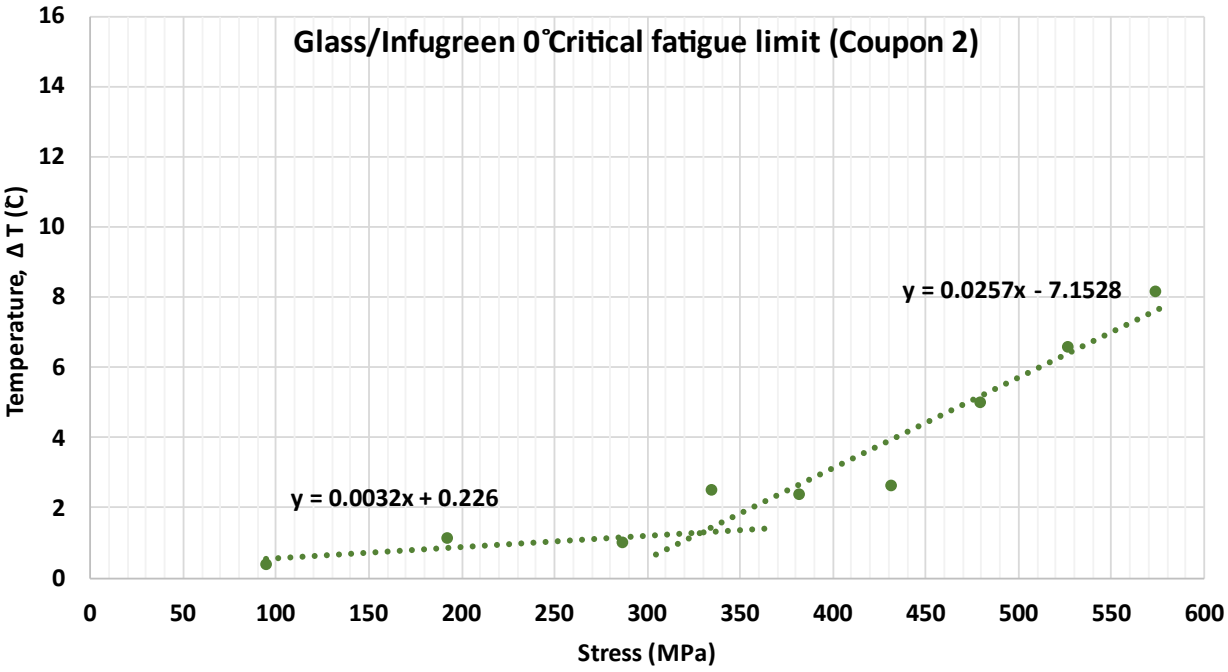

Figure 4. 51 Change in specimen temperature at the end of each load block as a function of the maximum stress applied for 0° GF/Infugreen to determine the critical stress limit.

This project has received funding from the European Union's Horizon 2020 research and innovation programme under grant agreement No 952966.

4.5.3. Fractography and failure analysis

The fatigue tested 0° GF/Elium and GF/Infugreen specimens were examined using SEM. As in previous configurations, a specimen each from the low-cycle and high-cycle regimes of the S-N curves of the composites tested. Figure 4. 52 shows the fatigue tested GF/Elium composite specimens. Blooming failure was extensively observed in the specimens. Fibre splitting and breakage was widely seen in all the specimens. Failure was seen to initiate at either edge of specimens with fibres splitting and their subsequent breakage seen. With increase in number of loading cycles, the specimens eventually failed with extensive fibre splitting as seen in Figure 4. 52. A similar failure behavior was seen in both low-cycle and high-cycle tested specimens. Figure 4. 53 presents SEM images captured from the fracture surface of low-cycle fatigue tested GF/Elium specimen. Fibre splitting and broken fibres could be seen. Matrix cracking and fibre-matrix debonding was seen to occur prior to fibre failure. Evidence of matrix adhesion on the broken fibres could be obtained. Fibre surfaces were seen to be rough and jagged on account of matrix adhesion. The micrographs also indicated matrix deformation to have occurred prior to specimen failure. Figure 4. 54 presents the SEM images from the fracture surface of a high-cycle fatigue tested GF/Elium specimen. The fracture characteristics were similar to that seen in case of the low-cycle fatigue tested specimen. Typical mechanisms such fibre-matrix debonding, fibre splitting and fibre breakage was seen. Matrix plastic deformation could also be observed. Damage was seen in the vicinity of the construction fibres, possibly initiating at these locations due to the weaker interfacial interaction between the construction fibres and the matrix.

Figure 4. 55 shows the GF/Infugreen specimens tested under fatigue loading. Specimen failure was seen to occur due to extensive fibre splitting and breakage as seen in the Figure. However, as compared to GF/Elium composites, fibre splitting was not as extensive. The difference in plastic deformation between the thermoplastic Elium resin and thermoset Infugreen resin is likely to have led to a difference in the failure behavior observed. However, across the GF/Infugreen specimens tested, a similar failure behavior was seen. For SEM observations, small sections from the specimens were carefully extracted and observed. Figure 4. 56 shows the SEM images taken from the fracture surface of a low-cycle fatigue tested GF/Infugreen specimen. The fatigue loading direction is indicated in the images. The images indicate the typical failure mechanisms observed as in the case of the GF/Elium composite. However, the fibre surfaces appeared to be smoother as compared to those of the GF/Elium composite, indicating lesser matrix adhesion to the fibres. Evidence of fibre-matrix debonding could be clearly seen. The ply surface exposed due to delamination was also observed (see Figure 4. 56 (b)). In addition to fibre breakage, the presence of bundled construction fibres in a direction perpendicular to that of loading was observed. The matrix surface appeared smoother as compared to that of Elium resin indicating a difference in the extent of plastic deformation undergone by the two matrix systems during fatigue loading. Figure 4. 57 presents the SEM images drawn from the fracture surface of the high-cycle fatigue tested GF/Infugreen specimen. No significant difference in fracture features as compared to that of low-cycle fatigue tested specimen could be seen. Again, fibre debonding and fibre breakage was seen. The fibre surfaces were smoother as compared to those of GF/Elium composite. Figure 4. 57 (d) shows the specimen surface beneath a delaminated region. Most of the fibres appeared intact with a few broken fibres also seen. Fibre-matrix debonding was clearly seen and the matrix surfaces were also similar to those observed in case of the low cycle fatigue tested specimen. A comparison of the fracture features of the two types of composites indicated a difference in matrix plastic deformation

This project has received funding from the European Union's Horizon 2020 research and innovation programme under grant agreement No 952966.

during fatigue loading and fibre-matrix interactions possibly leading to differences in the observed fatigue stress levels of the two types of composites tested.

Figure 4. 52 Figure 1. GF/Elium 0° fatigue test specimens after failure.

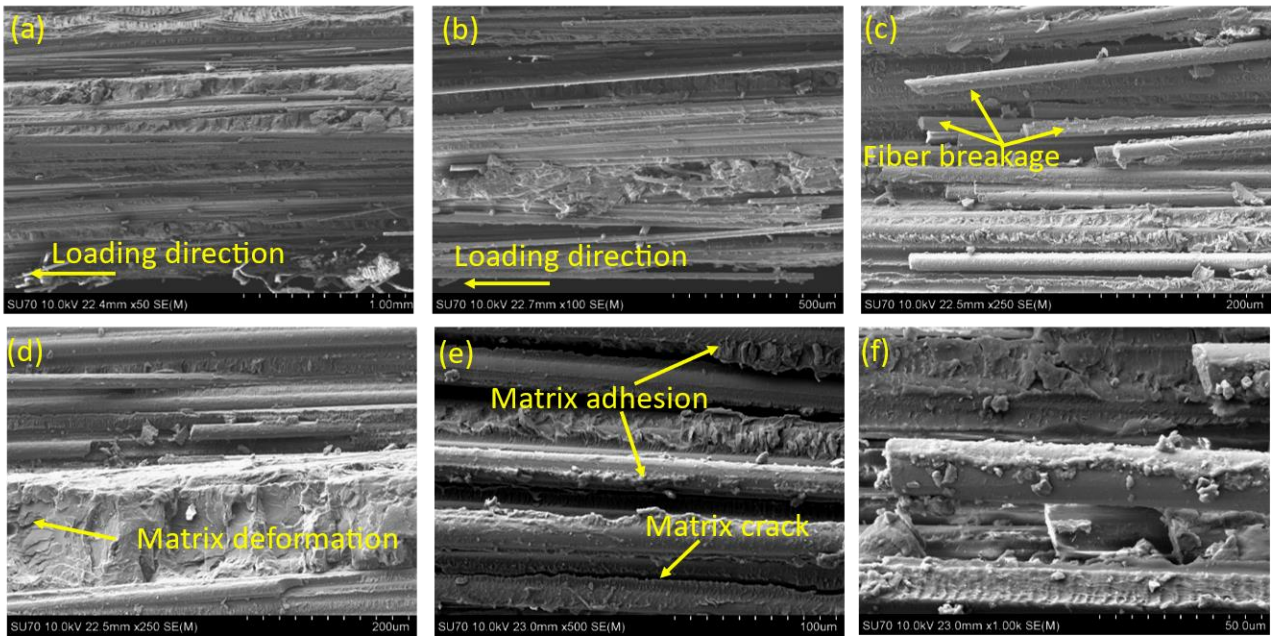

Figure 4. 53 Figure 2. SEM images from a low-cycle fatigue tested GF/Elium 0° specimen.

This project has received funding from the European Union's Horizon 2020 research and innovation programme under grant agreement No 952966.

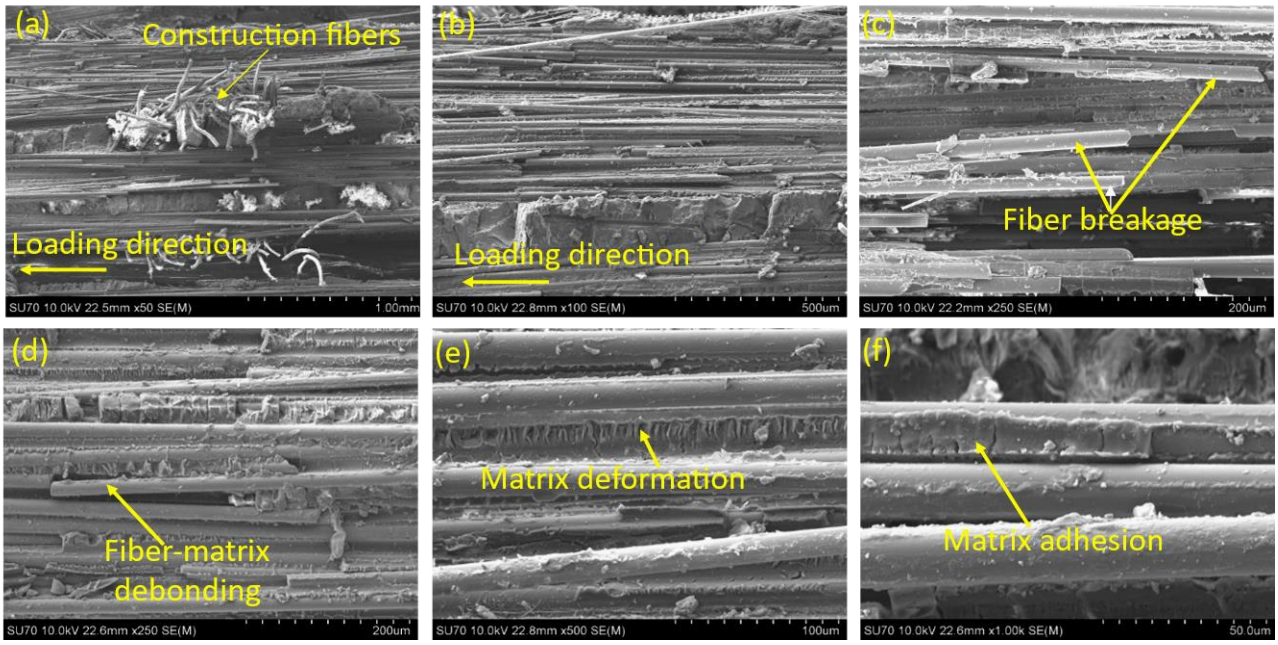

Figure 4. 54 Figure 3. SEM images from a high-cycle fatigue tested GF/Elium 0° specimen.

Figure 4. 55 Figure 4. GF/Infugreen 0° fatigue test specimens after failure.

This project has received funding from the European Union's Horizon 2020 research and innovation programme under grant agreement No 952966.

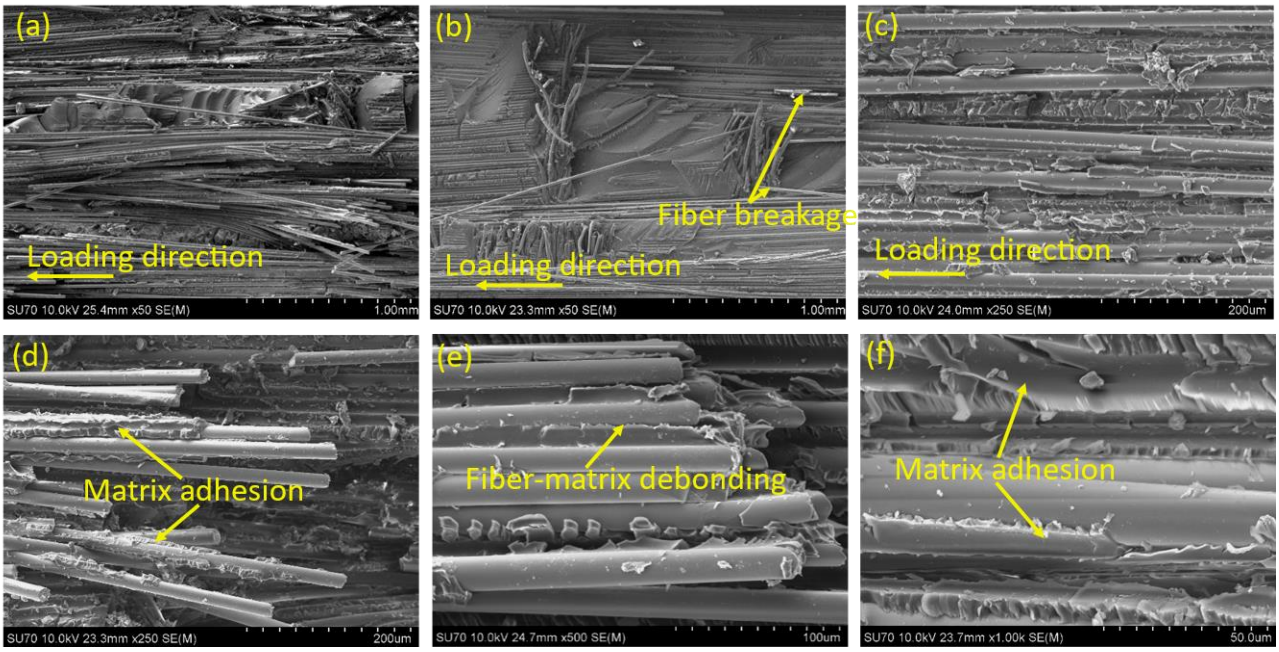

Figure 4. 56 Figure 5. SEM images from a low-cycle fatigue tested GF/Infugreen 0° specimen.

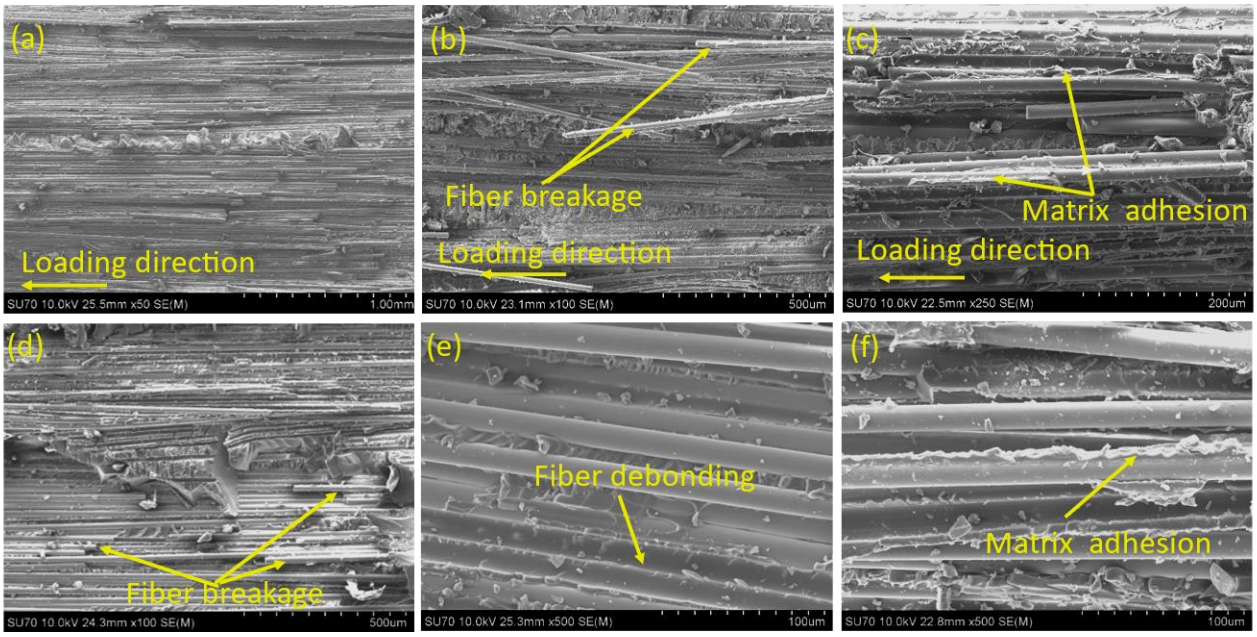

Figure 4. 57 Figure 6. SEM images from a high-cycle fatigue tested GF/Infugreen 0° specimen.

From visual inspection of failed test coupons and observation of coupons under fatigue loading, it is understood that the progression of failure is different for GF/Infugreen and GF/Elium coupons. For both the materials, the initiation of damage occurs at the edges. The fibre tows running out of the edge delaminates first as they are not gripped end-to-end. After all the jutted fibres delaminate at the edges, stress is redistributed across the cross-section of the coupon. This phenomenon is illustrated in Figure 4. 58(a). After this, the mechanism leading to failure differs for GF/Infugreen and GF/Elium coupons. For, GF/Infugreen, splitting of the coupon is observed few cycles before the complete failure. After splitting, the coupon takes few more cycles of load then leading to complete failure by breakage close to the grips. This phenomenon is illustrated in Figure 4. 58(b). Whereas for GF/Elium a sudden complete failure (Catastrophic failure) by

This project has received funding from the European Union's Horizon 2020 research and innovation programme under grant agreement No 952966.

fibres blooming from the coupon is observed (Figure 4. 58(c)). As discussed previously, this difference in failure mechanism may be due to the difference in plastic deformation between the thermoplastic resin and thermoset resin.

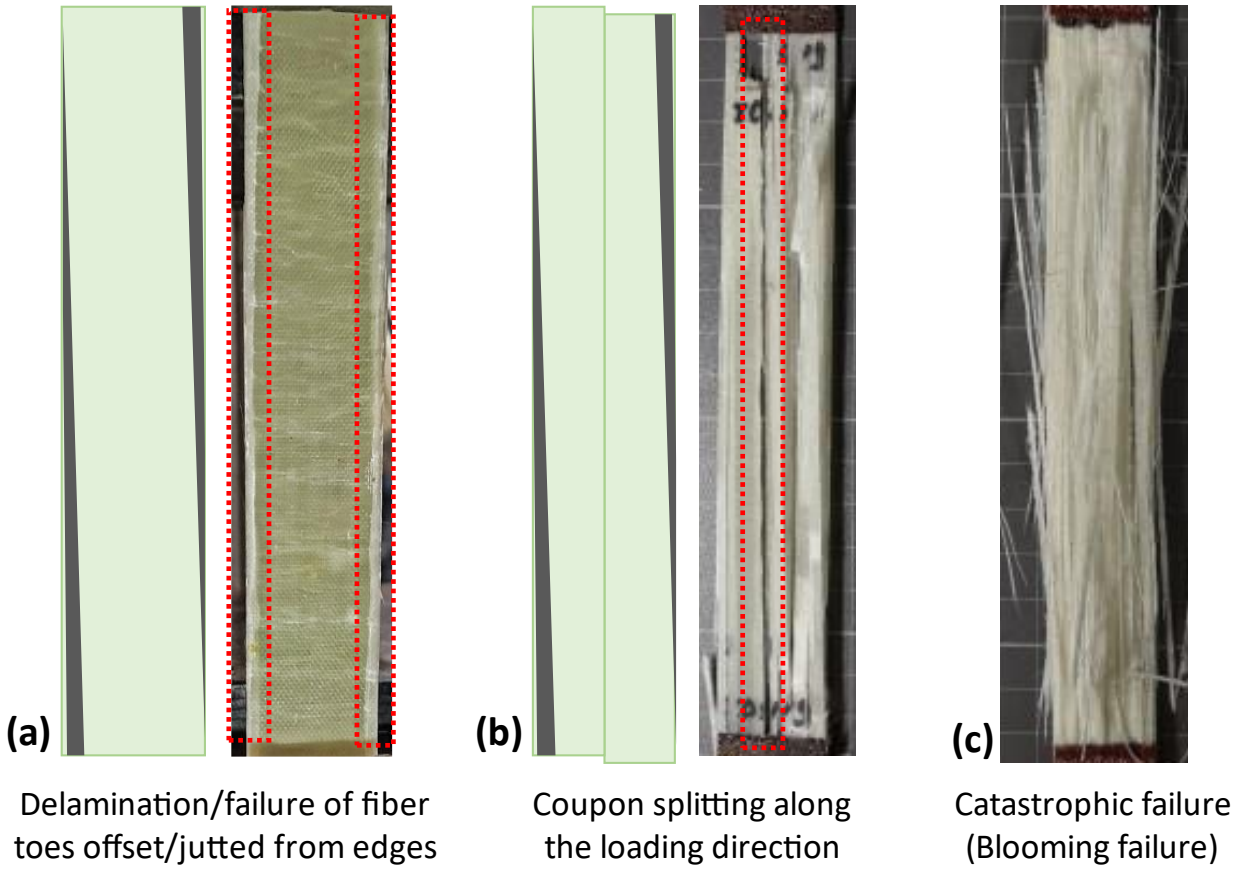

Figure 4. 58 Failure progression of 0° specimens during fatigue testing.

This project has received funding from the European Union's Horizon 2020 research and innovation programme under grant agreement No 952966.

4.6. Fatigue of bonded joints

To study the fatigue behaviour of bonded joints, two types of adhesives were considered viz. Araldite® 2015-1 (marine grade adhesive) and reversible adhesive newly developed by Corso Magenta in single-lap joint configuration. Additionally, trail tests for bonded joints made using Corso Magenta's reversible adhesive was performed. The adherend was multi-directional carbon fibre/thermoset (Infugreen 810) (MD-CFRP) composite for both Araldite 2015-1 and reversible adhesive joints. All the coupons were manufactured at INEGI's facility and shipped to ULim for testing whereas aging of reversible adhesive joint was done at Corso Magenta's facility. Static lap shear tests were performed on the bonded joints to obtain lap shear strength which was further used to design the tension tension fatigue tests. It was found that the lap shear strength of marine grade adhesive and reversible adhesive was 11.19 MPa and 2.02 MPa respectively. Though the static test results for marine grade adhesive joints were consistent, the poor performance of reversible adhesive did not yield consistent results. Further, the already weak reversible adhesive joints performed much poorer after ageing due to further weakening of the joint. The tension-tension fatigue tests to establish the S-N curve for the adhesively bonded joints were conducted at a frequency of 8 Hz with an R ratio of 0.1. Figure 4. 59 shows the S-N curve for MD-CFRP single-lap joints made of marine grade and reversible adhesive. Though, the results for marine grade adhesive looks consistent, in theory all the failures were unacceptable. At all stress levels the failure mode was adhesive failure which is clear from Figure 4. 60. In few cases, the manufacturing defects like voids induced premature failure and scaring of surface fibres during surface preparation has led to fibre peel off (Figure 4. 60). In case of CFRP – Reversible adhesive single-lap joint, the weak adhesion was clearly seen from the adhesion failure and leftover crystalline formation (Ref. Figure 4. 61) indicating that the adhesive did not create an acceptable bond. Similar outcome was observed for aged reversible adhesive coupons, which also exhibited poor performance due to adhesive failure. The static lap shear strength was inconsistent and below 1 MPa which did not allow to continue with fatigue testing.

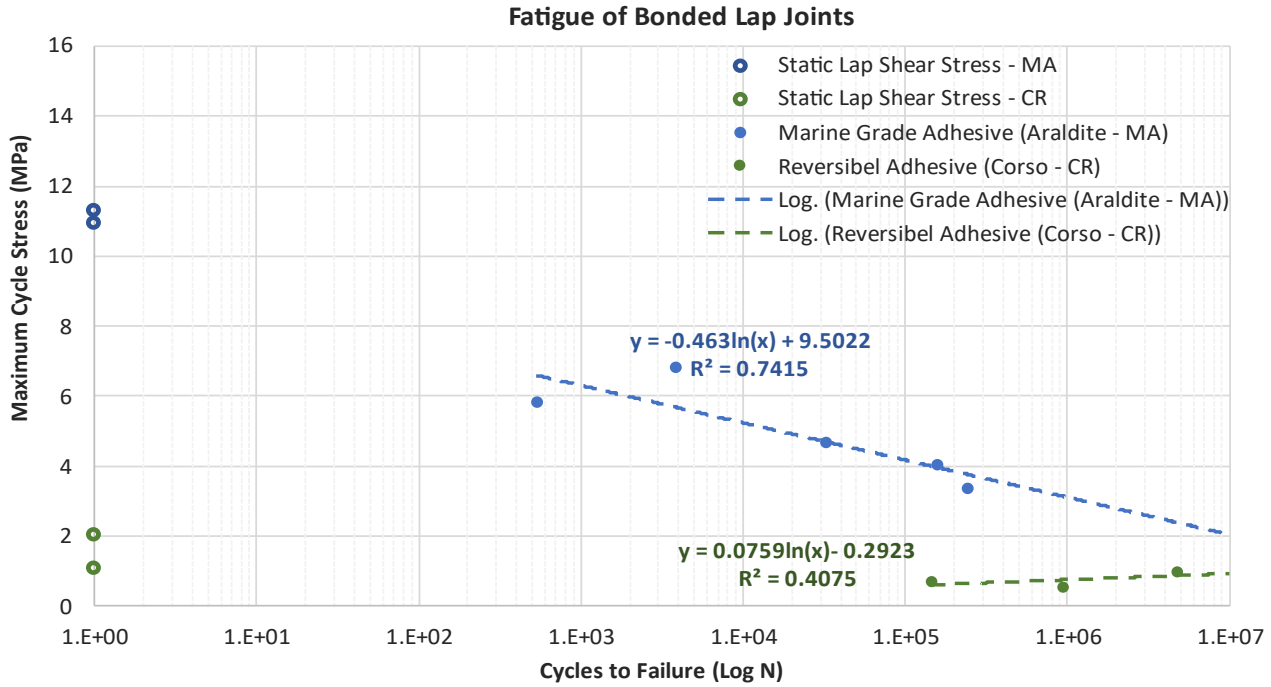

This project has received funding from the European Union's Horizon 2020 research and innovation programme under grant agreement No 952966.

Figure 4. 59 S-N Curve for single-lap joint of marine grade and reversible adhesive with MD-CFRP.

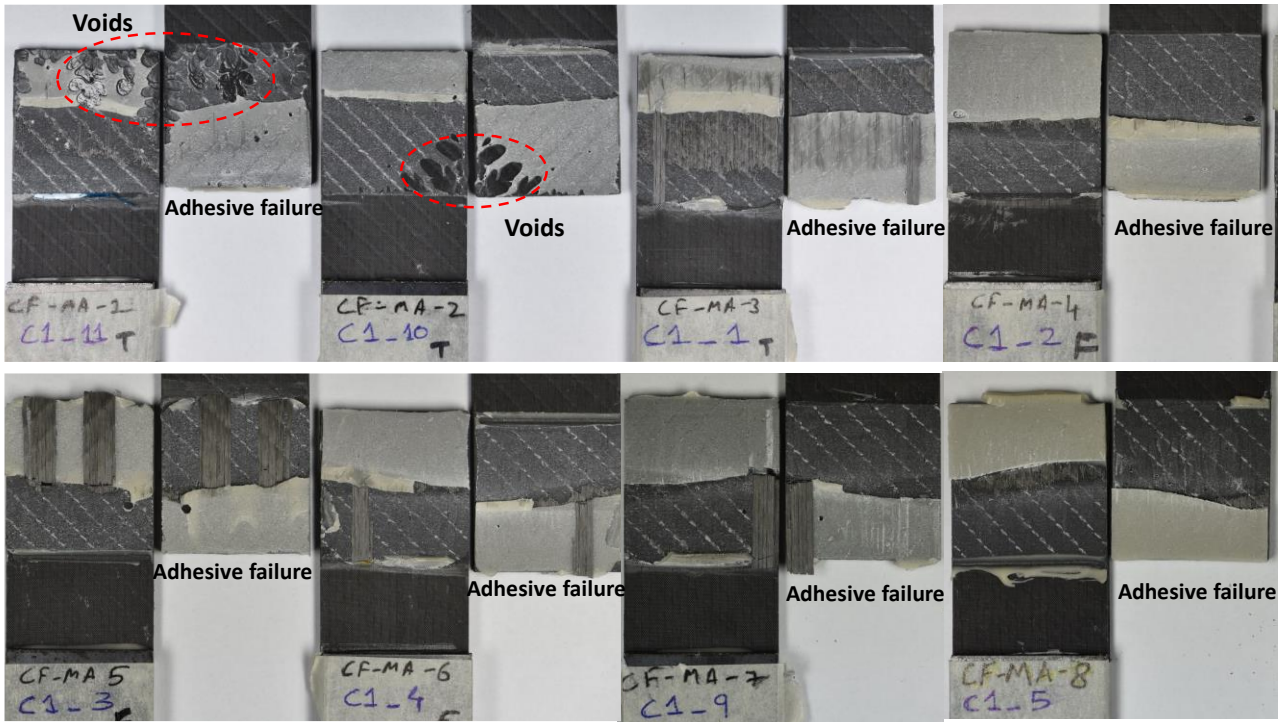

Figure 4. 60 CFRP – Marine grade adhesive single-lap joint after failure due to fatigue loading.

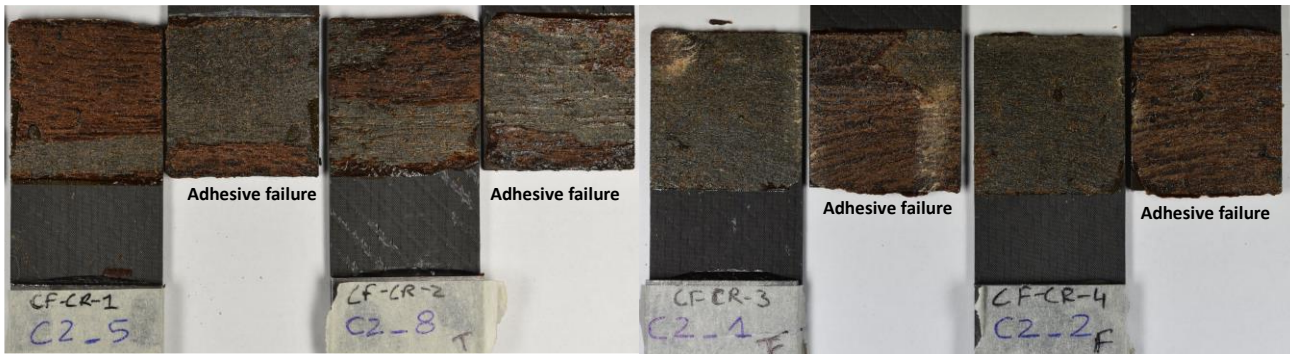

Figure 4. 61 CFRP – Reversible adhesive single-lap joint after failure due to fatigue loading.

This project has received funding from the European Union's Horizon 2020 research and innovation programme under grant agreement No 952966.

5. QUASI-STATIC COMPRESSION TESTS

In parallel to assessing the fatigue performance of composite materials, the composite specimens from the selected materials were also tested under quasi-static compression static loading. The characterized properties were supplied to other partners in the consortium in order to inform their numerical models. Further, the stress-strain curves were plotted to obtain further insight to the mechanical response under compression loading for these materials. A careful examination of failure modes and fractography characteristics were made for representative case under each laminate material as listed in The results from the compression tests indicate that Elium based laminates possess higher strength characteristics compared to Infugreen based laminates. The fractography revealed typical plastic behaviour of Elium resin with traces of Elium visibly adhering to the fibre surface in the vicinity of the fracture zone. However, the post fracture fibre surface was found to be cleaner in the case of Infugreen based laminates, suggesting brittle behaviour. These observations were found to be consistent with the observations made in Task 2.1.

Table 3. The following section provide descriptions of manufacturing procedure used, test method followed, and the results obtained in detail.

5.1. Materials and Manufacturing

For the compression testing, the resin systems used are same as the two systems (Elium and InfuGreen) as described in the previous section of fatigue testing. For the consistency with the material employed for Task 2.1, two types of reinforcements were used for compression studies viz. Saertex UD 1182 g/m^2 E-Glass fibre based on non-crimp Hybon 2026 1200 fibre (Quasi-UD) and Saertex U-C 438 g/m^2 Carbon fibre based non crimp fabric. Due to the different sizing present in glass and carbon fibres, the laminates employing thermoplastic (Elium) were prepared using two different grades viz. Elium 188XO for glass fabric and Elium 188O for carbon fabric, as recommended in the technical datasheets for Elium188 [13,18]. The laminates were prepared using Vacuum assisted resin infusion technique and cured initially at room temperature. The samples of width 13 mm and length 140 mm as per ASTM D6641 [3], were extracted from the infused laminates using the abrasive waterjet cutting technique. The extracted test specimens were post-cured 60° C for 24 hrs and at 60° C for 16 hrs for thermoplastic and bio epoxy-based laminates respectively. Table 5. 1 lists all the layups along with the type of reinforcement and matrix which was used for compression testing. In total, specimens of eight types were tested to incorporate a fibre dominant ($[0]_n$) and a matrix dominant ($[90]_n$) layup with each fibre (Carbon and Glass) for both the resins (Elium and InfuGreen). The number of plies in each layup were decided based upon examination of failure modes. The Fibre volume fraction (V_f) for the fibre dominant layups $[0°]_{ns}$ was determined to normalize the characterized values for an equivalent laminate of 55 % fibre volume fraction to eliminate any bias conveyed due to difference in the fibre volume fraction (V_f) amongst various 0° layups. The absolute V_f was determined using thickness measurement in

This project has received funding from the European Union's Horizon 2020 research and innovation programme under grant agreement No 952966.

accordance with ISO 14127 [19] The process involves measurement of the thickness of the cured laminates at different locations. Further, by using the areal weight (gsm) of the fabric and fibre density from the manufacturer's datasheet, the following formula (Equation 1) is employed to calculate the fibre volume fraction. An areal weight of 1170 gsm and 410 gsm was considered for glass and carbon fabric, respectively. This excludes the weight of the synthetic stitching present in the fabric.

Table 5. 1 Laminate constituents and lay-ups for compression testing.

Material systems	Lay-up	Reinforcement	Resin	Initiator	Fibre Volume Fraction (V_f) (%)
Glass/Thermoplastic (GF/Elium)	$[0]_{2S}$	U-E 1182 g/m²	Elium 188 XO	Perkadox GB-50X	60.70 (0.66)
	$[90]_{2S}$	U-E 1182 g/m²	Elium 188 XO		-
Glass/Thermoset (GF/Infugreen)	$[0]_{2S}$	U-E 1182 g/m²	SR Infugreen 810	SD8824	58.71 (0.86)
	$[90]_{2S}$	U-E 1182 g/m²	SR Infugreen 810		-
Carbon/Thermoplastic (CF/Elium)	$[0]_{4S}$	U-C 438 g/m²	Elium 188 O	Perkadox GB-50X	48.94 (0.77)
	$[90]_{2S}$	U-C 438 g/m²	Elium 188 O		-
Carbon/Thermoset (CF/Infugreen)	$[0]_{4S}$	U-C 438 g/m²	SR Infugreen 810	SD8824	49.76 (0.20)
	$[90]_{4S}$	U-C 438 g/m²	SR Infugreen 810		-

5.2. Test methods

The compression testing was performed using Combined loading compression (CLC) test fixture as per ASTM D6641 [3]. Figure 5. 1 depicts the test setup employed. The tests were conducted under displacement control mode with the crosshead displacement rate of 1.3 mm/min. A gage length of 13 mm was maintained as per test standard. Two strain gages were bonded on the specimen, one on each face. The average of both the strain gage readings was used to calculate the modulus. A strain range of 0.001- 0.003 was used using chord modulus method. The tests were stopped after a rapid or sudden drop in load was observed. The tested specimens were then inspected for failure mode to validate their conformity as per ASTM D6641 [3].

This project has received funding from the European Union's Horizon 2020 research and innovation programme under grant agreement No 952966.

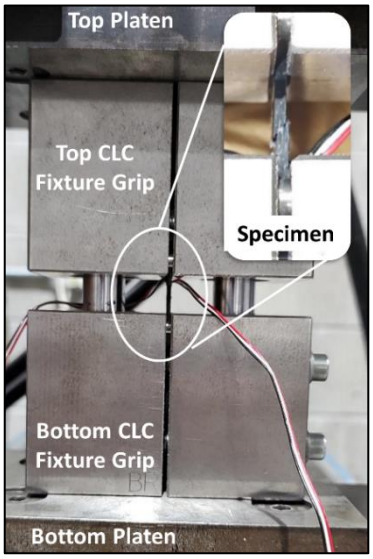

Figure 5. 1 The CLC test fixture demonstrating a representative specimen under testing.

For the specimens tested under compression loading, a valid representative specimen in each tested layup was taken for fractography analysis using scanning electron microscopy (SEM) using Hitachi SU-70 high-resolution scanning electron microscope (SEM). The specimens were carefully selected representing the failure mode observed in each test configuration. A small piece was cut out of the selected specimen with a cut plane oriented parallel to the plane of the fracture. A schematic representation providing the perspective of the region analysed under SEM is depicted in Figure 5. 2. This procedure of cutting of the tested specimen into smaller piece is performed to fit the specimen into the SEM setup to avoid hitting with the pole piece. The fracture surface was exposed to gold sputtering at 20 mA for at least 40 s before conducting analysis under SEM. A beam voltage of primarily 10 kV and in some cases 5 kV was selected to prevent overcharging of the specimens under microscope.

This project has received funding from the European Union's Horizon 2020 research and innovation programme under grant agreement No 952966.

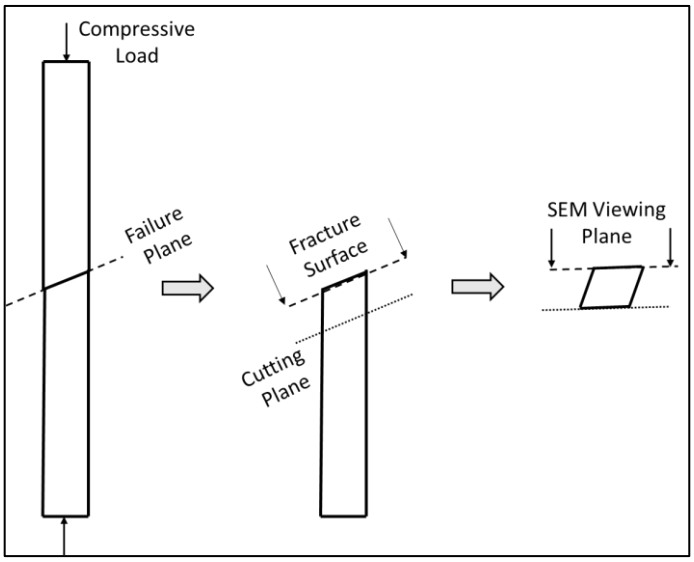

Figure 5. 2 Schematic representation of specimen preparation for SEM for compression specimen

5.3. Compression test results

In this chapter the results obtained from compression testing are reported. A summary of all characterized average properties is presented in Table 5. 2 and Figure 5. 3. Thereafter, the compression stress-strain response curves as plotted in Figure 5. 5 and Figure 5. 6 for 0° and 90° specimens respectively. Further, the post-test images of specimens for each laminate configuration highlighting the typical failure, are depicted in Figure 5. 7 and Figure 5. 8 for 0° and 90° specimens respectively. The fractography observations are then discussed using the images obtained from SEM which are depicted in Figure 5. 9.

Table 5. 2 Tabulated summary of the average values of the characterized properties under compression.

Material systems	**Lay-up**	**Average Properties**	**Maximum Strength (σ_{max}) (MPa)**	**Modulus (E) (GPa)**	**Strength at Failure initiation ($\sigma_{failure}$) (MPa)**
Glass/Thermoplastic (GF/Elium)	$[0]_{2S}$	σ_{11}, E_{11}	692.9 [*627.8] (91.9)	47.1 [^42.7] (2.9)	688.3 [*623.7] (91.1)
	$[90]_{2S}$	σ_{22}, E_{22}	149.0 (10.8)	16.7 (0.7)	145.9 (10.7)
Glass/Thermoset (GF/Infugreen)	$[0]_{2S}$	σ_{11}, E_{11}	529.2 [*495.7] (29.5)	45.3 [^42.4] (0.7)	527.0 [*493.7] (33.3)
	$[90]_{2S}$	σ_{22}, E_{22}	142.6 (4.5)	15.7 (0.3)	136.0 (8.1)
Carbon/Thermoplastic (CF/Elium)	$[0]_{4S}$	σ_{11}, E_{11}	577.9 [*649.5] (42.8)	90.4 [^101.6] (9.0)	553.9 [*622.5] (42.3)
	$[90]_{2S}$	σ_{22}, E_{22}	133.0 (5.6)	7.7 (0.3)	132.3 (4.8)
Carbon/Thermoset (CF/Infugreen)	$[0]_{4S}$	σ_{11}, E_{11}	488.1 [*539.5] (100.2)	98.3 [^108.6] (10.8)	483.4 [*534.3] (104.9)
	$[90]_{4S}$	σ_{22}, E_{22}	119.8 (2.7)	7.4 (0.2)	118.9 (3.4)

This project has received funding from the European Union's Horizon 2020 research and innovation programme under grant agreement No 952966.

Note- GF: Glass Fibre, CF: Carbon Fibre; Failure is defined here the instance during the test where first significant drop in load is observed, the specimen may still be bearing the load beyond failure initiation and reach a peak value. Standard deviation values in round parenthesis; Normalized values in square brackets. *Normalized Strength =Strength × 0.55/Absolute V_f; ^Normalized Modulus=Modulus × 0.55/Absolute V_f;

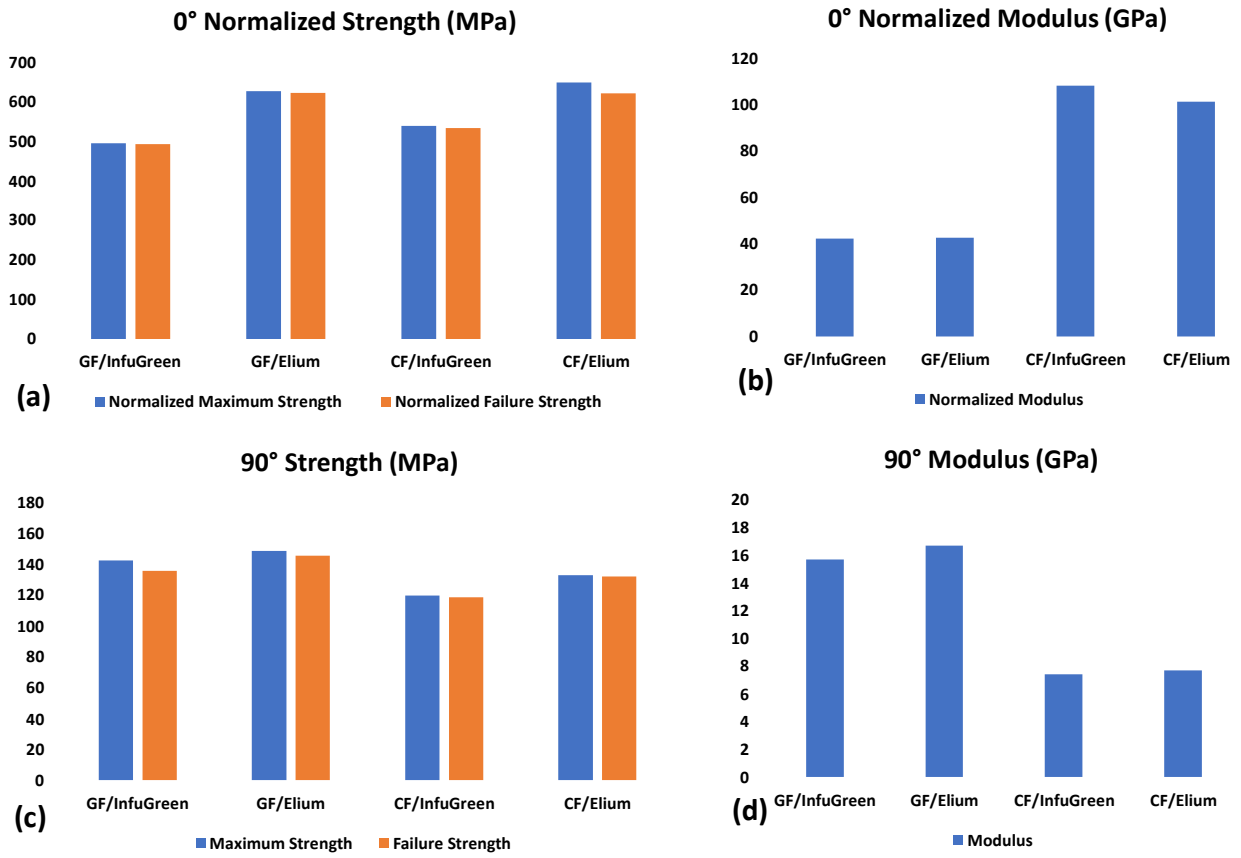

Figure 5. 3 Bar graphs depicting the average values of a) Normalized Strength for 0° b) Normalized Modulus for 0° c) Strength for 90 ° d) Modulus for 90° specimens.

5.3.1. Compression Characteristics

From the results obtained (refer Table 5. 2), it is observed that for 0° specimens, the maximum strength (normalized) of carbon fibre-based laminates is higher than the glass fibre-based laminates. The maximum (normalized) strength is dominated by the fibre characteristics and hence is higher in case of the carbon fibre based as they have higher load bearing capacity than glass fibres in general. However, for the same reinforcement, while comparing the maximum normalized strength, it is observed that the thermoplastic (Elium) based laminate exhibit higher strength as compared to the thermoset (InfuGreen bio-epoxy) based laminate. Similarly, in case of 90° specimens, the Elium based laminates for both the reinforcements possess higher strength compared to InfuGreen based laminates. Thus, in general it is perceived that the Elium based laminates have higher strength characteristics under compression than the Infugreen based laminates.

This project has received funding from the European Union's Horizon 2020 research and innovation programme under grant agreement No 952966.

Furthermore, as expected for the 0° case the modulus in glass fibre-based laminates is lower than carbon fibre-based laminates due to lower stiffness offered by glass fibres compared to carbon fibres. However, notably the modulus values for 90° glass fibre laminates are very high compared to the carbon-fibre based laminates. This observation is attributed to the fact that in case of glass fibre-based laminates, the fabric constitutes of 3% secondary supporting fibres (as shown in Figure 5. 4) which gets oriented in the loading direction for 90° specimens. These secondary fibres offer the additional stiffness to the 90° laminate. Whereas, in case of carbon fabric employed, the secondary fibres do not get aligned along the loading direction in 90° specimens. Hence, the 90° carbon fibre based laminate exhibit lower modulus. Overall, in case of 90° specimens within each reinforcement, the Elium based laminates exhibit slightly higher modulus compared to InfuGreen based laminates. However, the difference is very marginal.

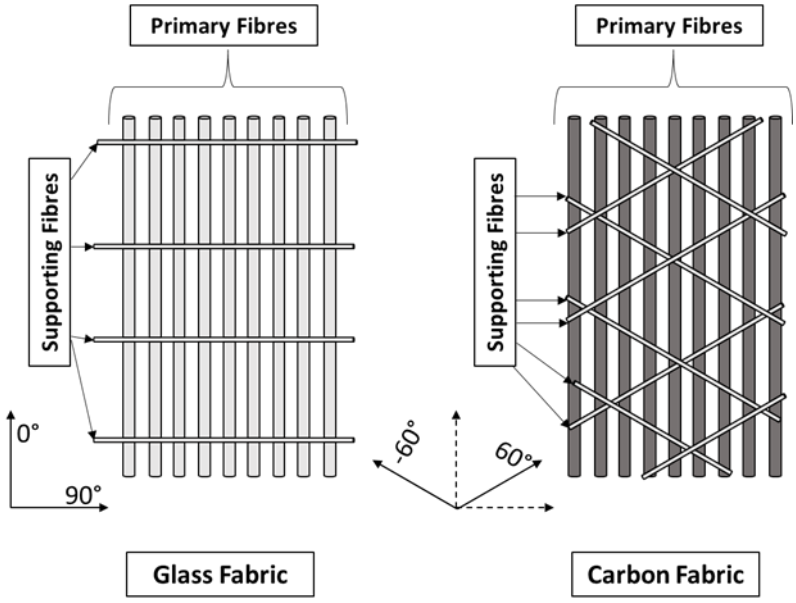

Figure 5. 4 Schematic representation of fabric structure depicting arrangement of primary (load bearing) and secondary (supporting) fibres.

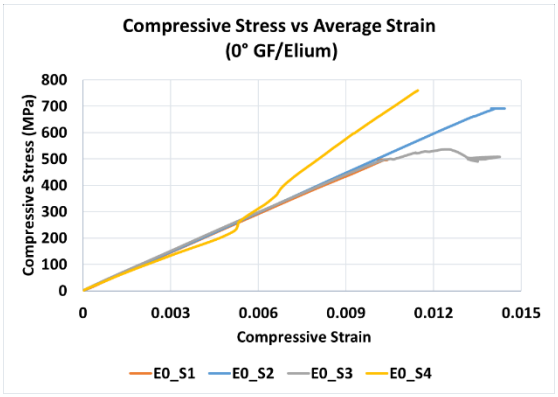

(a)

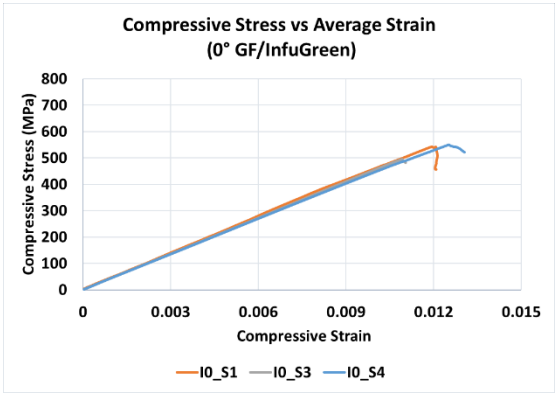

(b)

This project has received funding from the European Union's Horizon 2020 research and innovation programme under grant agreement No 952966.

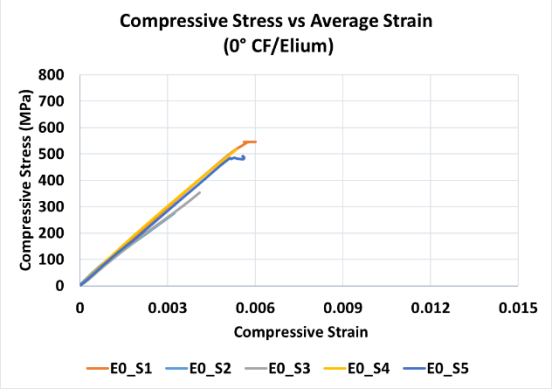

(c)

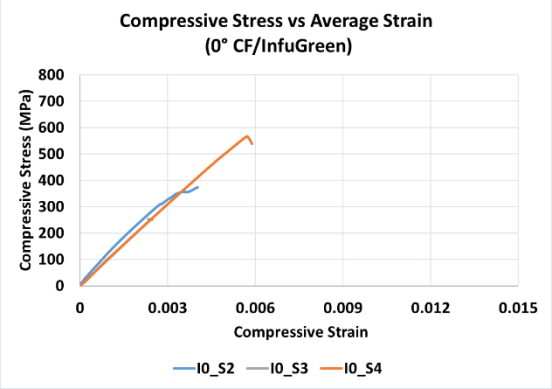

(d)

Figure 5. 5 Stress-strain response curves for 0° (a) GF/Elium (b) GF/InfuGreen (c) CF/Elium (d) CF/InfuGreen specimens

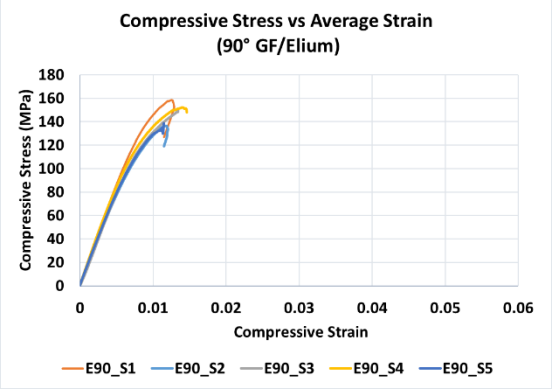

(a)

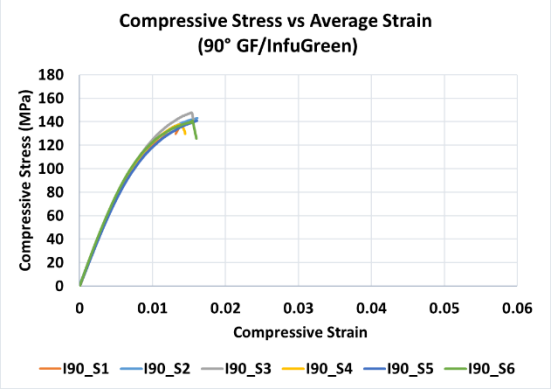

(b)

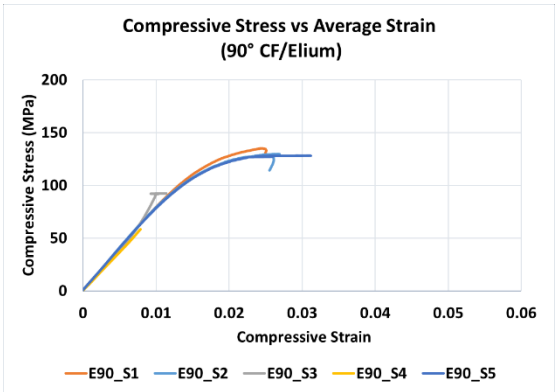

(c)

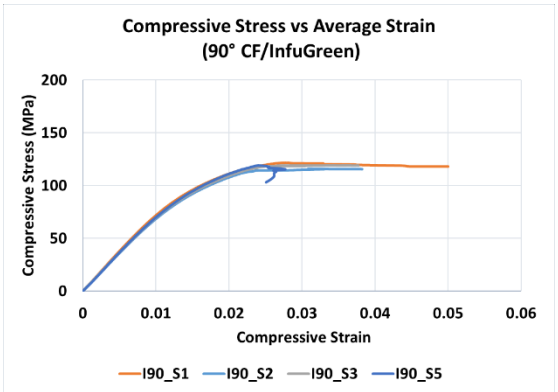

(d)

Figure 5. 6 Stress-strain response curves for 90° (a) GF/Elium (b) GF/InfuGreen (c) CF/Elium (d) CF/InfuGreen specimens

Note- The strain gages failed prior to specimen failure in some samples, hence a few curves present the data captured up to the point of recorded data available.

5.3.2. Compression failure analysis & fractography observations

Figure 5. 7 and Figure 5. 8 depict the post-test images of the specimens. For 0° specimens (for both reinforcements and both the resin systems), it is observed that kinking of the fibres is one of the predominant failure modes observed. The SEM images from Figure 5. 9 provide further insight to these

This project has received funding from the European Union's Horizon 2020 research and innovation programme under grant agreement No 952966.

observations. From the SEM images (Figure 5. 9(e) & (g)) the kinked fibres can be clearly seen, which further leads to breakage of fibres. For 90° specimens however, the predominant mode of failure was fracture with crack plane transverse to the loading direction. Further investigations using SEM for the fractured surfaces reveal distinctive fibre matrix interface characteristics for Elium and InfuGreen for both the type of reinforcements. In case of Elium based laminates, the resin remained adhered to the fractured fibres (for both Glass and Carbon case). Furthermore, the signs of plastic flow which is typical to thermoplastic can be observed in case of Elium based laminates. On the other hand, a cleaner fibre-matrix interface is observed in case of InfuGreen based laminates. Moreover, from Figure 5. 9 (d), it is evident that the InfuGreen exhibit a brittle failure mode, which is typical phenomenon of epoxies.

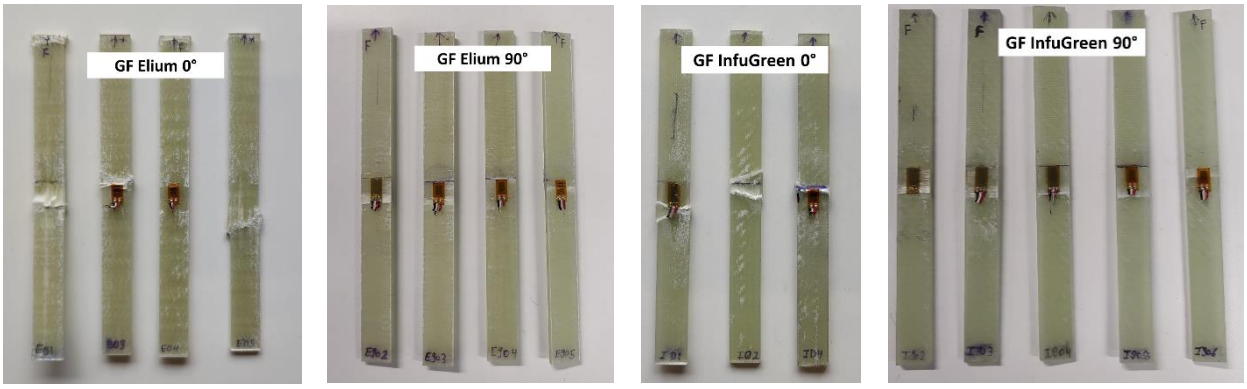

(a) (b) (c) (d)

Figure 5. 7 Post testing specimen images depicting typical failure observed for glass-fibre reinforced (GF) specimens (a) GF/Elium 0° (b) GF/Elium 90° (c) GF/InfuGreen 0° (d) GF/InfuGreen 90°

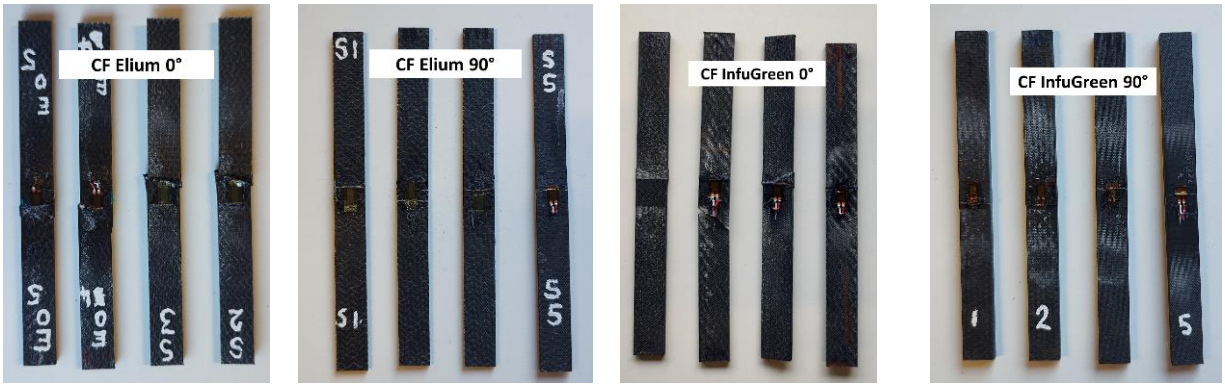

(a) (b) (c) (d)

Figure 5. 8 Post testing specimen images depicting typical failure observed for glass-fibre reinforced (CF) specimens (a) CF/Elium 0° (b) CF/Elium 90° (c) CF/InfuGreen 0° (d) CF/InfuGreen 90° specimens.

This project has received funding from the European Union's Horizon 2020 research and innovation programme under grant agreement No 952966.

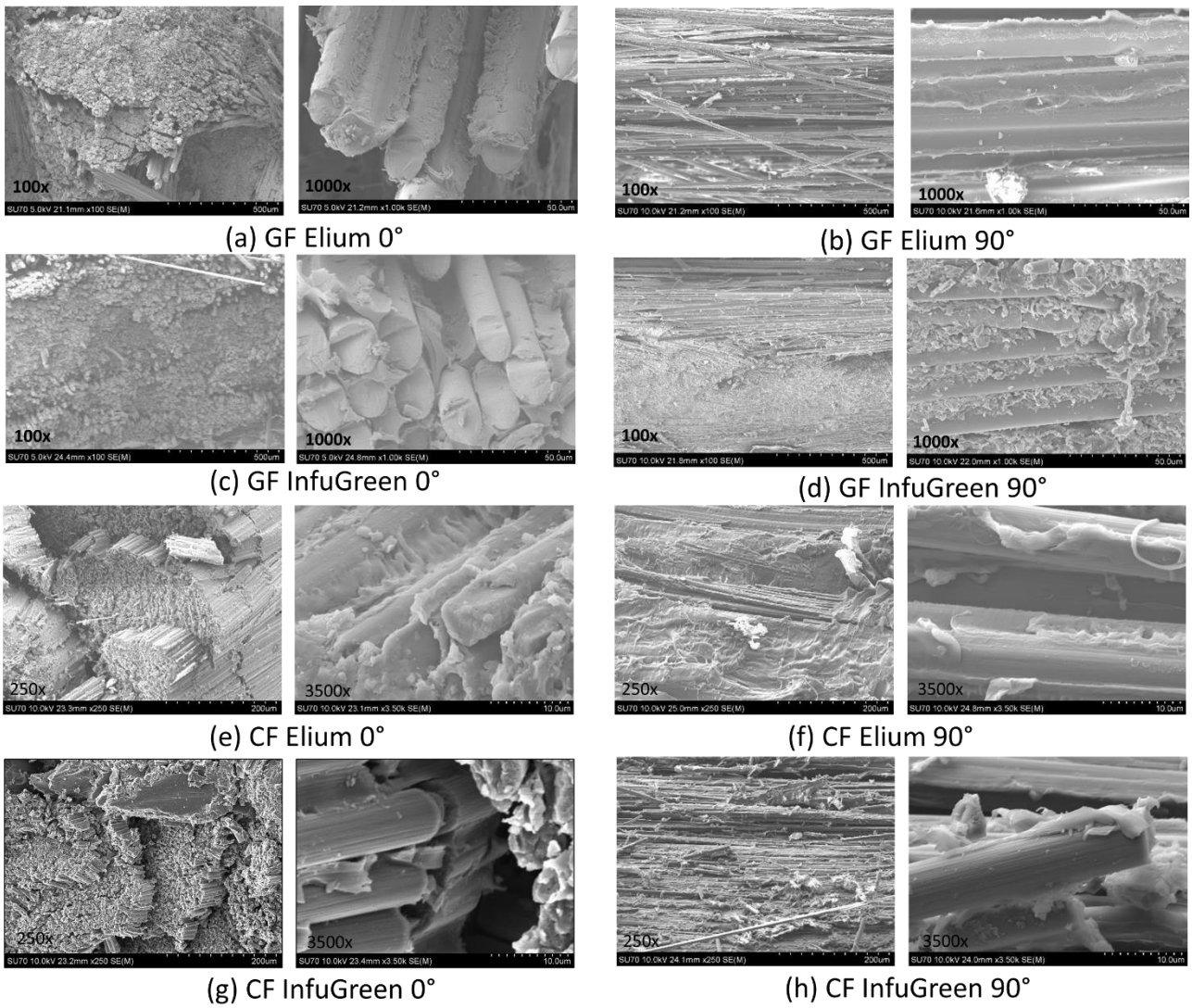

Figure 5. 9 SEM images under different magnification scales for (a) GF/Elium 0° (b) GF/Elium 90° (c) GF/InfuGreen 0° (d) GF/InfuGreen 90° specimens (d) CF/Elium 0° (e) CF/Elium 90° (f) CF/InfuGreen 0° (g) CF/InfuGreen 90° specimens

This project has received funding from the European Union's Horizon 2020 research and innovation programme under grant agreement No 952966.

6. CONCLUSIONS

The work performed in Task 2.4 during months 1-29 of the Fibregy project is presented in this report. It includes a very brief literature review followed by an extensive description of the experimental fatigue test campaign and associated results. The document also includes a description of the compression tests and associated results. The main conclusions and future research recommendations on the fatigue and compression of glass fibre reinforced composites are summarised below:

6.1. Fatigue

Constant amplitude load controlled fatigue tests were performed on various layup configurations of GF/Elium and GF/Infugreen specimens (90°, ±45°, Quasi-isotropic [0°, +45°, 90°, -45°], ±30°,0°) and two types of adhesive bonded joints to characterize fatigue behaviour by obtaining the S-N curves. The outcome is summarised in the Table 6. 1. In addition to obtaining the S-N curves, a novel approach to understand the high cycle fatigue behaviour of composites by estimating the critical stress limit was investigated by performing step-wise temperature stabilisation tests (Thermography).

The critical findings and observations from the fatigue test campaign are summarised as follows:

- The S-N curves for GF/Elium and GF/Infugreen in 90˚, ±45˚, quasi-isotropic, ±30° and 0° lay-up configurations were obtained, and suitable curve fitting was done with the available data.
- Unidirectional composites where all the fibres are oriented in one direction (90˚ and 0˚) and multidirectional composites where the lifetime is clearly dominated by one orientation (Quasi-isotropic) with respect to the loading direction yielded a linear S-N curve on a semi-log plot whereas composites with oblique fibre orientations with respect to the loading direction (±45˚, ±30˚) yielded a non-linear S-N curve on a semi-log plot.
- The fatigue behaviour of GF/Infugreen was better than GF/Elium in 90˚ lay-up configuration (Characterised by matric dominant failure) due to the higher static strength of Infugreen resin.
- The fatigue behaviour of GF/Elium was slightly better than GF/Infugreen for oblique lay-up (±45˚, ±30) composites.
- The fatigue behaviour of GF/Infugreen was better than GF/Elium for composites with fiber dominant failure modes (0° and Quasi-isotropic layups).
- The critical stress limit estimated from step-wise (temperature stabilisations) tests was in agreement with the stress level obtained from interpolation of the S-N curve. The positioning of the critical stress limit on the S-N curve suggests that the coupons can endure ≥ 10 million cycles before failure at that stress level. However, further testing of specimens to failure at the critical stress level is required for confirmation.
- The temperature stabilisation (Thermography) approach appears to be a time and cost efficient method for estimating the critical stress level.
- The fractography studies revealed that the fibre-matrix failure was a clean failure with no matrix residue remaining on fibres for GF/Infugreen whereas for GF/Elium there was evidence of matrix adhering to the fibres.
- Suggested future fatigue testing research:

This project has received funding from the European Union's Horizon 2020 research and innovation programme under grant agreement No 952966.

- The temperature stabilisation method yielded promising results in this study. However, several aspects of designing and processing the results can be enhanced with further understanding of the test parameters. For this, a detailed study on influence of test parameters on the obtained critical stress values is recommended.
- To better understand the damage mechanism interrupted fatigue tests with non-destructive testing methods like computed tomography is recommended.

Finally, all of the tests performed in Task 2.4 is presented in the Table 6. 2.

Table 6. 1 Fatigue test summary with S-N curve and thermography for GF/Infugreen and GF/Elium in 90˚, ±45˚, ±30˚, quasi-isotropic (QI) and 0˚ lay-up configurations.

Composite configuration	Glass/Infugreen		Glass/Elium	
	S-N Curve	**Critical Stress Level (Thermography)** (MPa)	**S-N Curve**	**Critical Stress Level (Thermography)** (MPa)
[90°]	$y = -2.04 \ln(x) + 53.0$ ($R^2 = 0.9583$)	18.81	$y = -2.25 \ln(x) + 48.03$ ($R^2 = 0.9347$)	16.37
[±45°]	$y = 56.227 x^{-0.079}$ ($R^2 = 0.9854$)	16.70	$y = 78.666 x^{-0.102}$ ($R^2 = 0.9899$)	17.22
QI	$y = -16.7 \ln(x) + 366.9$ ($R^2 = 0.9959$)	104.33	$y = -21.05 \ln(x) + 396.3$ ($R^2 = 0.9894$)	65.5
[±30°]	$y = 3304 x^{-0.5816} + 118.1$ $R^2 = 0.9922$	94.84	$y = 3304 x^{-0.5816} + 118.1$ $R^2 = 0.9922$	91.03
[0°]	$y = -60.27 \ln(x) + 1184$ ($R^2 = 0.9423$)	333.97	$y = -43.07 \ln(x) + 941.88$ ($R^2 = 0.9285$)	271.05

Table 6. 2 Total number of valid tests and invalid tests (in brackets) performed in each case in Task 2.4.

Test configuration	Static Tests	S-N Curve tests Valid (Invalid)	Thermography tests
GF/Thermoplastic (Elium) [90°]	2	11 (1)	2
GF/Thermoset (Infugreen) [90°]	2	9 (2)	2
GF/Thermoplastic (Elium) [±45°]	1	8	3
GF/Thermoset (Infugreen) [±45°]	1	9	3
GF/Thermoplastic (Elium) Quasi-isotropic	2	7	3
GF/Thermoset (Infugreen) Quasi-isotropic	2	7	3
GF/Thermoplastic (Elium) [±30°]	2	10 (1)	3
GF/Thermoset (Infugreen) [±30°]	2	10 (1)	3
GF/Thermoplastic (Elium) [0°]	2	11	2
GF/Thermoset (Infugreen) [0°]	2	10 (4)	2
Bonded joint - Araldite 2015-1	3	5	N/A

This project has received funding from the European Union's Horizon 2020 research and innovation programme under grant agreement No 952966.

Bonded joint - Reversible adhesive	3 (1)	5 (2)	N/A
Bonded joint - Reversible adhesive (Aged)	0 (2)	-	N/A

6.2. Compression

The key observations from the compression tests can be summarised as follows:

- Elium based laminates have higher strength characteristics under compression than the Infugreen based laminates.
- The Elium based 90° laminates exhibited a very marginally higher stiffness compared to the InfuGreen based 90° laminates.
- Fibre kinking is the dominant failure mode in 0° specimens while fracture in the direction transverse to loading direction is the predominant failure mode in 90° specimens.
- Plastic behaviour is evident from SEM observations for thermoplastic (Elium) and a brittle behaviour is evident for the bio-epoxy (InfuGreen).
- Suggested future research work on compression testing:
    - Investigate the fatigue behaviour under compression loading and compare failure modes with those observed during quasi-static tests.
    - Impact incidents during service cause damage to the composite structures by introducing subsurface defects such as delamination and fibre breakage. It is beneficial to assess the effect of such damages by performing Compression After Impact (CAI) testing, which can aid in assessing the residual structural integrity.

Overall, the objectives listed in the DoA for Task 2.4 were successfully achieved. In addition, thermography tests were effectively performed to compliment the results obtained from the classical S-N curve approach. Further, the compressive behaviour of laminates was characterized to supplement the work carried out in Task 2.1 in support of numerical model development.

This project has received funding from the European Union's Horizon 2020 research and innovation programme under grant agreement No 952966.

7. APPENDIX

Table 7. 1 Fatigue test summary for GF/Infugreen 90° samples.

GF Gerster H2026 90° - Infugreen								
Test Details: R Ratio: 0.1, Frequency: 8 Hz, Ultimate tensile strength: 49.84 MPa								
Coupon ID	**Area (mm^2)**	**Max Load (kN)**	**Max Stress (MPa)**	**Cycles to failure**	**Normalised Stress**	**Temperature (Humidity)**	**Remarks**	**Test Valid**
I90-SN-1	101.97	-	-	-	-	19.3˚ C (60.0%)	Machine tuning coupon	N/A
I90-SN-2	102.21	5.09	49.84	1	1.00	19.4˚ C (60.1%)	Failure in Gauge section	Yes
I90-SN-3	106.23	5.31	50.00	1	1.00	19.4˚ C (60.1%)	Failure in Gauge section	Yes
I90-SN-4	106.04	4.40	41.50	365	0.83	19.4˚ C (59.0%)	Failure in Gauge section	Yes
I90-SN-5	103.29	4.40	42.60	111	0.85	19.5˚ C (58.9%)	Failure in Gauge section	Yes
I90-SN-6	103.35	4.00	38.70	2767	0.78	19.5˚ C (57.8%)	Failure close to grips	Yes
I90-SN-7	103.89	4.00	38.50	2309	0.77	18.1˚ C (56.8%)	Failure close to grips	Yes
I90-SN-8	104.81	3.70	35.30	3162	0.71	18.2˚ C (56.6%)	Failure in Gauge section	Yes
I90-SN-9	104.03	3.70	35.57	480	0.71	18.3˚ C (57.7%)	Premature failure	No
I90-SN-10	103.91	3.20	30.79	16966	0.62	18.5˚ C (58.2%)	Failure in Gauge section	Yes
I90-SN-11	104.73	2.80	26.73	511222	0.54	19.0˚ C (55.5%)	Failure in Gauge section	Yes
I90-SN-12	103.08	2.52	24.45	1200150	0.49	16.6˚ C (68.7%)	Incomplete (Runout)	N/A

This project has received funding from the European Union's Horizon 2020 research and innovation programme under grant agreement No 952966.

Table 7. 2 Fatigue test summary for GF/Elium 90° samples.

GF Gerster H2026 90° - Elium								
Test Details: R Ratio: 0.1, Frequency: 8 Hz, Ultimate tensile strength: 41.85 MPa								
Coupon ID	**Area (mm^2)**	**Max Load (kN)**	**Max Stress (MPa)**	**Cycles to failure**	**Normalised Stress**	**Temperature (Humidity)**	**Remarks**	**Test Valid**
E90-SN-1	95.50	4.00	41.85	1	1.00	17.2° C (72.2%)	Failure in Gauge section	Yes
E90-SN-2	98.03	3.51	35.79	1	0.86	17.3° C (70.0%)	Failure at defect location	No
E90-SN-3	95.56	3.20	33.49	648	0.80	17.8° C (64.4%)	Failure in Gauge section	Yes
E90-SN-4	96.46	3.00	31.10	3820	0.74	17.9° C (63.7%)	Failure in Gauge section	Yes
E90-SN-5	97.73	2.80	28.65	8753	0.68	18.0° C (64.1%)	Failure in Gauge section	Yes
E90-SN-6	96.11	2.50	26.01	30038	0.62	18.2° C (62.8%)	Failure in Gauge section	Yes
E90-SN-7	96.59	2.20	22.78	28508	0.54	16.7° C (60.2%)	Failure near grips	Yes
E90-SN-8	94.70	3.00	31.68	1201	0.76	18.9° C (62.5%)	Failure in Gauge section	Yes
E90-SN-9	94.83	2.80	29.53	5140	0.71	18.7° C (62.8%)	Failure in Gauge section	Yes
E90-SN-10	98.41	2.50	25.40	16968	0.61	18.7° C (65.0%)	Failure in Gauge section	Yes
E90-SN-11	96.84	2.20	22.72	21472	0.54	17.3° C (58.9%)	Failure in Gauge section	Yes
E90-SN-12	95.12	1.95	20.50	273608	0.49	17.0° C (62.5%)	Failure in Gauge section	Yes
E90-SN-13	95.84	1.45	15.13	2702064	0.36	18.6° C (77.3%)	Incomplete (Runout)	N/A

This project has received funding from the European Union's Horizon 2020 research and innovation programme under grant agreement No 952966.

Table 7. 3 Fatigue test summary for GF/Infugreen ±45° samples.

GF Saertex H2026 ±45° - Infugreen							
Test Details: R Ratio: 0.1, Frequency: 5 Hz, Ultimate tensile strength: 42.07 MPa							
Coupon ID	**Area (mm^2)**	**Max Load (kN)**	**Max Stress (MPa)**	**Cycles to failure**	**Normalised Stress**	**Remarks**	**Test Valid**
I45-SN-1	81.88	6.89	42.07	1	0.99	Failure in Gauge section	Yes
I45-SN-2	81.94	4.50	27.46	6455	0.64	Failure in Gauge section	Yes
I45-SN-3	83.01	5.00	30.12	1828	0.71	Failure in Gauge section	Yes
I45-SN-4	81.84	4.00	24.44	27035	0.57	Failure in Gauge section	Yes
I45-SN-5	81.59	5.50	33.71	801	0.79	Failure in Gauge section	Yes
I45-SN-6	81.93	6.00	36.62	404	0.86	Failure in Gauge section	Yes
I45-SN-7	81.75	6.50	39.75	92	0.93	Failure in Gauge section	Yes
I45-SN-8	81.89	3.50	21.37	168406	0.50	Failure in Gauge section	Yes
I45-SN-9	81.24	4.30	26.47	10263	0.62	Failure in Gauge section	Yes
I45-SN-10	80.57	3.01	18.68	2048113	0.44	Failure in Gauge section	Yes

This project has received funding from the European Union's Horizon 2020 research and innovation programme under grant agreement No 952966.

Table 7. 4 Fatigue test summary for GF/Elim ±45° samples.

GF Saertex H2026 ±45° - Elium							
Test Details: R Ratio: 0.1, Frequency: 5 Hz, Ultimate tensile strength: 53.83 MPa							
Coupon ID	**Area (mm^2)**	**Max Load (kN)**	**Max Stress (MPa)**	**Cycles to failure**	**Normalised Stress**	**Remarks**	**Test Valid**
E45-SN-1	77.47	8.34	53.83	1	1.19	Failure in Gauge section	Yes
E45-SN-2	76.91	7.00	45.51	242	1.00	Failure in Gauge section	Yes
E45-SN-3	77.03	6.50	42.19	494	0.93	Failure in Gauge section	Yes
E45-SN-4	76.60	6.00	39.16	973	0.86	Failure in Gauge section	Yes
E45-SN-5	76.76	5.50	35.83	1651	0.79	Failure in Gauge section	Yes
E45-SN-6	75.33	5.00	33.19	5411	0.73	Failure in Gauge section	Yes
E45-SN-7	76.96	4.50	29.24	11686	0.64	Failure in Gauge section	Yes
E45-SN-8	75.41	4.00	26.52	75317	0.58	Failure in Gauge section	Yes
E45-SN-9	77.88	3.01	19.33	809495	0.43	Failure in Gauge section	Yes

This project has received funding from the European Union's Horizon 2020 research and innovation programme under grant agreement No 952966.

Table 7. 5 Fatigue test summary for GF/Infugreen quasi-isotropic lay-up samples.

GF Gerster H2026 Quasi-isotropic - Infugreen							
Test Details: R Ratio: 0.1, Frequency: 5 Hz, Ultimate tensile strength: 341.44 MPa							
Coupon ID	**Area (mm^2)**	**Max Load (kN)**	**Max Stress (MPa)**	**Cycles to failure**	**Normalised Stress**	**Remarks**	**Test Valid**
IQI-SN-1	56.17	18.66	332.20	1	0.97	Failure in Gauge section	Yes
IQI-SN-2	54.55	19.13	350.68	1	1.03	Failure in Gauge section	Yes
IQI-SN-3	54.17	14.00	258.46	784	0.76	Failure in Gauge section	Yes
IQI-SN-4	54.04	11.00	203.56	20562	0.60	Failure in Gauge section	Yes
IQI-SN-5	53.59	11.40	212.71	8089	0.62	Failure in Gauge section	Yes
IQI-SN-6	53.72	15.30	284.83	106	0.83	Failure in Gauge section	Yes
IQI-SN-7	54.81	10.50	191.58	32693	0.56	Failure in Gauge section	Yes
IQI-SN-8	54.46	14.60	268.09	483	0.79	Failure in Gauge section	Yes
IQI-SN-9	54.67	7.18	131.32	1351483	0.38	Failure in Gauge section	Yes

This project has received funding from the European Union's Horizon 2020 research and innovation programme under grant agreement No 952966.

Table 7. 6 Fatigue test summary for GF/Elium quasi-isotropic lay-up samples.

GF Grester H2026 Quasi-isotropic - Elium							
Test Details: R Ratio: 0.1, Frequency: 5 Hz, Ultimate tensile strength: 313.84 MPa							
Coupon ID	**Area (mm^2)**	**Max Load (kN)**	**Max Stress (MPa)**	**Cycles to failure**	**Normalised Stress**	**Remarks**	**Test Valid**
EQI-SN-1	54.74	17.94	327.73	1	1.04	Failure in Gauge section	Yes
EQI-SN-2	54.97	16.49	299.96	1	0.96	Failure in Gauge section	Yes
EQI-SN-3	54.75	15.00	273.95	603	0.87	Failure in Gauge section	Yes
EQI-SN-4	53.68	10.00	186.30	21164	0.59	Failure in Gauge section	Yes
EQI-SN-5	55.00	9.50	172.74	37771	0.55	Failure in Gauge section	Yes
EQI-SN-6	54.46	14.30	262.55	371	0.84	Failure in Gauge section	Yes
EQI-SN-7	55.16	11.50	208.48	7334	0.66	Failure in Gauge section	Yes
EQI-SN-8	54.72	14.60	266.83	444	0.85	Failure in Gauge section	Yes
EQI-SN-9	54.56	5.75	105.40	1038015	0.34	Failure in Gauge section	Yes

This project has received funding from the European Union's Horizon 2020 research and innovation programme under grant agreement No 952966.

Table 7. 7 Compression 0° test summary (GF/Elium 0° samples)

SAMPLE	b - WIDTH (mm)	h - THICKNESS (mm)	Load at Failure (kN)	Strength @ Failure (MPa)	Modulus, E (GPa)	Maximum Load (kN)	Maximum Strength (MPa)
E0_S1	12.78	3.076	29.885	760.2	48.4	29.892	760.3
E0_S2	12.89	3.050	27.162	691.3	48.0	28.042	713.7
E0_S3	12.95	3.129	21.759	537.2	49.1	21.759	537.2
E0_S4	12.96	3.136	30.891	759.9	42.8	30.907	760.3
E0_S5	12.95	3.119	27.975	692.9	Tested without gages	27.975	692.9
AVERAGE	**12.90**	**3.102**	**27.534**	**688.3**	**47.1**	**27.715**	**692.9**
ST DEV	0.08	0.037	3.552	91.1	2.9	3.556	91.9
CV (%)	0.58	1.21	12.90	13.23	6.08	12.83	13.26

Table 7. 8 Compression 90° test summary (GF/Elium 90° samples)

SAMPLE	b - WIDTH (mm)	h - THICKNESS (mm)	Load at Failure (kN)	Strength @ Failure (MPa)	Modulus, E (GPa)	Maximum Load (kN)	Maximum Strength (MPa)
E90_S1	13.01	3.140	6.467	158.3	17.2	6.467	158.3
E90_S2	13.00	3.187	5.641	136.2	16.0	5.648	136.4
E90_S3	13.02	3.170	6.162	149.4	16.5	6.563	159.1
E90_S4	13.07	3.156	6.282	152.3	17.5	6.282	152.3
E90_S5	13.07	3.160	5.507	133.3	16.1	5.727	138.7
AVERAGE	**13.03**	**3.163**	**6.012**	**145.9**	**16.7**	**6.137**	**149.0**
ST DEV	0.03	0.017	0.417	10.7	0.7	0.424	10.8
CV (%)	0.26	0.55	6.93	7.35	4.09	6.91	7.25

This project has received funding from the European Union's Horizon 2020 research and innovation programme under grant agreement No 952966.

Table 7. 9 Compression 0° test summary (GF/InfuGreen 0° samples)

SAMPLE	b - WIDTH (mm)	h - THICKNESS (mm)	Load at Failure (kN)	Strength @ Failure (MPa)	Modulus, E (GPa)	Maximum Load (kN)	Maximum Strength (MPa)
I0_S1	13.11	3.220	22.889	542.2	46.1	22.889	542.2
I0_S3	12.93	3.156	19.952	488.9	45.2	20.219	495.4
I0_S4	13.05	3.247	23.303	550.1	44.6	23.303	550.1
AVERAGE	**13.03**	**3.207**	**22.048**	**527.0**	**45.3**	**22.137**	**529.2**
ST DEV	0.09	0.047	1.827	33.3	0.7	1.674	29.5
CV (%)	0.70	1.46	8.29	6.31	1.65	7.56	5.58

Table 7. 10 Compression 90° test summary (GF/InfuGreen 90° samples)

SAMPLE	b - WIDTH (mm)	h - THICKNESS (mm)	Load at Failure (kN)	Strength @ Failure (MPa)	Modulus, E (GPa)	Maximum Load (kN)	Maximum Strength (MPa)
I90_S1	13.20	3.195	5.622	133.3	15.4	5.855	138.9
I90_S2	13.24	3.217	6.050	142.1	15.7	6.320	148.4
I90_S3	13.00	3.168	4.974	120.8	16.0	6.078	147.6
I90_S4	13.14	3.159	5.713	137.6	15.9	5.713	137.6
I90_S5	13.19	3.175	5.931	141.7	15.3	5.952	142.2
I90_S6	13.13	3.138	5.792	140.6	16.1	5.792	140.6
AVERAGE	**13.15**	**3.175**	**5.680**	**136.0**	**15.7**	**5.952**	**142.6**
ST DEV	0.08	0.028	0.378	8.1	0.3	0.221	4.5
CV (%)	0.64	0.87	6.66	5.98	1.96	3.71	3.17

This project has received funding from the European Union's Horizon 2020 research and innovation programme under grant agreement No 952966.

Table 7. 11 Compression 0° test summary (CF/Elium 0° samples)

SAMPLE	b - WIDTH (mm)	h - THICKNESS (mm)	Load at Failure (kN)	Strength @ Failure (MPa)	Modulus, E (GPa)	Maximum Load (kN)	Maximum Strength (MPa)
E0_S1	13.21	3.770	28.840	579.2	98.1	28.840	579.2
E0_S2	13.18	3.660	27.342	566.9	77.7	28.878	598.7
E0_S3	13.16	3.603	28.120	593.0	84.7	29.504	622.2
E0_S4	13.19	3.661	26.317	545.0	98.3	28.076	581.5
E0_S5	13.20	3.724	23.845	485.1	93.3	24.955	507.7
AVERAGE	**13.19**	**3.683**	**26.893**	**553.9**	**90.4**	**28.051**	**577.9**
ST DEV	0.02	0.065	1.944	42.3	9.0	1.803	42.8
CV (%)	0.13	1.75	7.23	7.63	9.97	6.43	7.41

Table 7. 12 Compression 90° test summary (CF/Elium 90° samples)

SAMPLE	b - WIDTH (mm)	h - THICKNESS (mm)	Load at Failure (kN)	Strength @ Failure (MPa)	Modulus, E (GPa)	Maximum Load (kN)	Maximum Strength (MPa)
E90_S1	12.74	2.000	3.436	134.8	7.8	3.444	135.1
E90_S2	12.85	1.960	3.270	129.8	8.0	3.270	129.8
E90_S3	12.96	1.983	3.584	139.4	7.5	3.649	141.9
E90_S4	12.97	2.067	3.460	129.1	7.4	3.481	129.9
E90_S5	12.93	1.967	3.258	128.1	7.9	3.260	128.2
AVERAGE	**12.89**	**1.995**	**3.402**	**132.3**	**7.7**	**3.421**	**133.0**
ST DEV	0.10	0.043	0.138	4.8	0.3	0.162	5.6
CV (%)	0.74	2.14	4.05	3.60	3.37	4.73	4.24

This project has received funding from the European Union's Horizon 2020 research and innovation programme under grant agreement No 952966.

Table 7. 13 Compression 0° test summary (CF/InfuGreen 0° samples)

SAMPLE	b - WIDTH (mm)	h - THICKNESS (mm)	Load at Failure (kN)	Strength @ Failure (MPa)	Modulus, E (GPa)	Maximum Load (kN)	Maximum Strength (MPa)
I0_S1	13.17	3.602	27.585	581.7	Tested without gages	27.648	583.0
I0_S2	13.27	3.636	18.543	384.4	99.1	19.179	397.6
I0_S3	13.21	3.627	19.235	401.5	87.1	19.436	405.7
I0_S4	13.23	3.622	27.124	566.2	108.6	27.124	566.2
AVERAGE	**13.22**	**3.622**	**23.122**	**483.4**	**98.3**	**23.35**	**488.1**
ST DEV	0.04	0.014	4.899	104.9	10.8	4.67	100.2
CV (%)	0.32	0.39	21.19	21.70	10.94	20.00	20.52

Table 7. 14 Compression 90° test summary (CF/InfuGreen 90° samples)

SAMPLE	b - WIDTH (mm)	h - THICKNESS (mm)	Load at Failure (kN)	Strength @ Failure (MPa)	Modulus, E (GPa)	Maximum Load (kN)	Maximum Strength (MPa)
I90_S1	13.20	3.195	5.622	133.3	15.4	5.855	138.9
I90_S2	13.24	3.217	6.050	142.1	15.7	6.320	148.4
I90_S3	13.00	3.168	4.974	120.8	16.0	6.078	147.6
I90_S4	13.14	3.159	5.713	137.6	15.9	5.713	137.6
I90_S5	13.19	3.175	5.931	141.7	15.3	5.952	142.2
I90_S6	13.13	3.138	5.792	140.6	16.1	5.792	140.6
AVERAGE	**13.15**	**3.175**	**5.680**	**136.0**	**15.7**	**5.952**	**142.6**
ST DEV	0.08	0.028	0.378	8.1	0.3	0.221	4.5
CV (%)	0.64	0.87	6.66	5.98	1.96	3.71	3.17

This project has received funding from the European Union's Horizon 2020 research and innovation programme under grant agreement No 952966.

8. REFERENCES

[1] Fibregy DoA (Description of the action). Annex 1, Grant Agreement, Number 952966 2020.

[2] ISO 13003:2003(E): Fibre-reinforced plastics — Determination of fatigue properties under cyclic loading conditions. 2003.

[3] D6641/D6641M Standard Test Method for Compressive Properties of Polymer Matrix Composite Materials Using a Combined Loading Compression (CLC) Test Fixture n.d. https://www.astm.org/d6641_d6641m-16e02.html (accessed May 26, 2023).

[4] Soukissian T, Karathanasi F, Axaopoulos P. Satellite-Based Offshore Wind Resource Assessment in the Mediterranean Sea. IEEE J Ocean Eng 2017;42:73–86. https://doi.org/10.1109/JOE.2016.2565018.

[5] Kensche CW. Fatigue of composites for wind turbines. Int J Fatigue 2006;28:1363–74. https://doi.org/10.1016/j.ijfatigue.2006.02.040.

[6] Mandell JF, Reed RM, Samborsky DD. High cycle fatigue of wind turbine blade materials. Am Soc Mech Eng Sol Energy Div SED 1992;12:105.

[7] Sørensen BF, Goutianos S. Prediction of fatigue limit for unidirectional carbon fibre/epoxy composites. IOP Conf Ser Mater Sci Eng 2018;388. https://doi.org/10.1088/1757-899X/388/1/012017.

[8] Luong MP. Fatigue limit evaluation of metals using an infrared thermographic technique. Mech Mater 1998;28:155–63. https://doi.org/10.1016/S0167-6636(97)00047-1.

[9] La Rosa G, Risitano A. Thermographic methodology for rapid determination of the fatigue limit of materials and mechanical components. Int J Fatigue 2000;22:65–73. https://doi.org/10.1016/S0142-1123(99)00088-2.

[10] Haddad M, Zitoune R, Bougherara H, Eyma F, Castanié B. Study of trimming damages of CFRP structures in function of the machining processes and their impact on the mechanical behavior. Compos Part B Eng 2014;57:136–43. https://doi.org/10.1016/j.compositesb.2013.09.051.

[11] Hejjaji A, Zitoune R, Toubal L, Crouzeix L, Collombet F. Influence of controlled depth abrasive water jet milling on the fatigue behavior of carbon/epoxy composites. Compos Part A Appl Sci Manuf 2019;121:397–410. https://doi.org/10.1016/J.COMPOSITESA.2019.03.045.

[12] Elium 188XO liquid thermoplastic resin Technical Data Sheet. Tech Data Sheet 2017.

[13] Datasheet T. ELIUM ® 188 O LIQUID THERMOPLASTIC RESIN TYPICAL CURED RESIN NON REINFORCED PROPERTIES. n.d.

[14] SR INFUGREEN 810 and hardeners SD882X, Green Epoxy systems for injection and infusion. Tech Data Sheet 2017.

[15] ISO 527-4, Plastics — Determination of tensile properties — Part 4: Test conditions for isotropic and orthotropic fibre-reinforced plastic composites. 2009.

This project has received funding from the European Union's Horizon 2020 research and innovation programme under grant agreement No 952966.

[16] Mandell JF. Fatigue Behavior of Short Fiber Composite Materials. Compos Mater Ser 1991;4:231–337. https://doi.org/10.1016/B978-0-444-70507-5.50011-1.

[17] J.F. Mandell. Fatigue Behavior of Fiber-Resin Composites. In: Pritchard G, editor. Dev. Reinf. Plast. - 2, London: Applied Science Publishers; 1982, p. 67.

[18] Datasheet T. ELIUM ® 188 O LIQUID THERMOPLASTIC RESIN TYPICAL CURED RESIN NON REINFORCED PROPERTIES; URL: ; URL: https://www.arkema.com/files/live/sites/shared_arkema/files/downloads/products-documentations/liquid-thermoplastic-resinfor-tougher-composites.pdf. n.d.

[19] ISO - ISO 14127:2008 - Carbon-fibre-reinforced composites — Determination of the resin, fibre and void contents n.d. https://www.iso.org/standard/37222.html.